5-2010

The Use of Preclinical Models to Improve the Treatment of Retinoblastoma

Katie Marie Nemeth
University of Tennessee Health Science Center

The Use of Preclinical Models to Improve the Treatment of Retinoblastoma

DOI
10.21007/etd.cghs.2010.0225

Comments
One year embargo expired May 2011

The Use of Preclinical Models to Improve the Treatment of Retinoblastoma

A Dissertation
Presented for
The Graduate Studies Council
The University of Tennessee
Health Science Center

In Partial Fulfillment
Of the Requirements for the Degree
Doctor of Philosophy
From The University of Tennessee

By
Katie Marie Nemeth
May 2010

ACKNOWLEDGEMENTS

I would like to acknowledge the many people who have contributed to my scientific development during my graduate studies. First, I would like to thank my mentor, Dr. Michael A. Dyer, for his commitment to developing my scientific thought process and training me in the skills needed for my future career. His patience and continual drive helped me achieve my scientific goals. Equally I thank the members of my committee, Drs. Suzanne Baker, Kip Guy, Dianna Johnson and Clinton Stewart, for their one-on-one meetings, stimulating conversations and continual support. In addition, I would like to acknowledge my earlier mentor Dr. Linda Harris who guided me through me early in my graduate career. I am also grateful to the members of the Interdisciplinary Program of Biomedical Sciences at University of Tennessee and St. Jude's Hospital, especially Drs. Pat Ryan, Don Thomason and Steven White, for their additional support. In addition, I would like to thank the Animal Imaging Core at St. Jude Children's Research Hospital for their friendship and endless effort in helping me collect the necessary data for my research. Their never-ending flexibility with my "dire" emergencies never ceased.

I am so grateful to many friends and peers that give me amazing support, challenging scientific conversation and friendships. I would like to acknowledge past and present fellows Drs. Claudia Benavente, Samantha Cicero, Brandon Cox, Stacey Donovan, Nikia Laurie and Erin Volk. Also, I would like to thank my family, especially my husband, Christopher J. Nemeth, for his never ending support and voice of reason. Last, but not least, I would like to thank my son Charles Matthew Nemeth for keeping me grounded during the writing process.

ABSTRACT

Rodent models play an essential role in the development of new chemotherapeutics and dosing regimes. It is often difficult to carryout a clinical study for pediatric cancers due to the small patient population. Retinoblastoma, a pediatric cancer of the eye, is one example of a pediatric cancer that can benefit from preclinical studies. Over the years various retinoblastoma rodent models have been developed used to test various combination of broad-spectrum systemic chemotherapy. It was found form these studies that the combination of topotecan and carboplatin was effective. However both drugs cause myelosuppression and therefore administrating both of these drugs systemically is not possible. An alternative effective therapy in the clinic was the use of a subconjunctival administration. We thought if we could administer both drugs, one by systemic and one by a subconjunctival injection, perhaps we could decrease the systemic exposure with good tumor response. Detailed pharmacokinetic studies were conducted to understand the subconjunctival injections of topotecan and carboplatin. It was found that both drugs could successfully penetrate the eye and increase drug exposure. In addition, in the presence of a tumor, drug exposure to the vitreous was greater.

Additionally comparative pharmacodynamic studies combining topotecan subconjunctival injection with carboplatin intraperitoneal or carboplatin subconjunctival injection with topotecan intraperitoneal were conducted. The tumor response, systemic toxicity and local toxicity were studied. There was tumor response in both combinations and no ocular toxicity was seen with a single eye subconjunctival injection for either drug. However, rats that received the combination with topotecan subconjunctival injection and carboplatin intraperitoneal experienced great toxicity and morbidity. The data and observations suggest the death is due to dehydration. Therefore it was concluded that the alternative combination was better.

The above data suggested an appropriate drug combination and schedule for a preclinical study. However, the noninvasive methods to follow tumor progression and choosing the correct genetic model needed to be determined. This was essential to ensure the preclinical study could be easily translated for future clinical studies. A characterization study of five modalities, retina camera, optomotry, tonometer, ultrasound and MRI, was done with retinoblastoma mice. We determined the feasibility of each technique. It was found that the retina camera could detect the tumor the earliest in a high throughput manner. Additionally, the tonometer and optomotry machines could assess ocular health. While the ultrasound and MRI could image the eye and tumor in one field of view, MRI could capture the posterior chamber in more detail along with the extraocular space. With different software programs, the tumor to eye ratio volume measurement were determined and compared to the gold standard of enucleation, embedding, serial sectioning and hand tracing. It was found that there was a better correlation between the ultrasound and hand tracing histological sections.

Concurrently, the tumor progression of six different genotypes was assessed. The tumor progression depended on the number and different genes deleted. Additionally, based on genotypes, it was determined there was not a strong genotypic trend in the increase in IOP or the loss of vision. From the studies of tumor progression

we have learn more about the influence of genes on tumor progression, which will benefit additional genetic studies in mouse model systems and human tumors.

TABLE OF CONTENTS

LIST OF TABLES

LIST OF FIGURES

LIST OF ABBREVIATIONS

μl	microlitters
μM	micromolar
ADME	absorption, distribution metabolism and elimination
AML	acute myloid leukemia
ANLL	acute non-lymphacytic leukemia
ANOVA	analysis-of-variance
AUC	area under the curve
AVV Vector	Adeno-associated virus vector
BAB	blood aqueous barrier
BBB	blood brain barrier
BCRP	breast cancer resistance protein
BRB	blood retina barrier
BSA	body surface area
BUN	blood urea nitrogen
CBC	complete blood count
CBP	carboplatin
c/d	cycles per degree
CE	ciliary epithelium
cm	centimeter
CNS	central nervous system
CT	computed tomography
d	day
dd	disc diameter
dl	deciliter
DNA	Deoxyribonucleic acid
E2F	eukaryote 2 factor
EBR	external beam radiation
FDA	federal drug administration
Fig.	figure
G1	Gap phase 1
G2	Gap phase 2
GCL	ganglion cell layer
GFP	green fluorescent protein
GFR	glomerular filtration rate
GI	gastrointestinal
h	hour
H&E	hematoxylin and eosin
Hg	mercury
i-BRB	inner blood retina barrier
INL	inner nuclear layer
IOP	intraocular pressure
i.p.	intraperitoneal
IPL	inner plexiform layer
IRBP	interphotoreceptor retinoid-binding gene
i.v.	intravenous

Kg ..... kilogram
LOH ..... loss of heterozygosity
LUC ..... luciferane
m^2 ..... meters squared
mg ..... milligrams
ml ..... milliliters
mm ..... millimeter
MP-RAGE ..... magnetization prepared rapid gradient echo
MRI ..... magnetic resonance imaging
mRNA ..... messenger ribonucleic acid
MRP ..... multidrug resistant protein
n ..... number
NE ..... neutrophil
ng ..... nanograms
Nr2e3 ..... nuclear receptor subfamily2, group E, member 3
O_2 ..... oxygen
OATP ..... organic anion transporter peptide
o-BRB ..... outer blood retina barrier
OCT ..... organic cation transporters
ONL ..... outer nuclear layer
OPL ..... outer plexiform layer
p ..... postnatal
p53 ..... protein 53
p107 ..... protein 107
p130 ..... protein 130
p-gp ..... P-glycoprotein
p/sec/cm^2 ..... photon per second per centimeter squared
PLT ..... platelets
q ..... long arm on chromosome
r^2 ..... a correlation constant value
RB ..... retinoblastoma gene
Rb1 ..... retinoblastoma protein
RBC ..... red blood cells
RE ..... Reese-Ellsworth
RPE ..... retinal pigment epithelium
sec ..... second
S phase ..... synthesis phase
SV40 Tag ..... Simian Virus 40 large t antigen
T ..... tesla
Tpt ..... topotecan
VEC ..... vincristine, etoposide, carboplatin
VEGF ..... vascular endothelial growth factor
WBC ..... white blood cells
3D ..... three-dimensional

CHAPTER 1. INTRODUCTION

1.1 ANATOMY OF THE EYE

The eye, a sensory organ, has been a useful model in the study of the vertebrate central nervous system (CNS) and its associated diseases [2]. It can be divided into three layers: the outer, middle and inner **(Fig. 1-1)**. At the front of the eye is the outer layer, which is composed of fibrous connective tissue that is further divided into the sclera and the cornea [2, 3]. The primary function of the sclera is to support the eye, while the cornea is responsible for the transmission of light through the pupil. The middle layer, known as the uvea, is composed of the choroid, ciliary body and iris [2, 3]. The iris is a smooth muscle at the front of the eye and is responsible for light regulation into the eye. Following these muscles is the ciliary body that supports the lens and helps secrete aqueous humor fluid. The choroid, at the posterior section, prevents reflection of the light and is responsible for the exchange nutrients and oxygen. The innermost layer of the eye, the retina, is where incoming light is transferred into electroimpulses [2, 3]. These action potentials travel by the optic nerve to the brain, initially to the lateral geniculate nucleus (LNC) and finally to the primary visual cortex [2].

When light enters the cornea the vision process begins. Light continues to travel through the cornea, pupil, lens, vitreous humor and finally reaches the retina. This final complex layer is composed of seven cellular groups [2, 3] **(Fig. 1-2)**. The ganglion cells are the first cell layer, where the initial light contact occurs, followed by the amacrine cells, bipolar cells, horizontal cells and photoreceptors. These final neurons, rod and cone cells, are the most commonly referred to because they are responsible for the photochemical reaction, converting light into electroimpulses. Each cell type has a specific role in sight [3]. Covering the majority of the retina, the rods are responsible for vision in low-light conditions. Contrary, the cones, fewer in number, function in bright light conditions and help distinguish the visual acuity in the special concentrated region called the fovea.

Vision is supported by many accessory structures in the ocular orbit. These include various muscle groups, a conjunctiva sac and vascular systems [2, 3]. Six external muscles that help search the visual field and track moving objects are divided into two main groups, the rectus and oblique [2]. The rectus muscles are further divided into the superior inferior lateral and medial. These muscles are responsible for moving the eye horizontally and vertically. Similarly, the oblique muscles, superior and inferior, are responsible for diagonal movement. Each group plays a role in viewing the entire field.

The conjunctiva sac and the vascular system are responsible for protecting and maintaining the eye [2, 3]. Located around the exterior globe is the conjunctiva composed of a thin epithelial membrane attaching to the lids and cornea epithelium creating a sac. Along with protecting the eye with mucus, it has an active role in repair [3]. The vascular system exchanges, either indirectly or directly, the nutrients and gases for the entire eye [3]. It is uniquely divided into two separate systems, the retinal and uveal vessels and arranged to avoid interference with the transmitted light [3]. Interestingly, the retina circulatory system is complex. The inner retina is directly

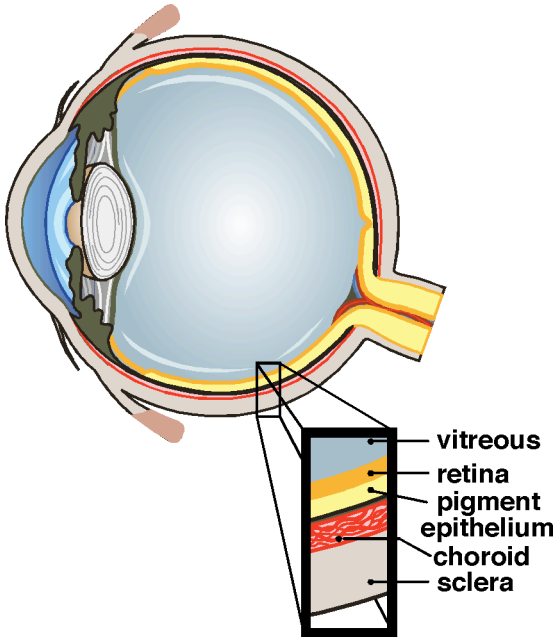

Figure 1-1. Anatomy of the Human Eye.
In the posterior chamber of the eye there are many layers. The small box represents the order of each tissue layer. Modified with permission. Dyer, M.A. and R. Bremner, *The search for the retinoblastoma cell of origin.* Nat Rev Cancer, 2005. **5**(2): p. 91-101 [4].

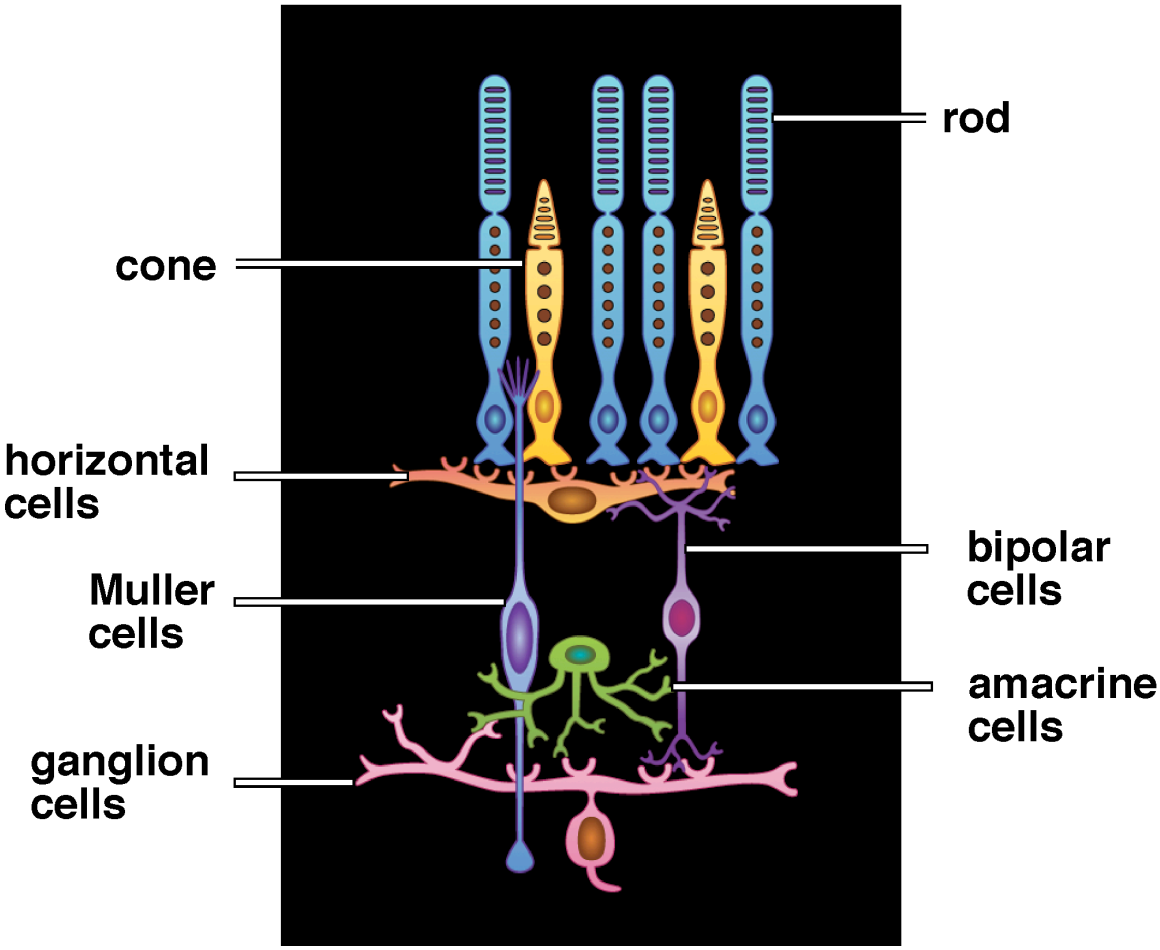

Figure 1-2. The Cellular Layers of the Eye.
There are seven cell types in the eye beginning in the anterior chamber with the ganglion, amacrine, Muller, bipolar, horizontal and rod and cone cells. Modified with permission. Dyer, M.A. and R. Bremner, *The search for the retinoblastoma cell of origin.* Nat Rev Cancer, 2005. **5**(2): p. 91-101 [4].

nourished by vessels, where as the outer part, including the photoreceptors, are nourished by diffusion. All three of these accessory structures are necessary and responsible for the movement, repair of the eye and exchange of nutrients.

In addition to the orbital supportive structures, intraocular fluid and its movement support the interior globe. Both the anterior and posterior chambers are filled with either aqueous humor or vitreous [3]. Movement of these fluids ensures additional exchange of nutrients [5]. The vitreous is a gelatinous protein rich fluid [3]. This static fluid is never replenished or renewed. On the other hand, the aqueous humor is secreted by the ciliary bodies and moves through the pupil into the anterior section of the eye. Here the canal of Schlemm drains it into the vascular and lymphic systems to maintain the eye pressure [3]. It maintains the eye pressure. If the flow is disrupted, fluid can accumulate resulting in increased intraocular pressure and decreased nutrient exchange, eventually leading to visual damage.

1.2 RETINA DEVELOPMENT

The retina is thin layer of tissue, composed of multiple cellular layers, that carries out the function of sight. The seven layers are divided into three cellular nuclear layers, the outer nuclear layer (ONL), inner nuclear layer (INL) and ganglion cell layer (GCL) and two synaptic layers, the outer plexiform layer (OPL) and inner plexiform layer (IPL) [6-8]. At the posterior part of the eye, the ONL is composed of photorecepter cells, rods and cones. These neurons send their impulses to the INL, bipolar cells. Additionally, the horizontal and amacrine cells also play an essential role by directing the signal to the GCL where the ganglion and amacrine cells are located. The ganglion cells transmit the output electric impulses to the correct locations in the brain.

Each of the cell populations originates from multipotent progenitor cells, which can give rise to any one of these seven cells [9, 10]. In the early stages of eye development a newly postmitotic cell line migrates to the proper location where it further differentiates. For a progenitor cell to complete this process different intrinsic changes, such as expression of transcription factors, make it “ready”, or competent [9]. Once competent, the cell is able to respond to additional external cues [9]. Both play a role to ensure a particular certain cell type is born. Interestingly, these transitions occur at specific developmental times, leading to a conserved birth order [6, 7]. For example, ganglion cells are always the first to develop, followed by cones, horizontal cells, amacrine cells, rod, Müller Glia and finally bipolar cells [7]. Interestingly, Cepko and colleagues found a cell’s fate is based on the last day it went through S phase [9]. Once a cell is committed as one type it cannot revert to a previous cell population [9]. If the proper external and internal signals are present the subsequent linage continues to develop [9, 10]. As expected cellular proliferation is tightly regulated to ensure the proper ratios of each cell type guaranteeing proper visual signals and function.

1.3 CELL CYCLE AND THE IMPORTANCE OF ITS REGULATION IN NEURAL DEVELOPMENT

The regulation of the cell cycle ensures that the proper cell numbers are present for each tissue and organ. The cell cycle can be divided into two different phases, interphase and mitosis. Interphase prepares the cells for division. It is further divided in G1 phase, where proteins and organelles are duplicated, S phase, where chromosomes are duplicated and G2 phase, where the remaining proteins needed for mitosis are synthesized. During mitosis the cell divides the chromosomes, organelles and cytoplasm equally between the two daughter cells. The four stages, prophase, metaphase, anaphase and telephase, ensure this proper duplication. Upon dividing the cell exits the cycle.

Multiple cell cycle proteins play essential roles in cellular division. In a non-dividing cell the retinoblastoma protein (*Rb1*) binds to *E2F* transcription factors, which are responsible for the transcription of additional genes required for transition to S phase. To date there are five *E2F* proteins (*E2F1-5*) and two additional Rb family members, *p107* and *p130* [11]. Each E2F member has a preference to bind to one of the Rb family members [12]. Interestingly, these cell cycle regulators have similar pocket domains, thus are referred to as the “pocket family” [13]. These proteins differ in their expression patterns throughout the cell cycle. For example, *p107* is highly expressed in cycling cells and *p130* is expressed at high levels near the exciting of the cycle [12].

The most well studied player of this group is the retinoblastoma protein *Rb1*. Its phosphorylation status was the first linked to the cell cycle. Once phosphorylated, by cyclins and cyclin dependant kinases, Rb1 losses its high affinity for the E2F protein and thus the cell becomes committed to divide. Once the cell finishes replication and exits the cell cycle and Rb1 gets hypophosphoralated allowing it to once again bind to E2Fs. If any of these proteins are not properly regulated, uncontrolled cellular division occurs and leads to an increase differences in cell number affecting the organs function or generates a mass leading to potential cancers [13].

As previously mentioned, a well-coordinated and fine-tuned cell cycle is important for maintenance, but also developmental stages. During different periods cellular intrinsic proteins help regulate the cell’s competence to differentiate [9]. If these proteins are interrupted, the cell competence changes, ultimately affecting the cell population and subsequent groups. For the eye, this can affect different cell types based on the linear birth order [9]. Thus, if earlier cells are increased, then the late population will be decreased which could affect the electroimpulse transmission and affect vision. [9]. Ultimately these changes can lead to pathological conditions, such as retinal degeneration and tumor formation, called retinoblastoma [14].

1.4 MOLECULAR ASPECTS OF THE RETINOBLASTOMA GENE AND PROTEIN

The discovery of the RB1 gene was first localized to chromosome 13q14 and cloned in 1986 [15, 16]. It spans a region of 27 exons and is conserved across many different species [7]. The gene encodes for *Rb1* protein, which is 105 KD and is best

known for its role in cell cycle regulation [17, 18]. In an hypophosphorylated state, this tumor suppressor binds to *E2f* transcription factors to prevent excessive cell division [10]. However, when *Rb1* is phosphorylated it's structure changes and the transcription factors are released to active genes needed for cells to pass through the G1 checkpoint. As the cell finishes the cycle and approaches the mitotic phase *Rb1* is dephosphorylated to its original hypophosphorylated state. When there is a mutation in this tumor suppressor the cell can cycle out of control leading to a potential malignant growth.

Various types of mutations, such as point mutations, small deletions and insertions, occur in the RB gene leading to a frame shift or a premature termination [10]. These changes inactivate the *Rb1* protein. When the protein's mutations were further investigated a loss of heterozygosity (LOH) was originally seen in the childhood disease; however this concept was further seen in other cancers, such as lung, bladder, brain and liver cancer [19, 20]. Interestingly, the somatic or germline mutations in the same gene can lead to different tumor types and ages of onset.

1.5 RETINOBLASTOMA THE DISEASE

Retinoblastoma mutations occur prior to birth present in both of the disease forms, non-inherited and inherited. The majority of disease cases, about 60%, are from non-inherited mutations [21]. The unilateral tumor begins with a single retinal cell acquiring two sporadic random mutations [22]. The remaining forty percent of cases are typically bilateral and caused by an inherited germline mutation in all cells of the body with a second somatic mutation in a retinal cell.

From his observation in the seventies, the mathematician Alfred Knudson developed the well-known "two-hit" hypothesis. He noticed children with bilateral retinoblastoma developed the disease earlier than those with the non-hereditary unilateral disease. This early onset was attributed to the first mutation occurring in a germline cell in utero. From these observations of retinoblastoma, the "two-hit theory" of cancer was born. This finding was the launching pad for the general understanding of cancer and the retinoblastoma disease. Shortly after this discovery, karyotype analysis revealed further detail that the insertional deletion was on chromosome 13 [17]. Further examination of cancerous cells found that both copies of chromosome 13 were the same. This loss of heterozygosity (LOH) explained that this inherited mutation was recessive and when the cell had two copies, its proliferation was uncontrollable [17, 23]. The discoveries in retinoblastoma continued to produce information about the commonalities of cancer. With the retroviral gene transfer of a wild type RB gene, it was found that cells with the endogenous inactivation in the RB gene were rescued from their uncontrolled proliferation. This experiment led to the definition of a tumor suppressor. In addition to retinoblastoma cases, Harbour and colleagues found abnormalities in the RB gene in small cell lung cancer samples [24]. Since these discoveries, the RB gene has been found to be abnormal in many adult cancers.

1.5.1 Diagnosis modalities

Retinoblastoma pathological effects are often confused with many other eye abnormalities. It is usually first detected by observing the eye's reflex to a bright light in a dimly lit environment. A healthy child's pupil reflexes red, but if a tumor is present the reflex will be a white or pinkish color [25]; however this reaction is difficult to distinguish from other diseases, such as leukocoria, toxocariasis, coats and cataracts. Therefore, ophthalmologists and other pediatric specialists use combination of approaches with different modalities to further confirm the pediatric disease of retinoblastoma.

The initial diagnosis is conducted with a retinal camera examination of the sedated child. This allows physicians to examine the entire globe for tumors and potential tumor seeding. This modality is sufficient for the initial diagnosis; however it has some limitations [26]. First tumor boundaries cannot be visualized in one field, limiting a comprehensive view of the tumor. Second, tumors at the periphery and extraorbital space cannot be detected. Third, the camera cannot be used for the more advanced cases, because tumor invasion in the anterior chamber obstructs the view. Taken together the retina camera can provide an assessment of ocular health, but cannot provide a conclusive evaluation, therefore further confirmation is necessary with other modalities.

To complete the initial ocular health evaluation, additional exams with a rebound tonometer and visual acuity test are conducted. The rebound tonometer detects changes in the eye's pressure normative values. Often the presence of a tumor can grow into the anterior chamber, press on the lens or tumor seeds can break off from the main mass and settle near the canal of Schlemm [26, 27]. Each event can lead to an increase in ocular pressure (IOP), which can damage the nerves leading to potential visual loss.

In addition, the visual acuity determines the severity of the tumor and placement of the tumor. A patient's vision is typically monitored using a Sneal eye chart. Often the placement of the tumor or ganglion cell damage interrupts the visual path and causes a decrease in vision. While both visual acuity and eye pressure are more informative, the tumor's stage is most effectively confirmed with additional imaging modalities.

With the advancement of high resolution imaging modalities, such as ultrasonography, magnetic resonance imaging (MRI) and computed tomography (CT), tumor growth can be fully characterized. These modalities are essential to determine the it's growth patterns, such as endophytic, exophytic, or combination of both. Generally an endophytic tumor invades the anterior portion of the globe, whereas an exophytic tumor invades the optic nerve and conjunctiva. If the tumor grows into the extraorbital cavity, it is likely to metastasize to the brain, spinal cord, bone marrow, or spread into the lymph nodes [26]. These cases require aggressive treatment. By combining the diagnostic abilities from each method a comprehensive picture of the tumor's stage is diagnosed.

Unlike the retina camera, ultrasound can be used to visualize the entire eye in a single field of view and its resolution of the anterior chamber and the retina's periphery are very good. Moreover, the power Doppler function can detect blood flow and echogenic debris in the vitreous [28]. In particular, vessels are detected by determining

the differences in sound wave frequencies between the vessels to the tissues. This diagnostic can provide information about the tumor's activity, such as nutrient exchange and waste elimination [28]. For example, a well vascularized tumor is likely to have better drug delivery compared to a tumor that is not well vascularized. Unfortunately, the major limitation of this diagnostic tool is the depth that sound waves can travel and therefore imaging of the extreme globe's posterior and invasion in extraocular space is difficult or impossible.

Prior to the ultrasound, the traditional imaging modality for retinoblastoma was the computed tomography (CT). It can detect intraocular, extraocular, intracranial spread and calcification of tumors [28]. However, it use is limited because radiation exposure to germline mutation patients is dangerous for the potentially to causing secondary tumors. This limitation, along with the poor detection of infiltration in the choroid, sclera and optic nerve made this tool unattractive and it has been replaced with the magnetic resolution imager (MRI).

With the development of the MRI the tumor can be viewed in various planes in the surrounding tissue environment such as: corneal, sagittal and transverse planes. This technology can clearly confirm the presence of the tumor, especially in the posterior chamber and brain. In addition, different software programs can be used to monitor tumor size and its change with treatment. Some researchers have suggested a correlation between the tumor size and the likelihood of tumor infiltration [29]. While the sensitivity is far superior to other diagnostic tools and continues to improve, MRI has some difficulty imaging tumor calcification and hemorrhages within the tumor [27]; however these limits are outweighed by its radiation free technology. Using these high-resolution image modalities helps classify the disease, decide about treatment options and monitor tumor response.

1.5.2 Retinoblastoma disease classification

Historically, there have been multiple different classification systems for retinoblastoma based on the available technology. These classifications have been used to establish a baseline, determine treatment progress and aid in the communication between medical doctors and clinical studies. The first system, and perhaps the most widely referred to today, is the Reese-Ellsworth (R-E1-5) classification. Originally developed in the 1960s, it was used to classify intraocular tumors and track the success of external beam radiation therapy (EBR). This system classifies the tumor's size and location into five different groups (**Table 1-1**). The tumor's size is determined by measuring the circumference of the optic nerve's head as a reference with the unit of measurement of disc diameter. The first group (R-E 1) is the least advanced form of the disease. In general, these tumors are less than 4 disc diameters and reside in the posterior globe; whereas the most advanced stage, R-E group 5, has massive tumors in over half of the eye and show marked vitreous seeding [30]. While this system is beneficial it only diagnoses the health of the globe.

Overtime treatment options have changed and additional classifications were developed [27]. These systems classify the intra-retinal tumor along with invasion and metastasis into the extraorbital space, brain or other system. Recently, Chantada and

Table 1-1. The Reese-Ellsworth Description of Salvaging the Eye.

Classification group	Change of salvage	Distribution of tumor
Group 1-A	Very favorable	Solitary tumor, less than 4 disc diameter (dd) in size at equator
Group 1-B		Multiple tumors, none over 4 dd in size, all at equator
Group 2-A	Favorable	Solitary tumor, 4 to 10 disc diameter in size or behind the equator
Group 2-B		Multiple tumors, 4-10 dd in size, behind equator
Group 3-A	Doubtful	Any lesion anterior to the equator
Group 3-B		Solitary tumors larger than 10 dd behind equator
Group 4-A	Unfavorable	Multiple tumors, some larger than 10 dd
Group 4-B		Any lesion extending anterior
Group 5-A	Very Unfavorable	Massive tumors involving over half the retina
Group 5-B		Vitreous seeding

Source: Reese, A.B. and R.M. Ellsworth, *Management of retinoblastoma.* Ann N Y Acad Sci, 1964. **114**: p. 958-62 [30].

colleagues were one group who proposed a system that allowed physicians to focus on the entire scope of the disease [31]. Their goal was to build comprehensive picture of the disease. Both of these staging systems are examples of current methods in which physicians can communicate the treatment options for different clinical protocols.

1.6 HISTORY OF CLINICAL TREATMENT

In 1809 James Wardrop was the first to publish a retinoblastoma clinical article that suggested enucleation as the standard treatment for the tumor [32]. For nearly a century, this was only clinical treatment option. It was Henry Stallard's discovery of retinoblastoma's radiosensitivity that lead to this less invasive treatment option [33]; however, it was not completely successful for all cases and often there was a reoccurrence of secondary tumors. Alternative local treatments have been investigated throughout the years.

It was not until the development of external beam radiation therapy (EBR) that a more successful direct and focal treatment was used [34]. This conservative focal treatment used radiation to locally target and limit the overall DNA damage. While this treatment was more safe and effective, it had adverse side effects, such as skull malformations and secondary tumors, seen primarily in children less than 12 months of age [35, 36]. Today, EBR treatment is reserved for recurrent or sever cases of older patients of retinoblastoma.

One way clinicians have addressed the limiting factors of EBR was to use chemotherapy agents. Early in the 1950s Kupfer was first to establish retinoblastoma's sensitivity to the chemotherapeutics, in particular nitrogen mustard. Unfortunately, the overall long term response was not successful [37]. His work led to further exploration of other chemotherapies [36, 38, 39]. These studies have sparked interest in combining focal treatment with drug treatments [40, 41]. An important comparative study looked at tumor response to EBR verse EBR with the chemotherapy drugs, vincristine, etoposide and carboplatin (VEC) [41]. While this study showed promising results, the use of EBR had continued concern physicians [36, 42, 43].

Eventually the development of additional therapies, such as laser thermotherapy, cryotherapy, brachytherapy and chemothermotherapy, gave physicians more treatment options. Each technique was specific to the tumor's size and location of malignant masses. Usually, laser photocoagulation, thermotherapy and cryotherapy are used to treat small tumors. Laser photocoagulation uses a laser to coagulate a posterior tumor's blood supply [26, 27]. Whereas tumors located in the peripheral, are treated with the cryotherapy freezing technique and thermotherapy, applies heat application to the tumor [26, 27]. However, if the tumor is too large and shows seeding it is managed with brachytherapy, a radioactive implant [44-46]. With these additional therapies the combinational treatment approach greatly expanded.

These different treatments paved the way for continued combinational studies. Various studies explored the use of focal therapies with the VEC drug combination [41, 47-49]. Of these studies, one reported a full ocular salvage of late stage retinoblastoma group [47]. Hence, ocular salvation and preservation of sight became possible for a

number of late stage retinoblastoma patients. Even though the tumor response was promising, the long-term effects of these drugs were questionable.

Several concerns mounted over the use of etoposide as it was suspected to cause the secondary cancer, acute myeloblastic leukemia (AML). In 1998, it was reported that the pediatric population was at a special risk for developing this secondary cancer [50-54]. In response, one group developed a protocol where they treated children with the combination of carboplatin and vincristine for 8 courses. In addition, they eliminated or delayed the use of focal therapies [55]. They found 60% of patients with early stage tumors had event-free survival for approximately 2 years [55]. Unfortunately, only 30% of children with late staged tumors (R-E IV-V) responded. This finding was similar to other reports of late stage tumor treatments. Even though there was a lack of success with the advanced tumor population, it concluded to be a success for children with early-stage intraocular retinoblastoma [55]. The results of this study emphasized that treatment outcome was heavily dependent on the tumor's initial stage.

With poor results for advanced diseases, a new therapy was needed. Therefore physicians explored other pediatric cancer treatments, in particular neuroblastoma [56, 57]. It was found that the topoisomerase I inhibitor, topotecan, was effective for this childhood cancer. Not only was it effective, but it could pass the blood brain barrier. These clinical findings were promising for retinoblastoma because the blood-brain barrier is similar to the blood-retinal-barrier protecting the eye. This finding was further supported by additional preclinical xenograft studies for pediatric nervous system cancers and in particular an orthotopic retinoblastoma xenograft model that used topotecan or topotecan in combination with other anti-cancer agents [58-60]. The later found good response and penetration to the eye with intravenous injection [60]. While these results were exciting, the chemotherapies were administrated by i.v. and thus there was a concern for the systemic exposure, especially for children with the germline mutation.

While this study supported the possibility of reducing the chance of AML, physicians wanted to improve the amount of drug exposure to the eye and decrease systemic exposure. It was thought a local delivery of the drug could lead to an increase in concentration; however, the eye structure proved to be challenging. A direct intravitreal injection was not feasible because of the risk of damaging the eye and the possibility disseminating tumor cells. Nevertheless, researchers circumvented this obstacle with by injecting in the surrounding orbital area [61-64]. Based on these studies, Abramson's group conducted a clinical study which treated patients with only subconjunctival injections of carboplatin [65]. With this new technique, he found a decreased in systemic side effects and partial to stable tumor responses. Unfortunately, there was still little success with the advanced tumors and the long-term prognosis was unfavorable [65, 66].

This new technique and the findings of retinoblastoma's sensitivity to topotecan led to additional therapeutic protocols. In one trial, patients received topotecan, vincristine, focal therapy treatments and a subconjunctival treatment of carboplatin. The current results are promising, but are being further being confirmed at St. Jude Children's Research Hospital (verbal communication). Similarly, an additional clinical trial focused on the subconjunctival injection of topotecan alone. This was similar to

Abramson's study in 1999, but it replaced carboplatin with topotecan [67]. While this study focused on toxicity, they also observed a partial response in six of the seven treated eyes [67]. While these recent clinical studies are exciting, further early phase clinical trials and animal studies with single agents or multiple drug combinations are needed to determine the ideal treatment and long-term effects**.**

1.7 THE PHARMACOLOGY OF TREATING RETINOBLASTOMA

To properly design preclinical and clinical studies the chemotherapeutics' pharmacologic properties need to be well defined. It is essential to determine what the body does to the drug and how the drug affects the body, its organs and cellular receptors. Before describing the pharmacology of the traditional retinoblastoma therapeutics, brief descriptions of general pharmacologic principles are essential.

Pharmacology may be considered as two basic components, pharmacokinetics and pharmacodynamics. When a drug is given, the body immediately starts to process it through a series of four pharmacokinetic steps: absorption, distribution, metabolism and elimination. By characterizing each process a comprehensive understanding of the amount of drug reaching the therapeutic site is determined. Drug absorption depends on the route of drug administration, such as oral ingestion or subconjunctival injection. Each site has unique characteristics in circulation and cellular characteristics, such as the number of membrane layers and cellular transport being either active or passive. In addition, the drug's biochemical properties, such as its aqueous solubility and its formulation or vehicle solution are factors that influence how the drug is processed [68].

Once the drug is dispersed to different organs and cellular fluids, its distribution throughout the body continues to be heavily dependent on the chemotherapeutics' physiological and physicochemical properties. In particular, regional blood flow has a large impact and quickly moves drug to major organs. Organs' membrane transporters, such as transporters efflux uptake and influence their exposure. Similarly, capillary permeability, intracellular and extracellular pH gradients and plasma proteins can affect the amount of free drug to cross cellular membranes throughout the body [68].

The third phase of a drug's pharmacokinetics is the metabolic conversion into metabolites, which typically ceases its activity; however, the exception to this is seen with prodrugs. These drugs are synthesized to become active when exposed to metabolic enzymes. In both of these cases different enzymatic systems carry out changes to the drug's structure, typically occurring in the liver [68]. After the drug's distribution, they are eliminated from the body.

The drug's elimination or clearance occurs primarily in the kidney, but can also occur by other routes, such as the liver and GI tract [68]. This last phase is important and highly dependent on an organ's function or developmental state. If either of these cases is abnormal, toxicity may occur. Elimination can be monitored in the clinic prior to drug dosing. For example, renal function is determined prior to dosing the chemotherapeutic carboplatin to avoid systemic toxicity. To fully understand a drug's pharmacokinetics the overall health of the clearance organs and the previous three phases are established and closely followed.

The understanding of a drug's pharmacokinetics is only one component to its pharmacologic fingerprint. Equally important is the drug's pharmacodynamic properties or its effects, such as the physiological effect and the mechanism of action, on the body or tumor. Typically drug targets are diverse. They can include receptor proteins, such as transcription factors, enzymes in a regulatory pathway, proteins involved in structure of the cell or even nucleic acids [68]. Drug binding to their target can lead to many cellular changes and to its ultimate response. By determining the pharmacokinetics and pharmacodynamics of a drug, the most effective and rational therapeutic use can then be translated from preclinical studies to clinical trials.

Etoposide was first synthesized in the1960's and surprisingly it took over thirty years for the FDA to approve the drug for the treatment of a number of cancers, such as lung cancer, non-Hodgkin's lymphoma, leukemia, Kaposi's sarcoma, neuroblastoma, retinoblastoma and various soft-tissue sarcoma [69, 70]. Due to solubility problems a prodrug, etoposide phosphate (Etopophos), was generated. Even in its new form, the protein binding is surprisingly high, about 90%, which greatly limits the drug's concentration [71]. Prior to its elimination, etoposide is cleared by both the kidney and liver, where its partially metabolized into inactive forms. While the pharmacokinetics were rapidly understood and explained how the drug was processed, its mechanism of action was not immediately known.

About one year after etoposide's approval, its target, topoisomerase II, was characterized. This enzyme creates a transient double strand break when bound covalently to DNA allowing the passage of nucleic acid segments through the break, thus regulating the over or under-winding of the DNA. The function of topoisomerase II is essential in all processes involving DNA, but plays a large role in the S to G2 phase transition [54]. When the drug is present, it prevents the release of the enzyme from the DNA resulting in an increase in the number of transient complexes [54]. The ternary complex inhibits the DNA religation, which in turns caused the lesions to be permanent. Over time an increase in DNA strand breaks lead to apoptosis.

As with most cytotoxic chemotherapeutic agents there are a number of acute to mild side effects, including alopecia, nausea and bone marrow suppression (the dose limiting toxicity) [54, 71]. While these side effects can be managed, disturbing complications of secondary cancers arose in children one to five years after treatment. Several groups reported a number of cytogenetic abnormalities responsible for the acute non-lymphocytic leukemia (ANLL) [51, 72, 73]. For the pediatric population, this side effect caused physicians to seek out other potential drugs for retinoblastoma.

An additional topoisomerase interactive drug, a synthetic analog of camptothecin, topotecan (Hycamtin) was investigated. Over the years, it has been used to treat many malignancies, such as sarcomas, nervous system and ovarian cancers [74]. It exists in two forms: the lactone (active drug) and carboxylate (inactive drug) [75]. The common toxicities are bone marrow suppression. They range from mild to acute, such as alopecia, nausea, fever, anemia, thrombocytopenia [76]. When administered intravenously, its metabolism begins in the plasma by a non-enzymatic hydrolysis. Its half-life has been reported to be approximately 2.5 hours [74]. Normal renal function is needed for rapid clearance from the plasma [74]. Uniquely, the bioavailability of the drug is not strongly influenced by the plasma proteins, with less than 20-50% of drug binding.

This makes it a perfect candidate for the treatment of different diseases of the central nervous system, such as the ocular system [74].

Topotecan is primarily a S-phase inhibitor and therefore heavily dependent on the administration schedule. Its target is the enzyme receptor topoisomerase I. Typically, this enzyme binds covalently to DNA, nicking a single strand of the double stranded helix allowing the nicked strand to rotate about the covalently held strand, thus relieving torsional strain on the DNA [76, 77]. This process is very important during DNA replication, as there is a constant need for unwinding and rewinding the DNA ahead of and behind the replication machinery. Topotecan targets the enzyme-DNA intermediate by reversibly binding and stabilizing the covalent complexes [76, 77]. During DNA replication, advancing replication forks collide with the stabilized complexes, which ultimately results in cell death [76, 77].

Another commonly used drug to treat retinoblastoma is the antineoplastic alkaloid, vincristine (vincristine sulfate). It is one of the chemotherapeutic drugs and has been used extensively to treat a variety of cancers, such as lymphosarcoma, Hodgkin's and lymphoblastic leukemia [78]. This drug is widely used because it has limited myelosuppressive effects and therefore can be combined with many different therapy regimens, such as the VEC protocol commonly used in retinoblastoma. While it has little to no effects on cell number of the blood, but it is known to cause neurotoxicity [78, 79].

As with many chemotherapeutic agents, vincristine is cell cycle specific by blocking cells in mitosis phase. Its mechanism of action is to bind tubulin proteins preventing the subunits from polymerizing into microtubules [78-80]. This interruption in structure affects the mitotic spindle, which is responsible for proper segregation of the sister chromosomes. This leads to cellular arrest in metaphase and eventual cell death [80].

The pharmacokinetic properties of this drug are known primarily because of the more recent performed with sensitivity and specific bioavailability techniques. With vincristine knowledge of the patient's hepatic function is important to avoid toxicity. This is because vincristine's metabolism occurs in the liver and its metabolites are excreted in the bile [79, 80]. The drug is strongly influenced by the liver and thus as a fairly long half-life [79, 80].

Carboplatin is another anti-cancer drug often used for retinoblastoma therapy. Unlike the previously mentioned drugs, it is not dependent on the cell cycle. Its mechanism of action causes cell death by adding platinum adducts to DNA creating cross-linkages between intra/inter strands of DNA [81]. Once it is added the platinum binding is irreversible and leads to cell death. The disposition of the drug is not affected by the binding of plasma proteins [81, 82]. Prior to being eliminated in the urine, its half-life is approximately 2-6 hours and heavily dependent on renal function.

Unlike other platinum agents, such as cisplatin, carboplatin is less nephrotoxic [81-83]. Like many anti-cancer drugs the dose-limiting toxicity is myelosuppression, in particular thromcytopenia [81, 82]. Given these mild toxic effects, this anti-cancer drug has been used to treat many different cancers, such as ovarian, cervical, head and neck

and non-small cell lung [84]. To date carboplatin is among the four commonly used anti-cancer drugs used in treating retinoblastoma.

1.8 PHARMACOLOGY CONSIDERATIONS

Retinoblastoma is a disease of the posterior chamber in the eye. Like many diseases beyond the globe's equator, its tumor's location has presented ophthalmologists with unique treatment challenges. While there are many routes to deliver drugs to the eye, such as systemic injection, topical treatment, intravitreal and periocular injections, each has unique limitations and risks [85, 86]. The systemic administration of chemotherapeutic agents has been explored early in the treatment of retinoblastoma. The major side effects are systemic toxicity and unnecessary exposure to the non-target tissues. This can be detrimental for children with germline mutations in *Rb1*. Moreover, studies have shown that drug exposure is greatly reduced before it reaches the eye.

The alternative delivery option is topical treatment, but it too has limitations, such as not reaching effective therapeutic levels in the posterior chamber [85, 86]. This is largely due to the blood-aqueous-barrier (BAB). The ciliary body and iris epithelium form cellular tight junctions and the iris's blood vessels prevent the exchange of most fluids, except those that are lipid-soluble [5]. Since both methods lead to inadequate amounts of drug delivery to the posterior chamber, ophthalmologists have searched for alternative local delivery techniques, such as intravitreal and periocular injections. Intravitreal injections were found to expose the eye to a greater drug concentration, but its invasive nature poses a risk in damaging vision. For retinoblastoma cases, this technique is especially dangerous because it could cause tumor dissemination. Therefore periocular injections, such as subconjunctival, have been explored extensively for this pediatric eye cancer [86]. The location of the injection is less invasive and typically does not cause vision damage. As previously mentioned, Abramson was the first physician to explore this method in a pediatric clinical study and found it to increase the drug concentration while lessening systemic exposure [65]. While the subconjunctival injection is a good option, it has many pharmacological challenges in the transscleral delivery, such as fixed physical and active barriers.

The many ocular membrane barriers serve as a protective mechanism, but cause obstacles in vitreal drug delivery. The conjunctiva, the first tissue, is a membrane with tight cellular junctions between adjacent cells. This limits the transport of solutes based on their molecular weight and radius [87]. Typically the human conjunctiva is 30-fold more permeable to drugs than the cornea and thus may be better than topical application [88]. In addition, its large surface area aids in the absorption of drugs [87, 88]. Once a drug has successfully passed out of the conjunctiva it encounters the globe and its primary protector, the sclera. The sclera's high permeability and porosity allows the diffusion of a range of solutes [89, 90]. Similar to the conjunctiva, it also provides a large surface area for absorption [89]. Once in the globe the drug next encounters a series of layers: the choroid, Brach's membrane and blood-retina-barrier (BRB). As with the previous tissues, the choroid also has molecular size and weight exclusion limits, which are species specific [91]. For example, one study found hydrophilic compounds had an inverse correlation between molecular weight and permeability in both bovine

and rabbit tissues [16]. In addition, it has been found that the choroid is more permeable than the following than Brach's membrane and the retina pigmented epithelium [16].

This final barrier is composed of many layers and referred to as the BRB, which is highly complex in drug transport. Experiments comparing this tissue to the sclera have found it is a tighter barrier for hydrophilic, large molecules drugs [16]. The inner layer is largely composed of the endothelial cells from retina vessels [16]. The BRB is composed of retinal pigmented epithelium and is often compared to the blood brain barrier (BBB) [92]. The BRB is further divided into the inner (i-BRB) and outer (o-BRB) layers [5, 93]. The latter division, o-BRB, is responsible for protecting the neuronal retina from the free diffusion of xenobiotics from the circulating blood and the retina. Its retina capillary endothelial cells form tight junctions and are surrounded by supportive cells [5, 93]. They are not very permeable to hydrophilic substances, but more so to hydrophobic substances [16]. Based on the location, these capillaries are difficult to study, like the i-BRB. This sub-division is made of the cellular tight junctions of the retinal pigment epithelium (RPE) cells, which prevents free passage of molecules from choroid to the retina. In addition it has a high level of melanin protein that potentially binds to the drug decreasing its concentration [91, 93]. Along with providing the physical barrier, these divisions also provide many active barriers, such as the blood, lymphatic vessels and drug transporters.

A drug's concentration can be immediately decreased after a subconjunctival injection largely due to the extensive blood and lymphatic system draining into the systemic circulatory system [85, 86, 91]. In addition, the episcleral veins, between the conjunctiva and sclera, are a potential obstacle [5, 85]. Once in the globe the drug passes to the choroid. Due to its enormous blood volume flow, the choroid poses the most significant threat on transscleral delivery [5]. Finally the drug reaches the vitreous where its static gelatinous environment does not threaten the drug's concentration. In addition to contending with these fluid obstacles, the drug encounters multiple transporters at each layer or barrier system.

Along with passive diffusion, active transport plays a key role in transscleral delivery. In general**,** drugs move into the vitreous by passive diffusion when the concentration is high or when the active transporter proteins are over saturated [16]; however, this is highly dependent on the drug's physicochemical characteristics. There are a number of active transporters in the eye's tissues that protects it from foreign compounds and can complicate drug delivery. The expression of transporters largely impacts the amount of drug, which reaches the ocular space. To date there is no comprehensive picture of the different transport proteins in ocular tissues. The current information is a collage from recent experiments, such as *in vitro* studies, cell culture work and tissue explants, with multiple species (**Appendix A**). For a drug to successfully pass to the vitreous it encounters many drug transporters in the posterior region and there is minimal understanding about their expression in these tissues. To date seven different transporters have been localized to this area of the eye and include P-glycoprotein (P-gp), organic cation transporters (OCT), the multidrug resistant proteins (MRP1), the organic cation transporters (OCT3), organic anion transporting polypeptide (OATP-2 and OATP-E) and breast cancer resistance protein (BCRP) [16, 87, 94]. While all of these transporters are well established in other tissues, their presence in the eye are still largely under investigation. As more information is gathered, it is important to

remember the factors of species variation and ontogeny of expression. Therefore, a summary of the possible effective transporters in the eye needs to be appreciated in pharmacokinetic studies.

1.8.1 Preclinical trials

1.8.1.1 Previous rodent models

Typically clinical trials are designed based on previous clinical and preclinical studies, which are important for determining the initial toxicity of single and combinational therapies. However, if the animal model does not recapitulate the human disease preclinical the results are difficult to interoperate. Over the years the development of more relevant animal models have lead to more accurate translation of preclinical studies to early phase clinical trials.

Shortly after Knudson's "two hit" hypothesis of retinoblastoma, there was much advancement in the field; however, the attempts to generate an ideal retinoblastoma model system were a continued challenge. The first models were created by a heterotransplantation of retinoblastoma cells in adult athymic "nude" mice [95]. From this study they transplanted fresh retinoblastoma tumor into the anterior chamber of the eye. Unfortunately, the tumors were avascular and no tumor extension into the extraocular cavity was seen. An alternative model was generated in rats when the human adenovirus plasmid was injected in newborns [96]. Ironically this model generation of this model was an accident. Their original goal was to develop pituitary adenomas with a SV40 Tag viral oncogene. This first viral induced retinoblastoma mouse was the launching pad for other groups to develop models with retina-specific tumors.

The first viral induced tumor mouse was generated shortly after and provided the foundation for other groups to develop retinoblastoma models [97-99]. In particular, researchers took advantage of the ocular promoters expressed at different developmental stages and locations. The first was generated with the promoter of the interphotoreceptor retinoid-binding protein (IRBP) gene [100]. In brief, the vector was designed using the IRBP promoter with SV40 Tag oncogene. While these animals developed tumors very young and in the outer retina, their histology indicated that the tumor arose from the entire photoreceptor layer. This was due to non-specific binding of the SV40 Tag to many cellular proteins, such as *pRB*1 and *p53* [100]. This problematic design was corrected by targeting *Rb1* specifically with a construct made of the alpha crystallin promoter and the human papillomavirus (HPV) *E7* oncogene [101]; however, this model was unsuccessful because the rodents' lens developed abnormally and there was additional onset of epidermal cancers. Thereafter, Mukai and colleagues created a retinoblastoma mouse with a specific IRBP promoter with *E7* and found tumors [102]. Unfortunately, their tumors were not specific to the neural retina and developed in the retinal pigmented epithelium and ciliary body [102]. Research continued to struggle with creating the ideal preclinical model for this pediatric cancer.

After the full characterization of the RB gene and the advancement of genetic mouse models, there was great excitement to create the "knockout" mouse from

embryonic cells with the mutated RB1 gene [103-105]. When researchers knocked out both copies of RB, embryonic lethality occurred. And when they created the heterozygous RB1 (+/-) mouse it never developed retinoblastoma [103, 105]. This was unlike the human cases where a single germline mutation leads genetic instability, loss of heterozygosity eventual ocular tumor. Following this surprise, researchers specifically targeted the RB gene in the cells of the retina to avoid embryonic lethality; however, the eyes were still tumor free [106, 107].

Advancing molecular genetic tools led to the valuable *Cre-lox* system, which made it possible to study embryonic lethal genes in adult animals [108]. Briefly, this recombination system targets a specific sequence of DNA with the Cre recombinase bacterial enzyme. This recombinase recognizes the inserted "lox" sequences and excises DNA. This results in the removal of an essential gene or sequences in the gene. This novel system provided the tools to generate an adult mouse lacking an intact RB gene. Various models were generated using this system and driven by specific developmental retinal promoters, Nestin, Chx10 and Pax-6 [103-105]. Much to scientists' dismay these mice were still tumor free and thought to be due to species variation.

Later studies suggested this phenotype difference could be due to the role of other RB family members compensating for the loss of *Rb1* specifically in the mouse. The final breakthrough occurred when the $RB1^{lox/lox}$ mouse was crossed with the knockout p107 mouse. Retinoblastoma tumors developed and their offspring were breedable [103-105, 109, 110]. In addition, it was found that retinoblastomas could developed when the $RB1^{lox/lox}$ mouse was mated with the knockout of the other pocket protein, p130 [111]. Taken together, the development of these model systems have aided in the advancement in of understanding retinoblastoma disease progression and conducting relevant preclinical trials.

An additional successful model system is the orthotropic retinoblastoma xenograft rat. This model was generated by injecting the human retinoblastoma cell lines, Y79, Weri or Y79-luciferase, into the vitreous of newborn rats, which are immune naive on the first day of life [60, 112, 113]. Unlike previous nude mouse models, the rats have an intact immune system, which allows for comprehensive drug studies. In addition, the ocular environment is still developing and allows for the study in the appropriate temporal environment. The major advantage is that the tumors developed within only two weeks, thus providing a rapid way to study tumor growth and preclinical drug combination therapy [60, 112, 113]; however, there are some drawbacks. The tumors were generated from these human cell lines in a developing rat ocular environment, are not sporadic and grew too rapid for long-term study. Nonetheless, this model continues to be beneficial when used in combination with genetic mouse models, especially for carrying out preclinical studies.

1.8.1.2 Summary of preclinical trials

The use of animal models, such as rodents, are important in understanding the tumorgenesis, genetic mechanisms involved in cancer and are key for preclinical studies. Ideally preclinical trials provide information for human clinical trials. Over the years the majority of preclinical studies have been done with the LHbeta-SV40 Tag

retinoblastoma mouse. These models have allowed for rapid study of drug combinations. These preclinical studies have included vitamin D analogs, attenuated viral treatments, focal therapies, combinational therapies and traditional retinoblastoma chemotherapeutics, chemotherapeutic agents and viral treatment [114-116]. While these treatments showed some tumor response, toxicities were often seen as well as the lack of complete tumor control.

Over the years there have been many unique approaches to preclinical treatments. There were two studies in the nineties that used vitamin D or its analogues [115, 117]. This therapy was based on the finding of calcium receptors on retinoblastoma tumors. While this was a unique and creative treatment possibility, the animals experienced a lot of toxic side effects and death. An additional alternative study included the use of attenuated viruses or viral gene therapy. Brandt and colleagues explored the use of the herpes simplex virus type 1 to deliver the gene [114]. The researchers reported this treatment to be successful in other nervous system cancer cases. When retinoblastoma tumors were targeted with this treatment their initial response was promising, but the long-term effects were not. More recently an alternative preclinical trial with AVV-virus gene-therapy was used to deliver interferon-beta to tumors with intravitreal injections [112]. Previously, interferon-beta was reported to have anti-tumor properties. Researchers found retinoblastoma to respond well and suggested this treatment to be used in conjunction with other systemic therapies. One drawback is the use of intravitreal injections in retinoblastoma cases because there is of the risk of tumor dissemination. With the potential risk of tumor spread, researchers have explored other focal treatments and subconjunctival treatments with standard retinoblastoma chemotherapeutics.

Similar to the clinical trials, there have been many reports studying the use of focal therapy treatment, such as EBRT and cryotherapy, alone or in combination with chemotherapy treatments or chemotherapy alone in the large T antigen mouse model [64, 118]. From these studies it appeared that the combination of focal therapy and the combination of carboplatin with EBRT had the most success. Additionally, preclinical studies using chemotherapy alone have generally found a 50% response or greater with subconjunctival injections of topotecan, carboplatin liquid, nanoparticle or carboplatin fibrin sealant [119, 120]. While these preclinical studies have shown potential promise, there were some influential factors not considered.

The majority of these studies was conducted in a short time frame and used the beta-subunit SV 40 large T-antigen retinoblastoma mouse models, which has many shortcomings. The first drawback was that the tumors were not of the correct genetic RB lesions. Second, retinoblastomas at different stages of development were not studied and the most influential disadvantage was the fact that the large T antigen nonspecifically binds to other oncoproteins, such as the tumor suppressor p53 [100]. While no preclinical study can be perfect, the use of other preclinical models that recapitulate the human disease would allow these studies to be more readily translated to the clinic.

1.8.2 Challenges in conducting these studies

While animal models give researchers much insight to the disease and its potential treatments, there are many challenges in conducting pharmacological experiments in preclinical models. The first challenge is the model system, both xenograft and transgenic mouse model. Xenograft models have many limitations, which revolved around the injection of highly passed cell lines in a non-native location of an immune compromised animal. All of these factors can potentially influence tumor response to treatment. A better alternative is transgenic mouse models. While they are often more acute in their disease presentation and location, their genetic changes can alter pharmacological responses, especially if the change occurs in every cell in the body or if the gene is driven by a non-native promoter [121]. While these challenges do exist, they can be mitigated in using multiple model systems and control cohorts.

The second and most challenging aspect is converting the dosage between different species. To do this calculation, two different methods, body surface area (BSA) and area under the curve (AUC) are used. Currently, the clinic uses body surface area as the standard to determine the drug dose [122]. This method was originally developed by an intensive preclinical study that found oxygen, caloric expenditure, organ size and function were similar across many species' body surface area [122]. Although BSA has provided to method in determine dose, its major drawback is the inability to account for interspecies difference in absorption, distribution and/or elimination parameters [123]. By ignoring these essential components, it is likely to over or under dose, which can potential lead to a reduced therapeutic result and potential chemotherapeutic resistant population.

The alternative is to determine the dose by using equivalent AUC values. AUC guided dosing, which accounts for these biological processes of different species. To determine the AUC, pharmacokinetic studies are conducted. Measuring the drug concentration at many time points and plotting these as concentration verse time. By determining the AUC, the clearance rate, metabolism, protein binding and ultimate drug exposure, are all taken into consideration in the final dosage. This value can be used to compare the animal exposure to human exposure enabling the rational selection of drug dosage.

The major drawback to using the BSA or AUC guided dosing is that not all studies can be easily compared. This is largely due to the limitation and ethical constraints of clinical sample harvesting. An example is the preclinical studies carried out by Laurie and colleagues [60]. In this study they looked at the vitreal drug exposure in rats. As this study gave exceptional insight to the vitreal drug exposure, it could not be compared to any human studies because of visual damage or tumor dissemination risks [65, 67]. To compare dosage among different species, alternative parameters can be used and compared. One parameter for subconjunctival injections is the species' eye volume. This can help estimate the available volume that can be injected. While in principle it is similar to the BSA measurement, this focuses directly on the region of interest; however it too has limitations because it fails to account for each biological parameter difference. Nonetheless these challenges provide a framework to learn more about clinical drug treatment.

As described in the following chapters, my graduate thesis work has addressed two specific issues relevant to the assessment and development of preclinical approaches for the treatment of retinoblastoma. First, I have conducted a preclinical study looking at the combination of a local and systemic administration of carboplatin and topotecan. I found a local injection increases the drug exposure in the vitreous and decrease systemic exposure. This is an important finding for children with the germline mutation. In addition, an ideal combination of two well-studied board spectrum chemotherapy agents, carboplatin in the subconjunctival space and topotecan i.p. has shown good tumor response with minimal systemic and local toxicity.

Along with determining the best chemotherapy combination in my preclinical model, I have optimized the use of clinical modalities for mice and determined tumor progression in various models. Not only does this non-invasive longitudinal study make the preclinical research truly translational, but also gives a sense of retinoblastoma growth and progression in various sporadic mouse models. These finding will lay the foundation for future preclinical studies and help define the role of different genes in retinoblastoma tumor formation.

CHAPTER 2. PHARMACOLOGY*

2.1 INTRODUCTION

Patients with retinoblastoma have not fully benefited from advances in drug development and methods to deliver chemotherapy locally to the eye, in part, because few preclinical models have been developed that faithfully recapitulate the human disease. Preclinical animal models are essential for studying childhood cancers such as retinoblastoma, because there are too few patients for large-scale clinical trials [124]. The recent development of several new rodent models of retinoblastoma has opened the door to key advances in the treatment of bilateral retinoblastoma [60, 125] and the preservation of vision in children with this debilitating disease. Using an orthotopic xenograft model of retinoblastoma, we have previously shown that the combination of systemic topotecan and carboplatin is more effective than the current standard of care used around the world (e.g., etoposide, vincristine and carboplatin) [60]. Unfortunately, the dose-limiting toxicity of each of these drugs is myelosuppression and thus, the systemic co-administration of these compounds in patients at therapeutic dosages is associated with intolerable toxicities.

Two alternative approaches are available to allow for the co-administration of these two highly active agents and yet avoid the side effects associated with their use. First, the drugs could be administered at different times during the chemotherapeutic schedule with close monitoring of blood counts to ensure that myelosuppression does not reach dangerous levels. The limitation of this approach is that the individual tumor cells will only be exposed to a single agent at any given time during chemotherapy. The second approach is to administer one drug locally to the eye to minimize systemic exposure so that the second drug could be administered systemically. The first study to demonstrate the feasibility of locally delivered chemotherapy for children with retinoblastoma was carried out by Abramson and colleagues who used subconjunctival administration of carboplatin (20 mg/eye) [65]. Indeed, retinoblastoma is ideal for local delivery of chemotherapy, because the eye is readily accessible and it may be possible to achieve high intraocular concentrations with lower systemic exposure.

In this study, we perform a side-by-side comparison of subconjunctival carboplatin with systemic topotecan to subconjunctival topotecan with systemic carboplatin. Pharmacokinetic experiments were performed to determine if carboplatin or topotecan was better suited to subconjunctival injection in our efforts to minimize systemic exposure and toxicities. We also performed toxicity studies and pharmacodynamic experiments to help guide future clinical trials using this approach. To the best of our knowledge, this is the first comprehensive preclinical study that incorporates pharmacokinetics, pharmacodynamics and functional assessment in a pediatric cancer model.

* Modified with permission. Nemeth, K.M., et al., *Improved retinoblastoma treatment using subconjunctival carboplatin and systemic topotecan in preclinical models*. Cancer, 2010 (in press) [1].

2.2 MATERIAL AND METHODS

2.2.1 Retinoblastoma orthotopic xenograft model

Newborn Sprague Dawley rats (Charles River Laboratories, Wilmington, MA) received an intravitreal injection of 1,000 Y79-Luc cells as described previously [125]. After approximately two weeks, the cells expanded and the tumor mass could be detected using Xenogen IVIS 200 system and Live Image Software 2.5 after an i.p. injection of D-luciferin (Caliper LifeScience, Hopkinton, MA). The D-luciferin dosage was 100mg/kg and animals were imaged 30 minutes after the injection.

2.2.2 Pharmacokinetic studies

Two-week-old rats were treated with topotecan (TPT; Hycamtin; GlaxoSmithKline, research Triangle Park, NC) at a dose of 10mg per eye, carboplatin (CBP; Paraplatin; Bristol-Myers Squibb, New York, NY) at a dose of 100mg/eye. For a typical experiment, 18 animals received subconjunctival injections of either topotecan or carboplatin in both eyes. At serial time points (pre, 15 minute, 0.5 minute, 1.5m, 4 and 6 hour) a cardiac puncture was performed, blood collected and plasma isolated. Once the cardiac puncture was completed, the animals were euthanized by cervical dislocation, the eyes were removed and the vitreous and retina were collected and flash frozen.

For topotecan, total topotecan (lactone plus carboxylate) was quantitated by a sensitive and specific reversed phase isocratic HPLC. Calibration curves were constructed using appropriate black control matrices. This method was linear over a range of 0.25 to 5000ng/ml, and the lower limit of quantitation was 0.25ng/ml. For carboplatin, total platinum was quantitated by sensitive atomic absorption spectroscopy method. Briefly, plasma and vitreous samples were spiked with 1N nitric acid, vortexed and centrifuged at 5000 rpm for 3 min. Concentrations of total platinum in supernatants were quantified using flames atomic absorption spectrometry after diluting the matrix in water containing 0.2% (v/v) Triton X-100 and 0.06% (w/v) cesium chloride. Samples (20μl) were injected in duplicate into a Perkin Elmer Analyst 6000 atomic absorption spectrometer (Perkein Elmer, Norwal, CT) with Zeeman Background corrections to measure platinum content. Peak area measurements were performed at a wavelength of 265.9 nm with a slit width of 0.7 nm. Total platinum concentrations were determined by interpolation on calibration curves constructed form drug-free matrices (plasma or vitreous).

An appropriate pharmacokinetic model was fit to the topotecan or carboplatin plasma or vitreous concentration-time data using the ADAPT software, version 5.0.0 (Biomedical Simulations Resource, Los Angeles, CA). Estimated model parameters included the volume of the central compartment (v_c), elimination rate constant (k_e) and when appropriate the inter-compartment rate constants (k_{cp} and k_{pc}). Systemic clearance (CL) was calculated using the model parameters. The area under the topotecan or carboplatin plasma or vitreous concentration-time curve from 0-6 hours (AUC_{0-6}) was calculated using the parameter estimates and the log-linear trapezoidal method.

For isolation of the different portions of the eye, we have optimized the procedure for this method over the past several years with a series of control experiments. Briefly, the eye is removed form the animal with a pair of #3 forceps and it is immediately rinsed in an excess of sterile saline (10ml/eye). Then the eye is dried on sterile cotton pads to ensure that any saline on the surface of the eye does not dilute the vitreous sample. The eye is then punctured in a dry, sterile 6 cm tissue culture dish with an 18 Ga needle and dissected with #5 forceps. The forceps are sterilized and cleaned between eyes and animals and we use a different set of forceps for the dissection than the enucleation. We also harvest the eyes with the lowest concentration of drug first (longest time points) to minimize the cross concentration from the sample to sample the forceps. A series of experiments by dissecting was never exposed to drug with forceps used for PK studies has shown that there is no detectable cross contamination across samples. The vitreous is collected form the dish with a sterile 20-microliter pipette tip and placed in a siliconized sterile eppendorf tube. The retina is then rinsed in 10 ml sterile saline, excess saline is removed and it is placed in another sterile siliconized eppendorf tube. A series of experiments that involved mixing of vitreous from an untreated animal with vitreous with a treated retina, sclera or lens showed no detectable cross contamination with these methods.

2.2.3 Tonometer

Intraocular pressure (IOP) of sedated mice was measured with the TonoLab Rebound Rodent Tonometer (Tonolab, Espoo, Finland). Mice were anesthetized using isoflurane and measurements were taken at the same time of the day, approximately six hours into the light cycle. The device was held so that the probe was between 1-4mm from the cornea of the eye. Six consecutive measurements were taken and average to obtain final value for each eye. Baseline measurements were taken before subconjunctival injections and then at 1, 2 and 7 days after subconjunctival injection.

2.2.4 Optomotry

Visual acuity was measured using the OptoMotry System (Cerebral Mechanics, Alberta, Canada) as previously described [126]. All tests were carried out in bright light conditions to measure cone function. Visual acuity of the mouse was measured with at least two consecutive measurements on independent days 24 hours before and after administration of drug. A second set of measurements was made on 2 consecutive days 1 week after administration of the drug.

2.2.5 Histology

Eyes were fixed in 4% paraformaldehyde overnight at 4°C, dehydrated through an alcohol series and washed in xylene. Eyes were paraffin embedded and sectioned (5 μm) in the sagittal plane through the optic nerve. The cornea, ciliary epithelium, retina and optic nerves were compared across treated and untreated eyes at 1, 2 and 7 days after administration of the subconjunctival injection.

2.2.6 Blood counts

To assess the hematopoietic toxicity of topotecan and carboplatin, a standard CBC with differential was obtained at the time points specified in the Results section. The facial vein was used for blood draws to prevent any disruption of the ocular structure that may arise as a result of retro-orbital draws. Nearly 30μl of blood was collected and mixed with 3μl of EDTA. The samples were processed immediately using the Forcyte Machine (Oxford Scientific, Oxford, CT) to count the number of neutrophil, platelets and red blood cells.

2.3 RESULTS

2.3.1 Pharmacokinetics of subconjunctival carboplatin and topotecan

Phase I clinical trials have demonstrated that subconjunctival carboplatin [65] or subconjunctival topotecan [67] are well tolerated in retinoblastoma patients as single agents. To determine the extent of intraocular penetration and systemic exposure for each drug after subconjunctival administration in our rodent models, we performed a series of pharmacokinetic experiments in juvenile rats (2 weeks old) as described previously [60]. The topotecan dose was 10 mg/eye with bilateral injections and the carboplatin dose was 100 mg/eye with bilateral injections. Based on the proportional volume of the human and rat eyes, these doses were based on those used in Phase I trials in children [65, 67] **(Table 2-1)**.

After subconjunctival injection of topotecan or carboplatin, vitreous, plasma and retina were harvested and retina were carefully rinsed in saline to remove any drug that was in the vitreous of the eye. The drug concentration was measured in each sample across time points. The AUC values for plasma and vitreous for carboplatin and topotecan were calculated from model parameters **(Fig. 2-1A,B and Table 2-2).** These data suggest that both carboplatin and topotecan efficiently penetrate the vitreous after subconjunctival injection. The $AUC_{vitreous}/AUC_{plasma}$ for topotecan was 2.0 and the AUC vitreous/plasma for carboplatin was 0.85 suggesting that topotecan penetrated the vitreous with slightly greater efficiency than carboplatin.

Next, we evaluated the pharmacokinetics of subconjunctival topotecan and carboplatin in tumor bearing juvenile rats to determine if the presence of a rapidly growing tumor in the vitreous altered the pharmacokinetic profile for these drugs. To establish tumors, 1,000 Y79-Luc human retinoblastoma cells were injected into the vitreous of newborn Sprague Dawley rats [60] The tumor burden was measured 7 days later using the Xenogen imaging system to detect luminescence from the luciferase reporter gene in the Y79 cells. The tumor burden is directly proportional to the photons/cm/sec^2 detected using the Xenogen imaging system [112]. When the tumor burden reached the level of 10^6 photons/cm/sec^2, we performed a pharmacokinetic experiment similar to that described above. The results show that the vitreal penetration of carboplatin was similar in eyes with tumor ($AUC_{vitreous}/AUC_{plasma}$ = 1.3) as compared to those without tumor ($AUC_{vitreous}/AUC_{plasma}$ = 0.85) **(Fig. 2-2A** and **Table 2-2)**. However,

Table 2-1. AUC Guided Dose Conversion from Human to Rodent.

Drug	Route	Human dosage	Human plasma AUC	Rodent equivalent dose	Rodent AUC dose
Topotecan	i.p./ i.v.	2.7 mg/m^2	80-120 mg/ml•hr	0.45-.9 mg/kg	0.2 mg/kg
Topotecan	s.c.	2 mg/eye	104 mg/ml•hr	0.01 mg/eye	n.a.
Carboplatin	i.p./ i.v.	560 mg/m^2	260-430 mg/ml•hr	180 mg/kg	35 mg/kg
Carboplatin	s.c.	20 mg/eye	n.a.	0.1 mg/eye	n.a.

Notes: i.p. = intraperitoneal; s.c. = subconjunctival; AUC = area under the curve.

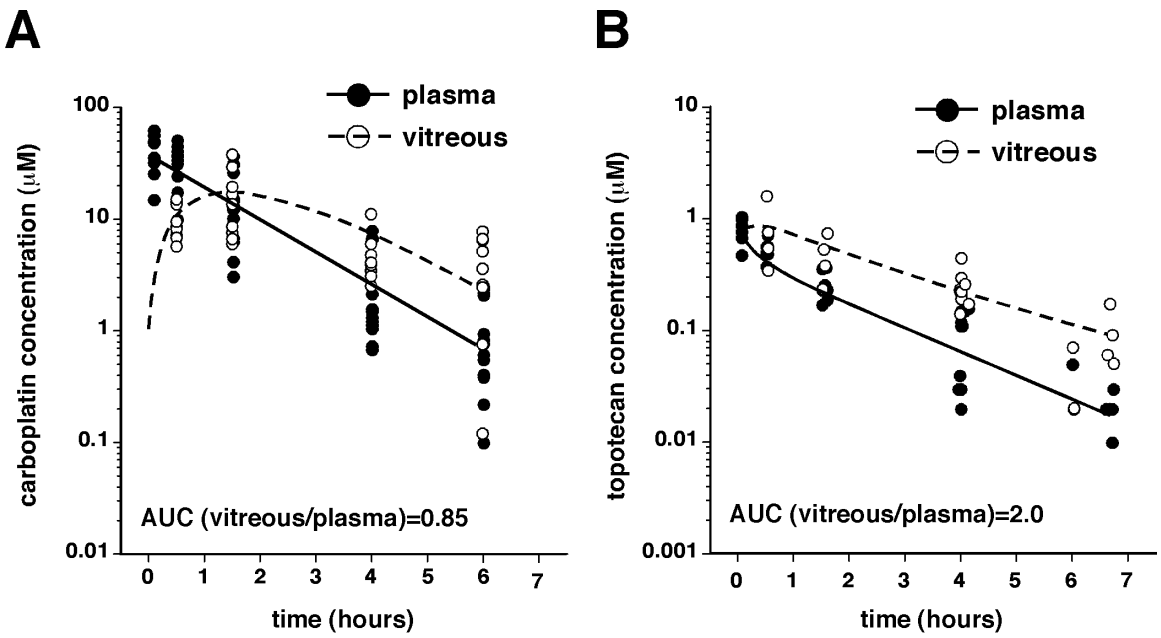

Figure 2-1. Pharmacokinetics of Carboplatin and Topotecan Following Subconjunctival Injection in 2-week Old Rats.
Ocular and systemic pharmacokinetic analysis of carboplatin (100 μg/eye in both eyes) (A) and topotecan (10 μg/eye in both eyes) (B). A two-compartment model was used to determine the AUC value. μM = micromolar; AUC = area under the curve.

Table 2-2. Subconjunctival AUC Values in Tumor and Non-tumor Rats.

		Non-tumor bearing			Tumor bearing		
Drug (dose)	**Route**	**AUC_{plasma}**	**$AUC_{vitreous}$**	**Ratio**	**AUC_{plasma}**	**$AUC_{vitreous}$**	**Ratio**
Topotecan (10μg/eye)	s.c.	1.1 μM•h	2.27 μM•h	1.98	1.4 μM•h	8.78 μM•h	6.12
Carboplatin (100μg/eye)	s.c.	53.6 μM•h	53.6 μM•h	0.85	32.2 μM•h	40.7 μM•h	1.26

Notes: i.p. = intraperitoneal; s.c. = subconjunctival; AUC = area under the curve.

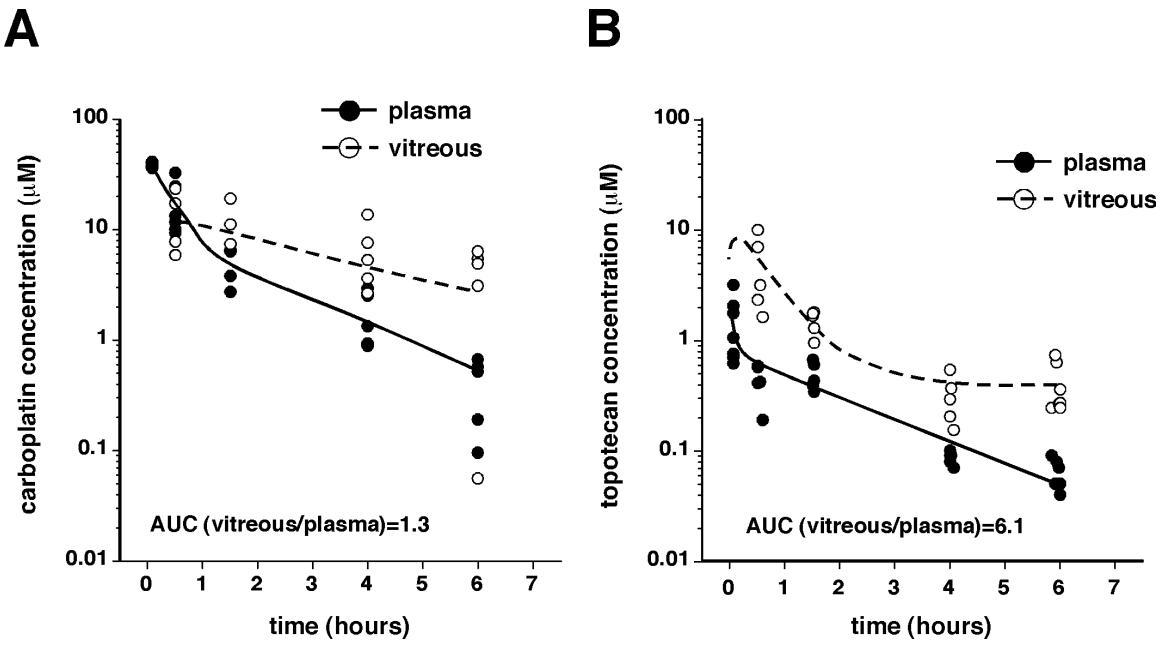

Figure 2-2. Pharmacokinetics of Carboplatin and Topotecan Following Subconjunctival Injection in 2-week Old Tumor Bearing Rats.
Ocular and systemic pharmacokinetic analysis of carboplatin (100 μg/eye in both eyes) (A) and topotecan (10 μg/eye in both eyes) (B). A two-compartment model was used to determine the AUC value. μM = micromolar; AUC = area under the curve.

the vitreal penetration for topotecan increases in eyes with tumor ($AUC_{vitreous}/AUC_{plasma}$ = 6.1) as compared to those lacking any tumor ($AUC_{vitreous}/AUC_{plasma}$ = 2.0) **(Fig. 2-2B** and **Table 2-2)**. For both drugs, the exposure of the vitreous relative to the systemic exposure ($AUC_{vitreous}/AUC_{plasma}$) was greater with subconjunctival injections as compared to the intraperitoneal injections **(Table 2-3)** as described previously [60].

2.3.2 Contralateral eye exposure to carboplatin and topotecan from a subconjunctival injection

As mentioned above, subconjunctival injection of topotecan or carboplatin leads to greater relative intravitreal exposure in orthotopic xenograft models than systemic administration using intraperitoneal injections. However, there is significant plasma exposure to topotecan and carboplatin when the drugs are injected into the subconjunctival space. To measure the exposure of the contralateral eye after a single subconjunctival injection of topotecan and carboplatin, we performed a pharmacokinetic experiment similar to those described above except only one eye was injected. At each time point we harvested the injected eye and the contralateral eye separately and measured the topotecan and carboplatin exposure. The AUC ratio (vitreous/plasma) values in the contralateral eye **(Table 2-4)** are less than that of the injected eye and are similar to those determined after intraperitoneal injections.

2.3.3 Comparison of the pharmacodynamics of subconjunctival topotecan to subconjunctival carboplatin

To test whether there was a difference in the retinoblastoma tumor response using subconjunctival topotecan/systemic carboplatin or subconjunctival carboplatin/systemic topotecan, we performed a pharmacodynamic experiment using our rat xenograft model. Y79-Luc cells were injected into the vitreous of newborn Sprague Dawley rats and when the tumor burden reached 1x 105 photons/cm/sec2, treatment was initiated. The animals were randomly divided into 3 groups (saline, subconjunctival topotecan (10μg/eye)/systemic carboplatin (10mg/kg) and subconjunctival carboplatin (100 μg/eye)/systemic topotecan (0.2 mg/kg-daily x 5) **(Fig. 2-3A-F)**.

The systemic exposure (AUC) and schedule of drugs used in this study recapitulate those used in clinical trials as closely as possible taking into account species-specific toxicity (**Appendix B**). In the saline treated group, the tumor burden increased by ~100-fold **(Fig. 2-3A)** and for the treated groups, there was an approximately 10-fold reduction in tumor burden compared to the saline injected group **(Fig. 2-3B,C)**. One of the most striking and surprising differences between the two treatment groups was the morbidity associated with subconjunctival topotecan and systemic carboplatin **(Fig. 2-3C)**. In this group, none of the animals survived past the 5th day of chemotherapy. A representative example of untreated and a treated (subconjunctival carboplatin/systemic topotecan) animal with corresponding histopathology are shown in **Fig. 2-3D-F**.

Table 2-3. Ocular and Systemic Topotecan and Carboplatin Exposure by Intraperitoneal and Subconjunctival Injections.

		Non-tumor bearing			Tumor bearing [3]		
Drug (dose)	**Route**	**AUC_{plasma}**	**$AUC_{vitreous}$**	**Ratio[2]**	**AUC_{plasma}**	**$AUC_{vitreous}$**	**Ratio[2]**
Topotecan (2 mg/kg)	i.p.	2.69 μM•h[1]	1.02 μM•h[1]	0.38[1]	n.a.	n.a.	n.a.
Topotecan (10μg/eye)	s.c.	1.14 μM•h	2.27 μM•h	1.98	1.44 μM•h	8.78 μM•h	6.12
Carboplatin (70mg/kg)	i.p.	559 μM•h[1]	330 μM•h[1]	0.59[1]	n.a.	n.a.	n.a.
Carboplatin (100μg/eye)	s.c.	53.6 μM•h	53.6 μM•h	0.85	32.2 μM•h	40.7 μM•h	1.26

Notes: i.p. = intraperitoneal; s.c. = subconjunctival; AUC = area under the curve.

[1] Values of i.p. AUC ratios were previously published. Source: Laurie, N.A., et al., *Topotecan combination chemotherapy in two new rodent models of retinoblastoma.* Clin Cancer Res, 2005. **11**(20): p. 7569-78 [60]. The dose was 2 mg/kg.

[2] The ratio of $AUC_{vitreous}$/ AUC_{plasma} is used to provide an estimate of the ocular exposure to each drug.

[3] For tumor bearing rats, 1,000 Y79-Luc cells were injected into the vitreous at P0 and then the animals were monitored daily from p7 using Xenogene Ivis 200.

Table 2-4. Comparison of Vitreal Exposure of Topotecan and Carboplatin.

Drug	Area under the curve ratio (vitreous/plasma)		
	Intraperitoneal[1]	Subconjunctival[2] (injected eye)	Subconjunctival[3] (contralateral eye)
Topotecan	0.38	2.0	0.35
Carboplatin	0.59	0.85	0.62

[1] Values of i.p. AUC ratios were previously published. Source: Laurie, N.A., et al., *Topotecan combination chemotherapy in two new rodent models of retinoblastoma.* Clin Cancer Res, 2005. **11**(20): p. 7569-78 [60]. The dose was 2 mg/kg.

[2] The dose for the subconjunctival injections was 10 μg/eye for topotecan and 100 μg/eye for carboplatin. Both were injected.

[3] The dose for the subconjunctival injection was 10 μg/eye for topotecan and 100 μg/eye for carboplatin. The left was injected and the right eye was analyzed in this experiment similar to those determined after intrapertioneal injections.

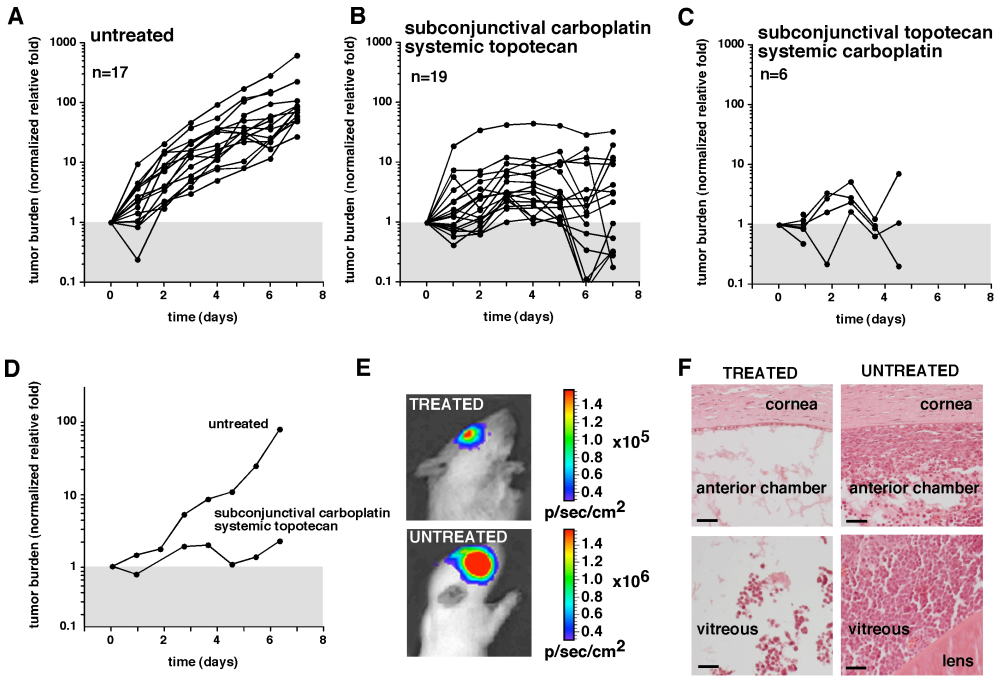

Figure 2-3. Pharmacodynamic of Subconjunctival Topotecan with Systemic Carboplatin and Subconjunctival Carboplatin with Systemic Topotecan. Juvenile rats received (A) saline injections, (B) received subconjunctival carboplatin (100 mg/eye) and systemic topotecan 0.2 mg/kg daily x 5 by intraperitoneal injection and (C) received topotecan (10 mg/eye) by subconjunctival injection and carboplatin (18 mg/kg) by intraperitoneal injection. All data were normalized to the starting tumor burden to provide relative growth and response (D-F). Data for a representative untreated animals and an animal treated with subconjunctival carboplatin and systemic topotecan including bioluminescence measurements and histopathologic analysis. Scale bar: 25 μm. N: the number of animals. p/sec/cm^2: photons per second centimeter square.

2.3.4 Analysis of ocular toxicity following subconjunctival topotecan or carboplatin

To test ocular toxicity of subconjunctival administration of either topotecan or carboplatin, we used a cohort of 12 C57Bl/6 mice divided into 4 groups (untreated, subconjunctival saline (10µl), subconjunctival topotecan (10µg/eye) and subconjunctival carboplatin (100µg/eye)) administered to one eye **(Fig. 2-4A-C)**. The eyes were examined 1, 3 and 7 days later for signs of inflammation or other periocular side effects associated with the injection. There were no visible signs of ocular toxicity associated with any of the injections **(Fig. 2-4A-C)**. We also monitored the animals for any signs of elevated intraocular pressure using a rodent tonometer and monitored visual acuity using the Optomotry system [126]. There was no evidence for changes in intraocular pressure or visual acuity for subconjunctival carboplatin or subconjunctival topotecan at any of the time points tested.

In a similar experiment, we combined subconjunctival injections with systemic administration to determine if there were any ocular toxicity from the exposure of the eye structures to both topotecan and carboplatin. Using 3 C57Bl/6 mice per group in 4 groups, we compared the ocular toxicity, visual acuity and intraocular pressure in animals receiving 10µg/eye topotecan with 18 mg/kg carboplatin by intraperitoneal injection and 100µg/eye carboplatin with 0.1 mg/kg topotecan. After 1, 3 and 7 days there was no difference in ocular appearance, intraocular pressure or visual acuity in any of the groups (**Fig. 2-5**). Histopathological analysis confirmed that there were no obvious changes in the retina, ciliary epithelium or cornea of the eyes exposed to subconjunctival carboplatin or topotecan (**Fig. 2-6**).

2.3.5 Myelosuppression and dehydration associated with subconjunctival topotecan and systemic carboplatin

Having established that there is no significant ocular toxicity associated with either subconjunctival carboplatin or topotecan (alone or in combination), we proceeded to study systemic toxicity associated with these drugs. We used 7 P8 rat pups and administered 100µg carboplatin to one eye and 0.2 mg/kg topotecan by i.p. administration. According to the schedule of topotecan administration in children with retinoblastoma, we proceeded to administer 0.2 mg/kg for the subsequent 4 days to mimic a dailyx5 schedule. Their weight was measured each day for a total of 9 days and compared to untreated littermates **(Fig. 2-7A)**. We could not detect any significant weight loss using this treatment protocol. We also collected blood by facial vein blood draw prior to treatment and on the 10 days after treatment to performed a CBC to monitor blood counts. There was no notable reduction in blood counts after treatment in this cohort of animals.

Next, we performed a similar experiment with subconjunctival topotecan (10µg) and systemic carboplatin (34 mg/kg) based on previous clinical data, AUC guided doses. Unfortunately, the rats couldn't tolerate the combination of topotecan and carboplatin using this route (subconjunctival topotecan and systemic carboplatin) and dosage.

In a second experiment, we reduced the carboplatin dose to 10 mg/kg and 3 of 6 animals survived to day 6 of treatment. In contrast to the subconjunctival carboplatin

Figure 2-4. Analysis of Ocular Effects of Subconjunctival Administration of Chemotherapeutics.
(A) Photos of eyes of C57Bl/6 mice 48 hours after subconjunctival injection of saline 10μl, 100μg of carboplatin or 10μg of topotecan. (B) Intraocular pressure, we used a rodent tonometer before and after administration or subconjunctival carboplatin and topotecan. Each bar represents the mean and standard deviation of 6 measurements form 3 independent animals. (C) Visual acuity measurement the optomotry system. Visual acuity was measure before and after injection in the groups of three animals per treatment group. The contralateral eye was again used as a control. The data represent the mean and standard deviation of the results from the 3 animals in each group and topotecan (10 μg/eye in both eyes). c/d = cycles per degree.

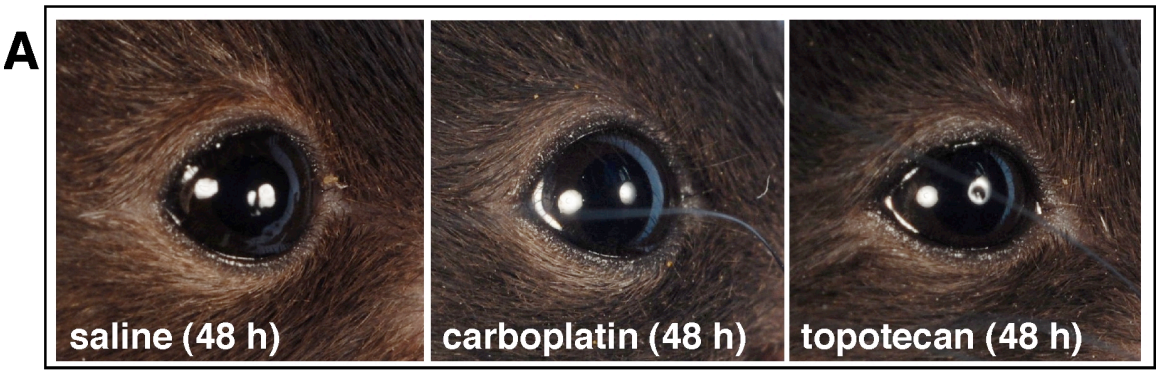
A
saline (48 h)
carboplatin (48 h)
topotecan (48 h)

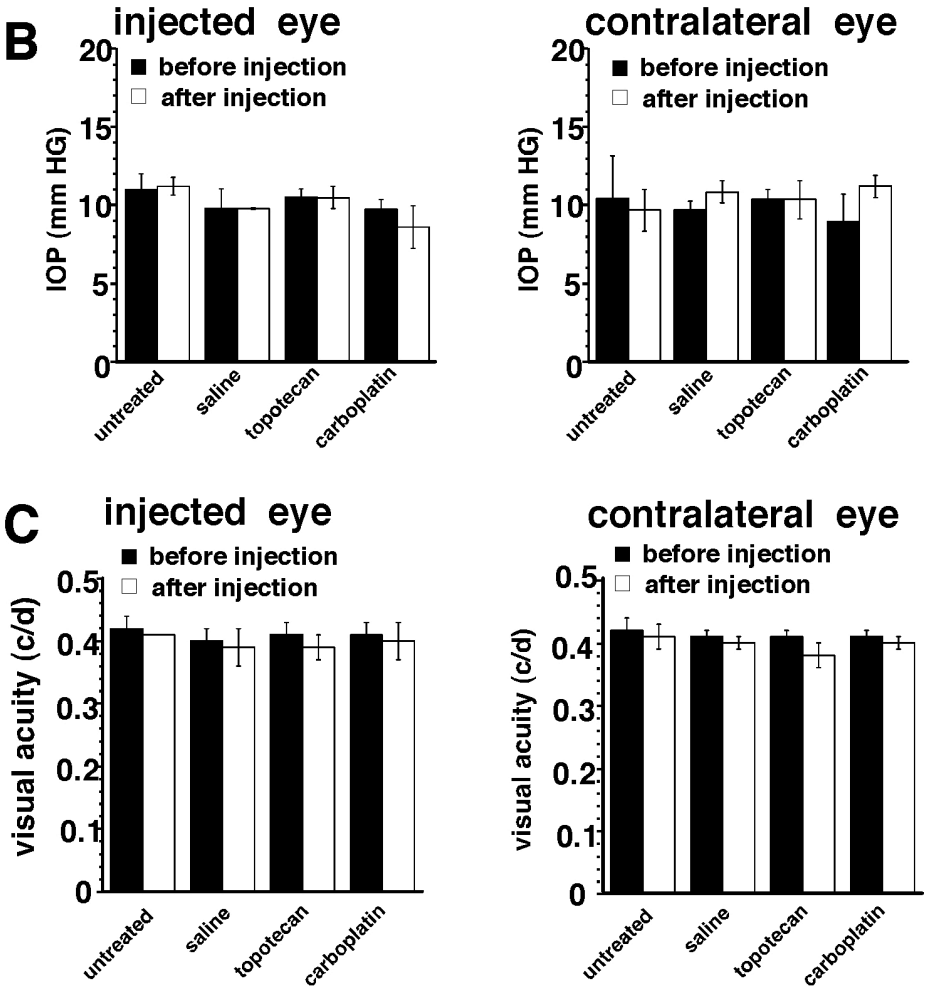
B
injected eye
contralateral eye
before injection
after injection
IOP (mm HG)
0
5
10
15
20
untreated
saline
topotecan
carboplatin
C
injected eye
contralateral eye
before injection
after injection
visual acuity (c/d)
0
0.1
0.2
0.3
0.4
0.5
untreated
saline
topotecan
carboplatin

Figure 2-5. Visual Acuity and Intraocular Pressure Measurements Following Combinations Chemotherapy.
We compared subconjunctival carboplatin with systemic topotecan or subconjunctival topotecan with systemic carboplatin in C57Bl/6 mice to determine if there was ocular toxicity. (A,B) Intraocular pressure, measurements were made before and after each combination. Controls were the contralateral eye and a 10μl saline injection to a parallel cohort. Each bar represents the mean and standard deviation of 6 measurements form 3 independent animals. There was no statistically significant difference across groups. (C,D). Visual acuity was measured before and after injection in groups of 3 animals per treatment (see above) and the contralateral eye was again used as a control. The data represent the mean and standard deviation of the results from the 3 animals in each group. There was no statistically significant difference in the visual acuity across groups. IOP = intraocular pressure; mm HG = millimeter mercury; c/d = cycle per degree.

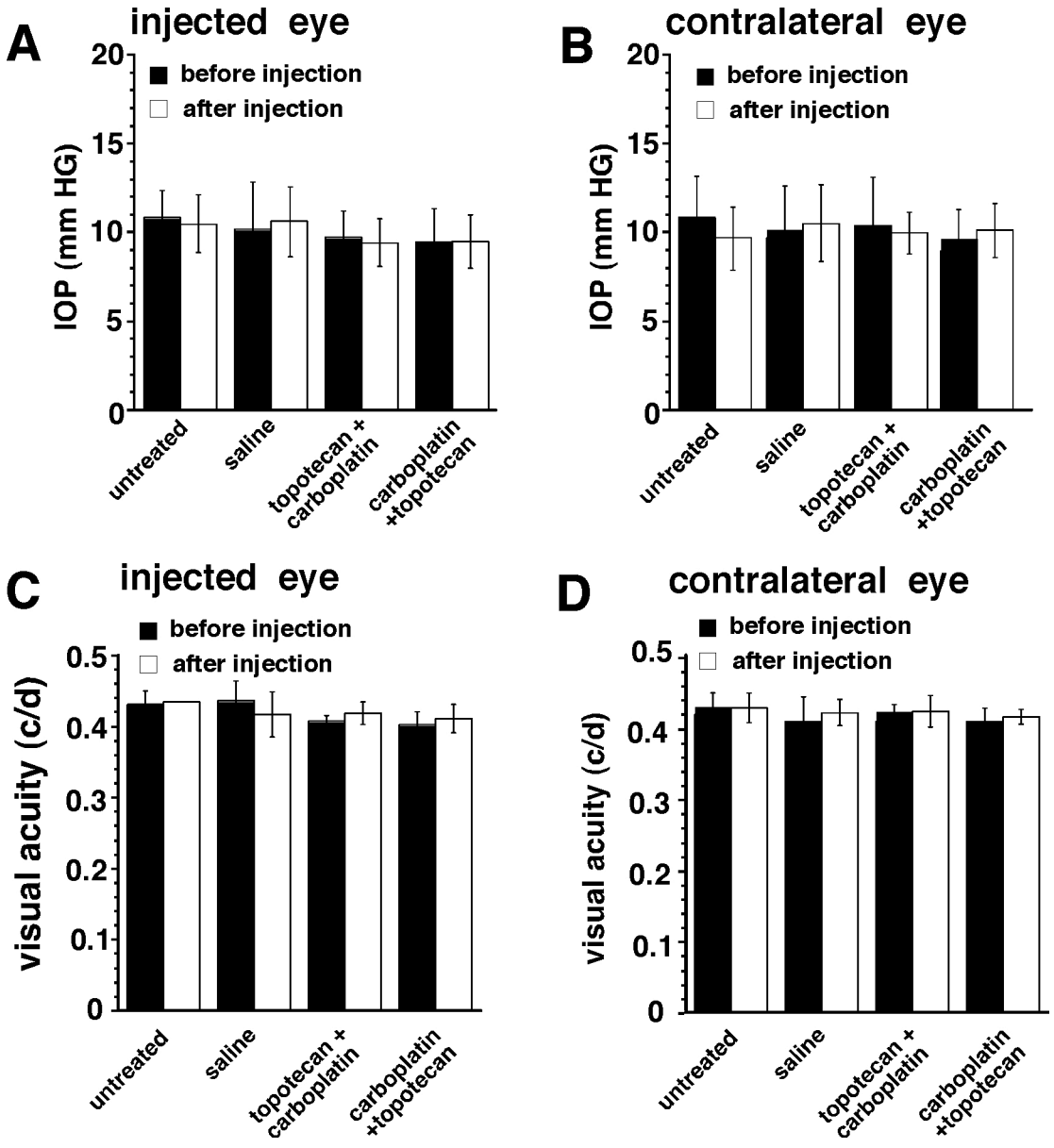
A
injected eye
before injection
after injection
IOP (mm HG)
20
15
10
5
0
untreated
saline
topotecan + carboplatin
carboplatin +topotecan
B
contralateral eye
before injection
after injection
IOP (mm HG)
20
15
10
5
0
untreated
saline
topotecan + carboplatin
carboplatin +topotecan
C
injected eye
before injection
after injection
visual acuity (c/d)
0.5
0.4
0.3
0.2
0.1
0
untreated
saline
topotecan + carboplatin
carboplatin +topotecan
D
contralateral eye
before injection
after injection
visual acuity (c/d)
0.5
0.4
0.3
0.2
0.1
0
untreated
saline
topotecan + carboplatin
carboplatin +topotecan

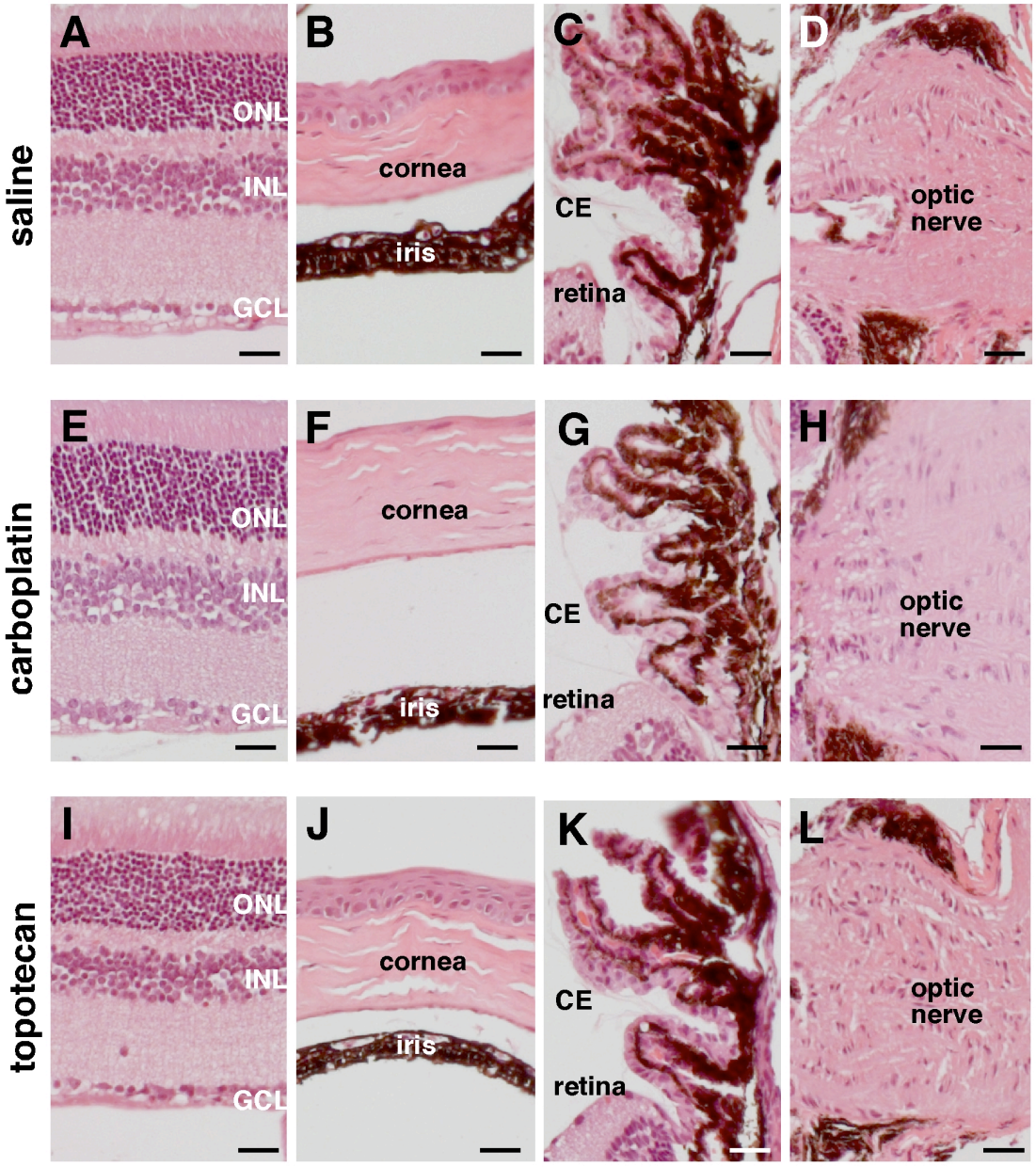

Figure 2-6. Histopathological Analysis of Ocular Structures Following Subconjunctival Injections of Topotecan or Carboplatin.
Representative images of H&E stained sections form paraffin blocks of eyes treated with subconjunctival saline (A-D), carboplatin (E-H) or topotecan (I-J). Retina, cornea, iris, ciliary epithelium (CE) and optic nerve (ON) are shown. ONL: outer nuclear layer, INL: inner nuclear layer and GCL: ganglion cellular layer. Scale bar: 25 μm.

Figure 2-7. Side Effects of Topotecan and Carboplatin Combination Chemotherapy Using Different Routes of Administration.

(A) The first group received saline injections, the second group received carboplatin (100 mg/eye) and topotecan 0.2 mg/kg daily x 5 by intraperitoneal injection and the third group received topotecan (10 mg/eye) by subconjunctival injection and carboplatin (10 mg/kg) by intraperitoneal injection. Body weight was measured each day for the subsequent 9 days. When the topotecan was administered by subconjunctival injection and the carboplatin was administered by i.p. injection and all the animals died by day 6 of treatment with signs of dehydration. (B) Blood chemistry for treated and untreated juvenile rats. Each bar represents the mean and standard deviation of 2-3 animals. (C) Blood cell counts for treated and untreated juvenile rats. Each bar represents the mean and standard deviation of 2-3 animals. Abbreviations: BUN, blood urea nitrogen; WBC, white blood cells; NE, neutrophils; RBC, red blood cells; PLT, platelets.

A

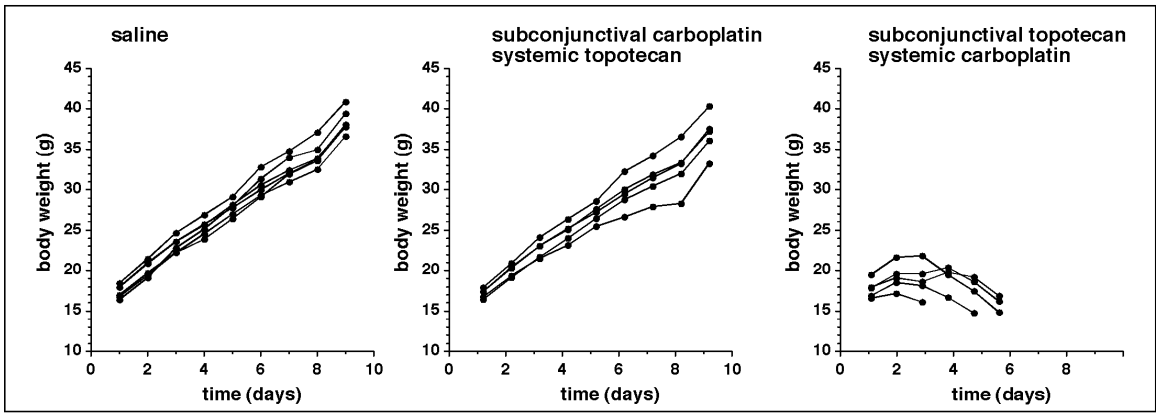
saline
subconjunctival carboplatin
systemic topotecan
subconjunctival topotecan
systemic carboplatin
body weight (g)
time (days)

B

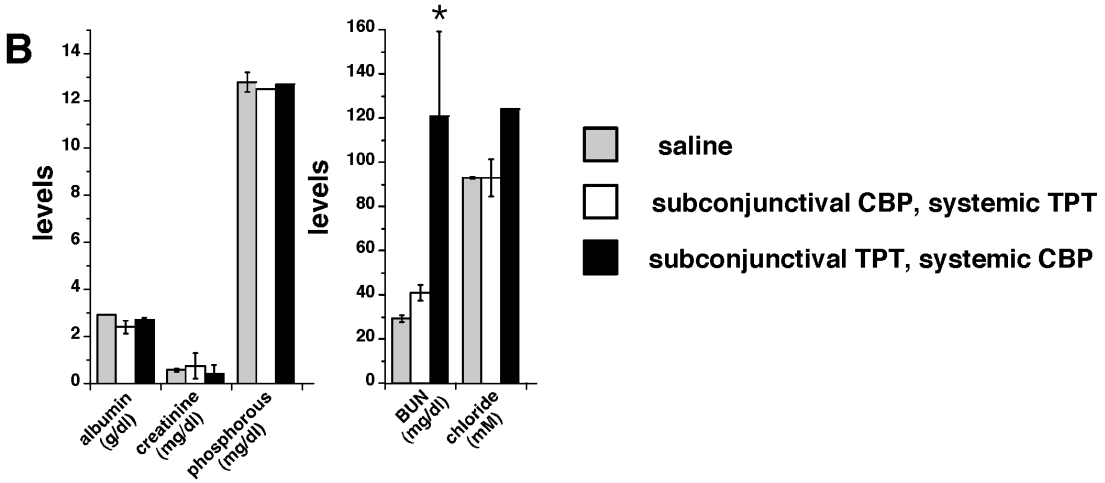
levels
albumin (g/dl)
creatimine (mg/dl)
phosphorous (mg/dl)
BUN (mg/dl)
chloride (mM)
saline
subconjunctival CBP, systemic TPT
subconjunctival TPT, systemic CBP

C

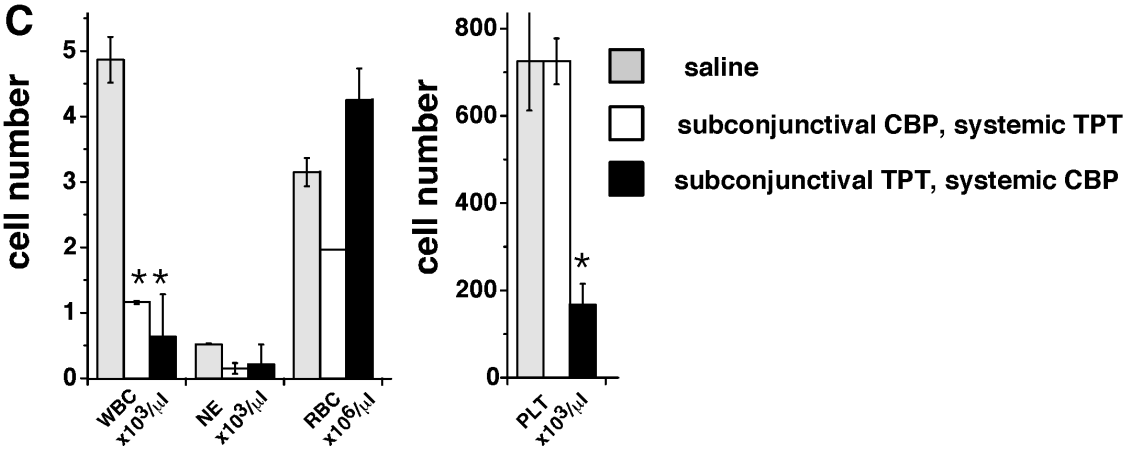
cell number
WBC x10³/μl
NE x10³/μl
RBC x10⁶/μl
PLT x10³/μl
saline
subconjunctival CBP, systemic TPT
subconjunctival TPT, systemic CBP

and systemic topotecan, this group exhibited signs of profound dehydration including significant weight loss, lethargy and tenting of the skin (**Fig. 2-7A** and data not shown**)**. Blood chemistries obtained from the rats that survived to day 6 of treatment were normal except for an elevated BUN consistent with chemotherapy-related dehydration **(Fig. 2-7B)**. In addition, blood counts obtained from those same animals were consistent with myelosuppression as evidenced by neutropenia and thrombocytopenia **(Fig. 2-7C)**. Taken together, these data show that there is significant toxicity associated with subconjunctival topotecan and systemic carboplatin as compared to subconjunctival carboplatin and systemic topotecan.

2.4 DISCUSSION

Retinoblastoma is unique among pediatric solid tumors because locally delivered chemotherapy can be combined with systemically administered chemotherapy to optimize intraocular drug exposure while minimizing the side effects associated with combination chemotherapy. In this study, we tested the feasibility, efficacy and toxicity associated with combining subconjunctival injection of one drug with systemic administration of the other drug. In this way, we hoped to avoid the side effects of intravenous combination chemotherapy while optimizing the vitreal exposure of both drugs and the anti-tumor effect. Using pharmacokinetic and pharmacodynamic approaches, we directly compared subconjunctival carboplatin with systemic topotecan against subconjunctival topotecan with systemic carboplatin. The combination of subconjunctival carboplatin and systemic topotecan resulted in greater efficacy and fewer side effects in the orthotopic xenograft juvenile rodent model. There were no detectable ocular side effects associated with this combination of chemotherapy following acute exposure or repeated dosing on a clinically schedule in rodents. Blood counts, vision, intraocular pressure, tumor growth and metastasis were closely monitored in this longitudinal study to provide the most relevant data in preparation for clinical trials using subconjunctival carboplatin combined with systemic topotecan. We did not include focal therapy such as laser therapy, which is an integral part of retinoblastoma treatment in children. Therefore, the overall outcome in terms of disease progression and saving vision and eyes will likely be much better in patients with retinoblastoma receiving subconjunctival carboplatin (20 mg/eye) and systemic topotecan starting at 3 mg/m^2/day (daily x 5 with a target AUC of 140±20 ng/ml•hr) along with focal therapy.

2.4.1 Pharmacokinetics

Pharmacokinetic studies are essential in retinoblastoma to determine how much drug penetrates the vitreous and to determine the relative plasma exposure for a given dosage of chemotherapy. This is particularly important for the combination of topotecan and carboplatin because if the systemic exposure of both drugs is too high it can result in dose-limiting myelosuppression. There were several key findings from our pharmacokinetic studies. First, subconjunctival delivery of topotecan and carboplatin led to an increased penetration of the eye as indicated by the vitreal level of drugs achieved. Second, the vitreous/plasma AUC ratios indicated that the intraocular penetration of topotecan (1.98) was better than carboplatin (0.85) following a subconjunctival injection.

Third, the presence of a tumor in the eye led to more efficient penetration of both drugs. Fourth, the subconjunctival route of administration led to greater vitreal exposure than the systemic route of administration for both drugs. Fifth, there was detectable exposure in the contralateral eye following subconjunctival injection in one eye as a result of the uptake of drug into the circulation. Overall, these data indicate that subconjunctival delivery of either drug is feasible for the treatment of retinoblastoma based solely on measures of intraocular and systemic exposure.

2.4.2 Toxicity

Measurements of visual acuity, intraocular pressure and cytotoxicity by histological analysis indicated that there was no detectable ocular toxicity associated with subconjunctival injection of either topotecan or carboplatin. In addition, when subconjunctival injection of topotecan or carboplatin was combined with systemic exposure of the other drug, we did not observe any changes in ocular physiology or histology. In contrast, chemotherapy-related dehydration and myelosuppression was a major challenge in these studies when subconjunctival topotecan was combined with systemic carboplatin. The juvenile rats could not tolerate the dose of 10 µg/eye topotecan with 34 mg/kg carboplatin. Even when the dose of carboplatin was reduced to 10 mg/kg the animals showed signs of severe dehydration and myelosuppression. In addition, there was some toxicity seen with the dose of 0.5mg/kg of topotecan daily x 5 with 10 µg/eye of carboplatin. Once the i.p. dosage was reduced to 0.2 mg/kg of topotecan the juvenile rats survived. In both combinations, this dose de-escalation is most likely due to the age of the rats. Clearly, in terms of side effects, subconjunctival carboplatin with systemic topotecan is much better tolerated for the juvenile rodents used in our studies. The other important advantage of the subconjunctival carboplatin with systemic topotecan route of administration is the fact that the topotecan can be delivered on a daily x 5 schedule. This provides continued chemotherapeutic exposure for several days and this is not possible when using subconjunctival topotecan with systemic carboplatin because carboplatin can only be administered on the first day of therapy in the humans.

2.4.3 Pharmacodynamics

Based on the toxicity data, the preferred route of administration for these two drugs is subconjunctival carboplatin and systemic topotecan; however, this is only preferred if the tumor response is similar or better as compared to subconjunctival topotecan with intraperitoneal carboplatin. Our pharmacodynamic studies in juvenile rats with orthotopic xenografts indicated that the tumor response using subconjunctival carboplatin and systemic topotecan was robust and comparable to the other route of administration. It was impossible to monitor the pharmacodynamic response to subconjunctival topotecan and systemic carboplatin past 5 days due to the animal morbidity. Therefore, administration of local carboplatin with systemic topotecan is preferred for the treatment of retinoblastoma.

The goal of these studies is to directly impact the clinical management of retinoblastoma patients by combining topotecan and carboplatin. More importantly,

these data establish the importance of preclinical studies for retinoblastoma and our systematic approach can now be used to screen other drug combinations for future efforts to preserve vision and save lives for children with retinoblastoma.

CHAPTER 3. LONGITUDINAL STUDY

3.1 INTRODUCTION

In the late sixties it was first reported that an immunodeficient “nude” mouse received a xenograft transplant [127]. With its ease and reproducibility, the xenograph flank model has become a major tool in studying human tumors. In this model the mouse’s flank is injected subcutaneously, with either a tumor cell line or a primary human tumor [128, 129]. This method allows for the study of the tumor in a three dimensional architecture [129] and to study the tumor’s sensitivity to chemotherapeutics *in vivo* providing information that is useful to confirm results obtained in previous *in vitro* studies [128]. In addition, the tumor’s response to treatment can be easily assessed with simple caliper measurements [130]. Most importantly these tumors are of human origin and response to potential chemotherapeutic is translatable to the clinic. While the flank xenograft model is valuable tool in predicting potential treatments, it has some drawbacks.

Along with the advantages of the model, the shortcoming need to be considered when designing and interpreting the data generated. It is important to consider the origin of the tumor cells. If from a tumor biopsy, the model will likely recapitulate the tumor closely; whereas, a tumor from a cell line is likely to be less similar to the human disease, being more homogenous and undifferentiated largely due to selective pressure from *in vitro* cell culturing [128]. The most basic drawback to the xenograph model is that the tumor does not grow naturally. This tumor is likely composed of a well-established successful cohort of cancer cells that may have additional genetic lesions or chromosomal abnormalities. Perhaps the most obvious and influential factors are from the stromal compartment where the tumor cells are injected. This includes a different vascular system and microenvironment than the original tumor environment, which can cause different tumor behavior, such as metastasis [128, 130]. All of these confounds will influence pharmacological studies. More specifically the pharmacological parameters, absorption, metabolism, distribution and excretion, will be altered, even if the treatment route is similar to the clinic. Perhaps the most basic and obvious drawback of the xenograph model is immunodeficient host, which makes the study to treatment impossible. All of these variables can impact the clinical translation and need to be recognized when analyzing the study results.

Due to concerns with the xenograph flank model and advances in mouse genetic technology, there has been a shift in model preference. This advancement has led to the generation of mouse models with the genetic mutations thought to be causative in human tumors. Transgenic preclinical models of retinoblastoma have also played an important role in identifying and optimizing new therapies for clinical trials. The first successful retinoblastoma model was developed in 2004 [110]. The elimination of RB1 and p107 genes ($Rb^{lox/-}$ $p107^{-/-}$) gave researches the potential to easily study in the disease in an animal; however, there was only a 60% penetrance and the tumors did not recapitulate the human form of the disease. Since this initial model there have been many different mouse models generated by crossing the $Rb^{Lox/-}$ mouse with mice, who lack different retinoblastoma family member, such as $Rb^{Lox/Lox}$;$p130^{-/-}$, $Rb^{Lox/Lox}$;$p107^{-/-}$ and $Rb^{Lox/Lox}$;$p130^{-/-}$; $p107^{lox/-}$ [131](unpublished data). Additionally, in 2006 Dr. Michael

Dyer's group reported the generation of a mouse (Rb $^{lox/-}$ p107$^{-/-}$p53 $^{lox/-}$) that showed an aggressive form of retinoblastoma, which recapitulated the human disease. This animal lacked the p53 tumor suppressor gene and its aggressive nature was later found to be due not only to the lack of p53, but also to the over-amplification of MDMX [125]. Each one of these models has resulted in successful and breedable models that have the potential to develop retinoblastoma. Even with these tools the translational study of retinoblastoma continues to be a challenge. This is in largely due to the lack of proper diagnostic tools or studies to monitor the ocular health in the presence of a tumor.

In the clinic, retinoblastoma is one of the easiest types of cancers to follow using ocular health and diagnostic imaging modalities. These exams confirm the presence of retinoblastoma and its response to treatment. With the development of different rodent modalities, similar tests can be used to monitor retinoblastoma progression in mouse models and address the preservation of vision after treatment. These tests include measurements of visual acuity and intraocular pressure (IOP), as well as tumor growth using retinal camera examination, high-resolution ultrasound and MRI analysis.

Recently reported as the gold standard of visual assessment in mice, optomotry is an appropriate measure for the development of baseline and future translational studies. In brief, this modality creates a virtual cylinder with 4 computer monitors that surround the mouse standing on a pedestal in the center of the screens. The screens contain moving alternative black and white bars that rotate either clockwise or counterclockwise. The mouse will track these moving bars and the vision of each eyes is tested with this involuntary response to the projected image [132]. The IOP was measured in a sedated mouse with the tonometer. This modality quickly assesses the pressure difference in the anterior chamber of the eye. Both preclinical and clinical tumors, can be imaged with a retina camera, although this test is sensitive and can be conducted in a high throughput manner, it has limitations. Often peripheral tumors are hard to locate and cannot be viewed in a single frame. Fortunately the ultrasound and MRI both have the ability to capture the entire eye in a single view. The ultrasound can detect anterior chamber tumors easily, but it has difficulty imaging the posterior part of the eye. Similar the MRI can image the tumors, but it can also detect posterior tumors clearly as well as extraorbital invasion. Each of these tools has become recently available; thus there has not been a published study which carried out a detailed characterization or long-term longitudinal study of retinoblastoma tumors form the various genetic lesion in the mouse models. Thus far, it has not been established whether one mouse model's tumor growth better recapitulates the pattern of growth seen in human retinoblastomas. By characterizing each diagnostic modality a better understanding of tumor growth will be obtained, allowing us to decode the impact of the genetic mutations in the mouse models and compare them to human retinoblastoma. In addition, this understanding strengthens the translational of future preclinical studies to early clinical trials.

3.2 MATERIAL AND METHODS

3.2.1 Mouse strains

C57BL/6 mice were purchased from Charles River Laboratories (Wilmington, MA) at approximately six weeks of age. *Chx10-Cre* mice were obtained from Dr. Connie Cepko (Harvard Medical School, Boston, Massachusetts). *Rb* $^{Lox/Lox}$ mice were obtained from the National Cancer Institute originally made by Dr. Anton Berns (Netherlands Cancer Institute, Amsterdam, Netherlands). The *p107s* (p107$^{-/-}$) and *p130*$^{-/+}$ mouse strains were obtained from Dr. Tyler Jacks (Massachusetts Institute of Technology, Cambridge, Massachusetts). *p53* $^{Lox/Lox}$ mice were from the National Cancer Institute. The AIPL$^{-/-}$ mouse was generated at St. Jude's Research Hospital by M.A. Dyer [133]. All animal studies were conducted in accordance with the SJCRH Institutional Animal Care and Use committee (IACUC) guidelines.

3.2.2 Kowa retina camera

The initial diagnosis and staging of retinoblastoma was visualized with a Kowa retinal camera (Tokyo, Japan). It was fitted to a base to ensure steadiness and a foot petal was used to control the shutter. The camera was reconfigured with a 78-diopter lens that was mounted 5 cm below the camera and was attached to a rod supported by the base. The visual field illuminator was set at level 6, previously shown to produce the best results for pigmented mice [134]. All effort was made to minimize reflection. The whiskers of the mice were trimmed and the pupils were dilated with 1% Tropicamide (atropine) (Bausch & Lomb Incorporated, Tampa, FL). Housing the mice in a dim cage for 10 minutes allowed the iris to dilate. No anesthesia was used to avoid possible complication of clouding of the eye. A conscious rodent was gently held approximately 3-5 cm under the lens. One hand was used to hold the mouse while the other hand was used to pull back the eyelids to avoid lid interference. Focusing was achieved by manually moving the mouse. In attempt to view the peripheral retina the mouse was angled. Observations were recorded both manual and digitally.

3.2.3 Magnetic resonance imaging (MRI)

Tumor-bearing mice were anesthetized using 2-3% isoflurane in O_2 for the duration of the data acquisition. They were imaged with a 7-Tesla Bruker Clinscan animal MRI scanner (Bruker BioSpin MRI GmbG, Germany) equipped wit Bruker 12s gradient (BGS12S) and a four channel phase-array surface coil placed on the mouse's head. 3D Magnetization Prepared Rapid Gradient Echo (MP-RAGE) protocol (T_r 2500 ms; T_E 2.5 ms; T_1 1050 ms) was used to produce T1 weighed images (coronal) using a matrix of 256 x 146 and FOV of 30 x 20.6 mm. The slice thickness for the T1 weighted images was 0.5 mm. Initial images were read on a Siemens workstation using Syngo MR B15 software (Siemens, Erlangen, Germany) and reviewed with MRIcro software (version 1.4). Three dimensional volume measurements were made using Diacom Works (DicomWorks, Lille, France) to calculate eye and tumor ratios.

3.2.4 Ultrasonography

Mice were anesthetized with 2-3% isoflurane in O_2 (2 liters/ minute), positioned laterally and secured on a heated platform. Although it was occasionally necessary to suture open the eyes open (Ethican 5-0 silk) for full globe protraction, taping of the upper and lower eyelids was usually sufficient for imaging purposes. Aquasonic 100 coupling gel (Parker Laboratories, Inc, Fairfield, NJ) was applied to the surface of the eye and a RMV 708 probe lowered stereotactically to the plane of the eye allowing acquisition of images. The Visual Sonics High Resolution microimaging Vevo 770 system (Visual Sonics, Inc., Toronto, Ontario, Canada) was used to record B-mode, 3-Dimensional (3D) and power Doppler images. High-resolution images were acquired (55MHz allowing an optimal focal depth of 4.5 mm) in the coronal plane using a field of view of 8x8x10 mm^3. Using the systems integrated rail and 3D motor, sequential acquisition of high-resolution coronal images with a step size of 102 μm allowed for an isotropic resolution of 0.1mm.

3.2.5 Tonometer

IOP of sedated mice was measured with the TonoLab Rebound Rodent Tonometer (Tonolab, Espoo, Finland). Mice were anesthetized using 2.5% isoflurane and measurements were taken at the same time of the day, approximately six hours into the light cycle. The device was held so that the probe was between 1-4 mm from the cornea of the eye. Six consecutive measurements were taken and averaged to give a final value for each eye.

3.2.6 Optomotry

Visual acuity was measured using the OptoMotry System (Cerebral Mechanics, Alberta, Canada) as previously described [132]. All tests were carried out in bright light conditions to measure cone function. Visual acuity of the mouse was measured with at least two consecutive measurements on independent days 24 hours before and after administration of drug. A second set of measurements was made on 2 consecutive days 1 week after administration of the drug.

3.2.7 Histology

Eyes were fixed in 4% paraformaldehyde overnight at 4°C, dehydrated through an alcohol series and washed in xylene. Eyes were paraffin embedded and sectioned (5 μm) in the sagittal plane through the optic nerve and stained with H&E. The cornea, ciliary epithelium, retina and optic nerves were compared across treated and untreated eyes at 1,2 and 7 days after administration of the subconjunctival injection.

3.2.8 Statistical calculations

Statistical tests were performed using GraphPad Prism Software for Mac Os X version 5.0 (GraphPad software Inc.). A one-way ANOVA and a Tukey's correction were used to compare groups.

3.2.9 Calcuation of volume

3.2.9.1 Histology bioquant software

Fixed globes were embedded in paraffin and sliced into 10μm thick sections. Every 10th section was stained with H&E (i.e., serial sections with 50μm spacing). These histological sections were viewed and hand traced at 4x magnification using BioQuant software program (BIOQUANT Image Analysis Corporation, Nashville TN). Due to the various tumor sizes and expansion of the stressed globe the number of images needed for a single composite of an eye varied. Three-dimensional digitized histology volumes were made by aligning each tracing to a predetermined focal point by the optic nerve head.

3.2.9.2 Ultrasound

Volume measurements of the eye and the tumor were determined with VEVO software (VisualSonics, Inc., Toronto, Ontario, Canada). From high-resolution 3D data sets, tissue perimeters were hand traced at 0.5 mm intervals and the eye and tumor labeled in unique colors to mark the different boundaries. The Visual Sonics software (VisualSonics, Inc., Toronto, Ontario, Canada) was then used then to render and calculate calibrated volumes. The tumor to eye ratio was calculated for each eye.

3.2.9.3 Magnetic resonance imaging MRIcro software

Volume measurement of the eye and tumor were determined by hand tracing each slice DicomWorks (DicomWorks, Lille, France). A traced slice was included if it had clear boundaries marking the eye and tumor distinct. Representative volume was determined using the voxel volume that was calculated by multiplying the image resolution in each of the three dimensions (x,y,z). The tumor to eye ratio was calculated for each eye.

3.3 RESULTS

3.3.1 Characterization of imaging and ocular health modalities

3.3.1.1 Characterization and measurement of intraocular pressure (IOP)

In the clinic, the IOP of a retinoblastoma eye can increase as the tumor grows into the anterior chamber, pressing against the lens or grows into the choroidal layer

[29]. Sustained elevated IOP can lead to blindness due to the compression of the optic nerve leading to degeneration of these ganglion cell axons. Before we could determine if retinoblastomas in the mouse models have the same effect as in humans, we needed to determine the IOP in wild type C57Bl/6 mice. We conducted a baseline study of IOP in four male mice, approximately six weeks of age. To determine the reproducibility of the tonometer measurements, as well as variation between day and among animals, IOP measurements were taken at the same time of the day for 4 consecutive days. Each measurement was performed in sextuplet and averaged. We found that there was little daily variation in the IOP as well as little variation among animals **(Fig. 3-1A,B)**. The IOP measurements we obtained are similar to the average IOP results previously described ranging from 10-20 mmHg [135]. These results were not significantly different.

Next we wanted to determine if the loss of RB1 and p107 affected baseline IOP. This data was important since all of the mice that have the potential to develop retinoblastoma are crossed with the Chx10-Cre; $Rb^{Lox/Lox}$; $p107^{-/-}$ mouse, thus lacking 2 genes. To answer these questions, young mice were monitored for 5 weeks, 7-8 hours into their light cycle and compared wild type animals **(Fig. 3-1C**). There was no statically difference among these comparisons.

Typically an increase in IOP is due to the disruption of fluid movement in the eye's anterior chamber of the eye. As mentioned above, retinoblastoma growth in the human can affect IOP; therefore, it was necessary to see if the rodent tonometer could detect a change in IOP in a mouse model of retinoblastoma. To look at this in detail, the p53 TKO model (Chx10-Cre; $Rb^{Lox/Lox}$; $p107^{-/-}$; $p53^{Lox/Lox}$) were enrolled and tested at approximately 6-8 weeks of age. A small pilot study of three animals was enrolled and each eye was monitored independently. This data showed a sudden increase in IOP of 18 mmHg **(Fig. 3-1D)**. Once this value or higher was reached the animals were humanly sacrificed.

3.3.1.2 Characterization of optomotry visual acuity system

As stated earlier, tumor location and size that leads to an increase in IOP can often lead to a loss of vision. Prior to determining if vision is affected by tumor growth in the preclinical models, the Optomotry System was characterized in our hands, with wild type mice (C57Bl/6 male mice) and compared to preexisting reports. Five mice were enrolled and their vision was studied for five consecutive days. As a negative control, a short-term study with an acute retinal degeneration mouse (aryl hydrocarbon receptor-interacting protein-like 1 or $Aipl1^{-/-}$) was also monitored [136]. This genotype is known to have early onset of retinal degeneration and at approximately 8 weeks nearly total loss of rods and cones, thus is blind [133]. There was little variation in vision between wild type mice and over the multiple day study **(Fig. 3-2A-C)**. As expected, the $Aipl1^{-/-}$ mouse never showed a response. A potential confound for this modality is that it is heavily dependent on the mouse's behavior and users attention. To our assurance our values were similar to previously published data [132].

Previously it was found that in the absence of the *Rb1* protein in a developing murine retina, rod photoreceptors fail to develop [137]. In addition, it was reported that occasional absence of rods might affect cone survival. To determine if rod degeneration

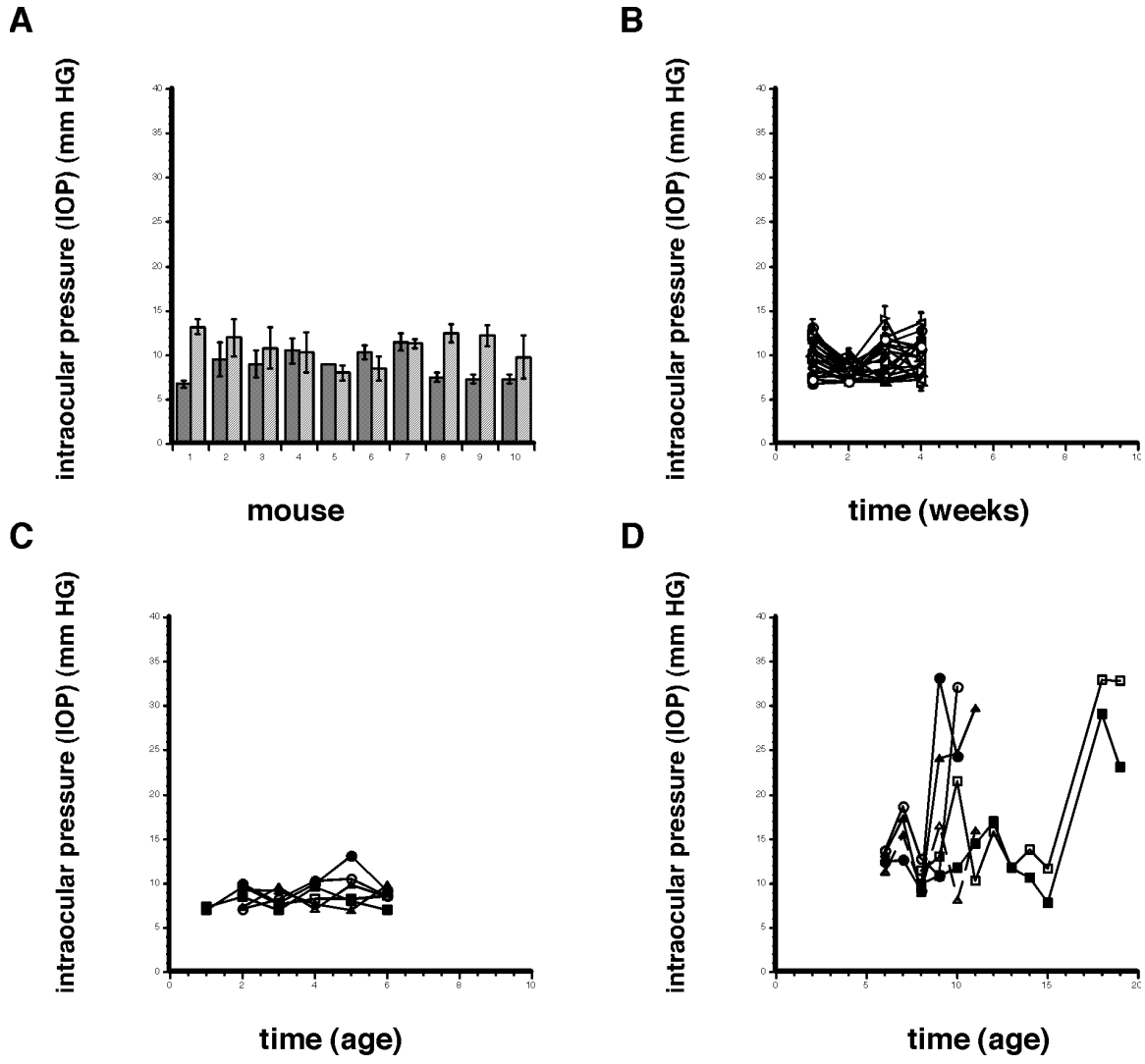

Figure 3-1. Tonometer Characterization of Wild Type C57Bl/6 and Retinoblastoma Mice.

(A) Each eye of four mice was measured individually with the tonometer to look for animal-to-animal variation. There was no significant difference among animals. (B) Each eye was measured individually over four days to assess day-to-day variation. Solid symbols represent the right eye, whereas open symbols represent the left eye. There was no significant difference across days. (C) Three 7D mice were followed over 6 weeks to determine genotype's IOP baseline. (D) The IOP of three p53 TKO mice were followed over thirteen weeks or until morbid status occurred. IOP = intraocular pressure; mm HG = millimeters of mercury.

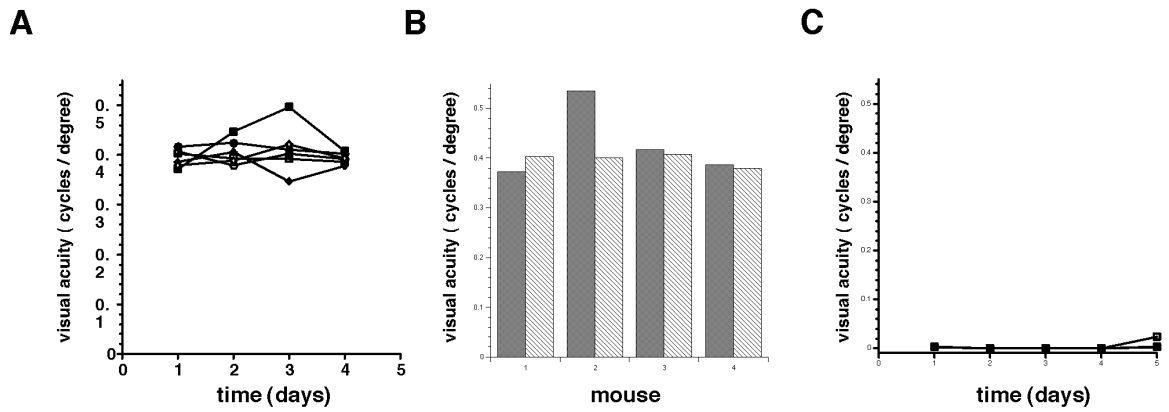

Figure 3-2. Optomotry Characterization of Wild Type C57Bl/6 Mice and AIPL1 $^{-/-}$ Mouse.

(A) Animal-to-animal variation each eye of four mice was measured individually. There was no significant difference. (B) Day-to-day variation each eye was measured individually over four days. Solid symbol or gray shading represents right eye and open symbol or striped shading is left eye. There was no significant difference. (C) Confirmation of the AIPL1$^{-/-}$ mouse was blind with optomotry modality.

could influence visual acuity in retinoblastoma mouse models, a pilot study where each eye was treated as its own subject was carried out in Chx10-Cre;Rb $^{Lox/Lox}$ mice as all retinoblastoma mouse models are crossed with this genotype. The test was run under bright light conditions which allowed us to solely measure cone function [138]. In comparison to wild type mice visual acuity, (0.370-0.460 cycle per degree), the Chx10-Cre; Rb $^{-/Lox}$ mice had similar visual acuity measurements (0.340-0.420 cycles/degree). This data was not statically significant. Additionally, all retinoblastoma mice are crossed with a p107$^{-/-}$ mouse to give the double knockout (DKO) (Chx10-Cre;Rb $^{Lox/Lox}$; p107$^{-/-}$). Therefore, it was important to determine if the visual acuity was similar to wild type and Chx10-Cre; Rb $^{Lox/Lox}$ mice. This short-term study was conducted and gave similar range of visual acuity (0.300-0.480 cycles/degree). This larger range was due to the poor behavior of these particular animals. In addition, different genotypes of tumor prone mice were followed to determine if loss of vision would occur over time **(Fig. 3-3A-F)**. A decrease in vision was seen for each of the six different genotypes of retinoblastoma.

3.3.1.3 Characterization of the Kowa retina camera

Along with visual health assessment in the clinic, children are sedated and imaging of their eye's posterior chamber is viewed with a retinal camera before and during treatment. This fundus inspection helps physicians document the tumor's status and response after therapy. Many groups have adapted these clinical cameras for rodents, which can also image the posterior chamber and assess associated pathologies [134, 139]. To determine if the Kowa retinal camera, adapted with a 78-diopter lens, could visualize the posterior chamber in our hands, we viewed a wild type C57Bl/6 mouse and the mutant Nr2e3$^{-/-}$ mouse. This mouse lacks Nr2e3 gene (nuclear receptor subfamily2, group E, member 3), which leads to retinal degeneration at a very young age [140]. This genotype was chosen because it has a distinct phenotype, a fundus covered in small spots [134]. Our images obtained with the Kowa retinal camera are quite similar to previously published images.

To the best of our knowledge there have need been published reports of retinoblastoma tumors images with the Kowa retinal camera. To determine if a tumor and tumor growth could be detected we looked at a number of retinoblastoma mouse models **(Fig. 3-4A-C)**. The tumor presence and growth was detected and captured with this modality.

3.3.1.4 Characterization and ultrasonic tumor detection

The retina camera is very good at detecting tumors in the posterior chamber, but a single frame of the entire retina cannot be generated. Traditionally, the clinic uses ultrasonography to closely characterize the size and vascularization of the tumor. Since it has never been reported before, it was necessary to determine if normal and tumor-bearing eyes could be successfully imaged. When compared to clinical B-scans, the scans of the rodent's eye were similar. As expected the tumor-bearing eye was successfully imaged and showed the presence of tumor **(Fig. 3-5)**. Unfortunately, the resolution of the margins at the posterior globe was not very clear.

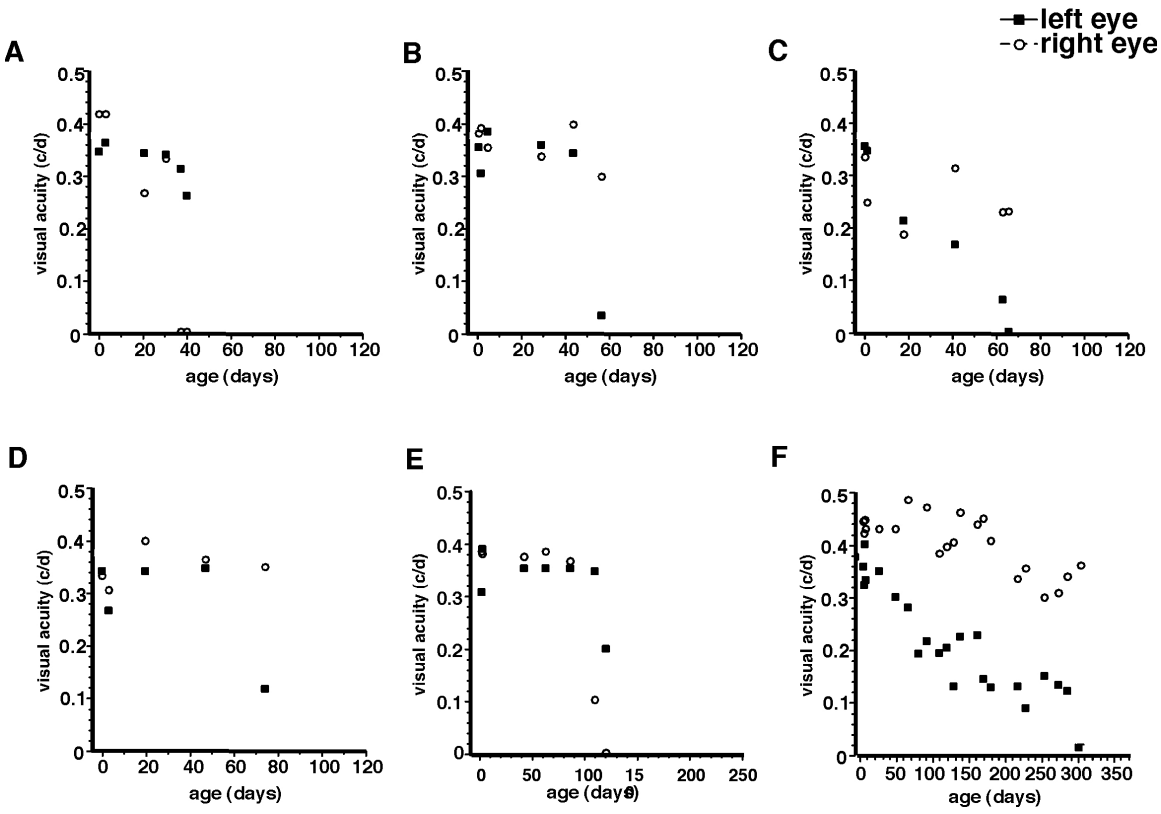

Figure 3-3. Loss in Vision Detected with Optomotry for Each.
A representation of visual acuity measurements for each genotype. The following genotypes included are (A) RB TKO, (B) p107s, (C) p53 TKO, (D) MDMX ^{tg}, (E) 3D and (F) 7D mice. The left eye is represented by a solid square, whereas the right eye is represented by an open circle. c/d = cycles per degree.

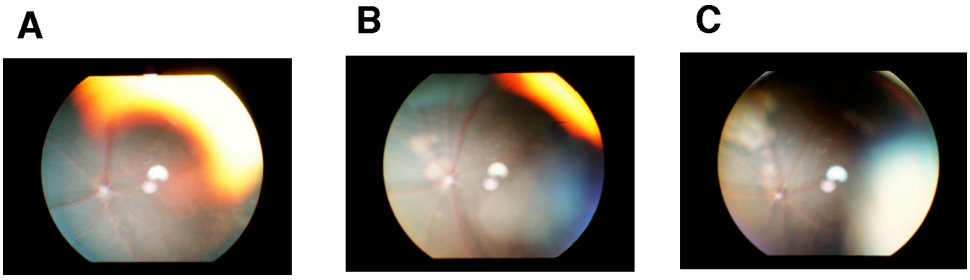

Figure 3-4. Kowa Retina Camera Detects Tumor Growth.
The first image is of a non-tumor eye (A). The second and third images (B,C) show tumor growth in the upper left quadrant. The two white dots in every photo is lens reflection.

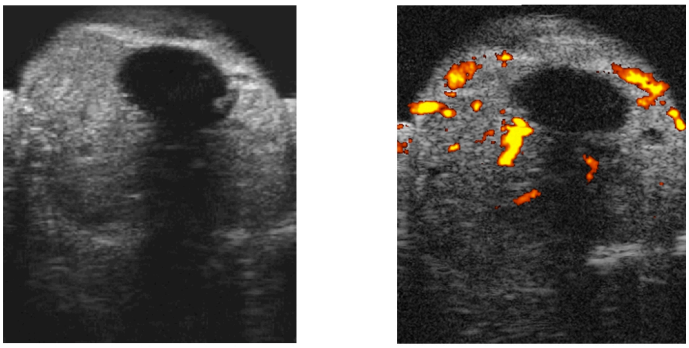

Figure 3-5. A Representation of an Ultrasound Image of Retinoblastoma Mouse. An ultrasound scan and Doppler image showing a tumor filled vitreous of the same tumor eye. The color markings represent blood flow in the tumor.

It is well known the vasculature is important in the delivery of chemotherapeutic agents. The additional benefit of ultrasound is the ability to visualize the blood vessels with the Power Doppler Imaging Mode. This allows the microvascularity in and around the tumor to be imaged and color mapped **(Fig. 3-5)**. To test if we were able to detect tumor vasculature in retinoblastomas 20 mice were scanned of different genotypes (p53 triple-knockout (Chx10-Cre; $Rb^{Lox/Lox}$; $p107^{-/-}$; $p53^{Lox/Lox}$), Rb TKO (Chx10-Cre- $Rb^{Lox/Lox}$; $p107^{-/-}$; $p130^{Lox/Lox}$) and MDMX (Chx10-Cre- $Rb^{Lox/Lox}$; $p107^{-/-}$;$MDMX^{tg}$). While the vascular system was visible in some mice, it was not present in all tumors; however, the absence of vessels in these tumors could not be ruled out because additional methods of detection were not conducted and may be considered in future studies.

3.3.1.5 Magnetic resonance imaging of tumor detection in tumor-bearing mice

Often the ultrasound can miss part of the tumor due to calcification and absorption of sound waves [141]. To complement the ultrasound approach, an anatomical MRI scan was used with a small animal 7T MRI system. This is the most straightforward, noninvasive method to study organs and determine tumor presence. To date, no one has followed tumor progression with MRI in retinoblastoma mice. This noninvasive modality produced two different scans, a longitudinal component (T1) and transverse component (T2). In general the T1 component is more detailed and can be used to determine tumor volume. In comparison to control, C57Bl/6, the tumor-bearing eyes showed an increase the presence of tumor in the vitreous over time.

To determine if the progression of rodent ocular tumors could be measured an abbreviated longitudinal study in p53 triple knockout mice (TKO) was conducted. Animals were enrolled in this study at 7-16 weeks of age and scanned weekly until the tumor invaded the anterior chamber, resulting in inevitable ocular rupture. The scan was conducted on three different tumor prone mice and each eye was analyzed independently (n=6) **(Fig. 3-6A-I)**. Each eye and tumor was hand traced and the tumor/eye ratio was determined using MRIcro software. An increase tumor volume was detected over time for each eye using MRI. At the same time of weekly MRI scans, the

Figure 3-6. Analysis of Tumor Development in Retinoblastoma Mice.
A longitudinal analysis of retinoblastoma tumor development in TKO p53 mice with weekly MRI scans (A,D and G) and intraocular pressure measurements with tonometer (C, F and I). For each scan session volume was calculated for tumor volume and eye size. A ratio between the two was calculated using MRIcro software (B, E and H). The ages of the mice were 7 weeks (A and D) and 16 weeks (G). For the first and second mouse (A) MRI scans were conducted at 7 (A1, D1), 8 (A2, D2), 9 (A3, D3) and 10 weeks (A4, D4); for third mouse (G) MRI scans were conducted at 18 (G1), 18.5 (G2), 19 (G3) and 20 weeks (G4). Weekly tonometer measurements were carried out on the three mice starring at 5 to 6 weeks of age. Open circle represents left eye and closed circle represents right eye. mm HG = millimeters of mercury.

A

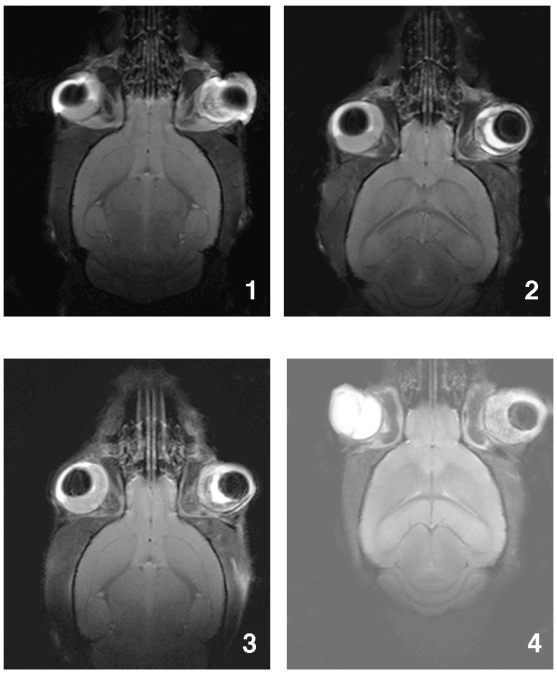
1
2
3
4

B

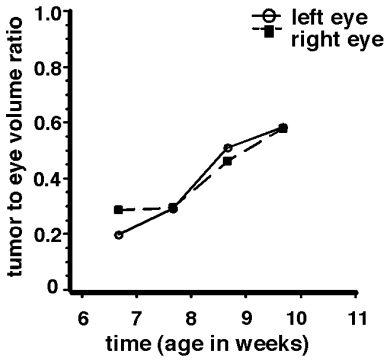
left eye
right eye
tumor to eye volume ratio
1.0
0.8
0.6
0.4
0.2
0
6
7
8
9
10
11
time (age in weeks)

C

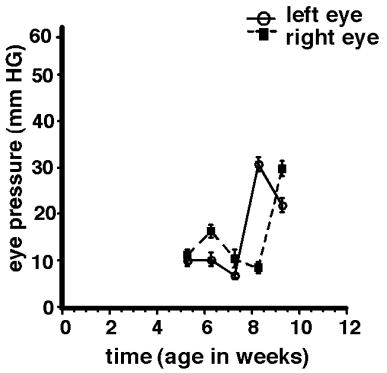
left eye
right eye
eye pressure (mm HG)
60
50
40
30
20
10
0
0
2
4
6
8
10
12
time (age in weeks)

D

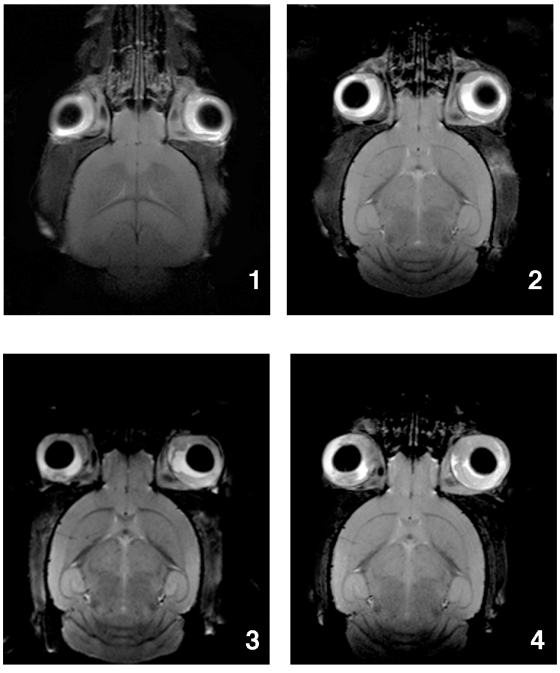
1
2
3
4

E

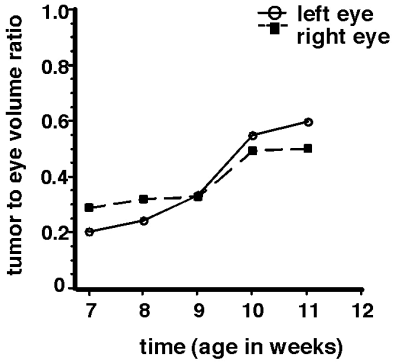
left eye
right eye
tumor to eye volume ratio
1.0
0.8
0.6
0.4
0.2
0
7
8
9
10
11
12
time (age in weeks)

F

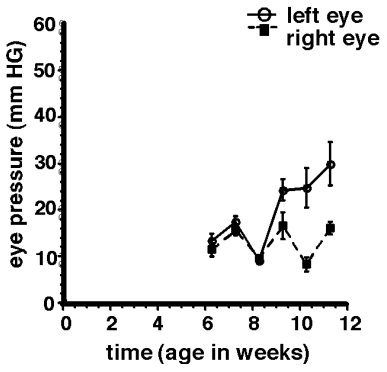
left eye
right eye
eye pressure (mm HG)
60
50
40
30
20
10
0
0
2
4
6
8
10
12
time (age in weeks)

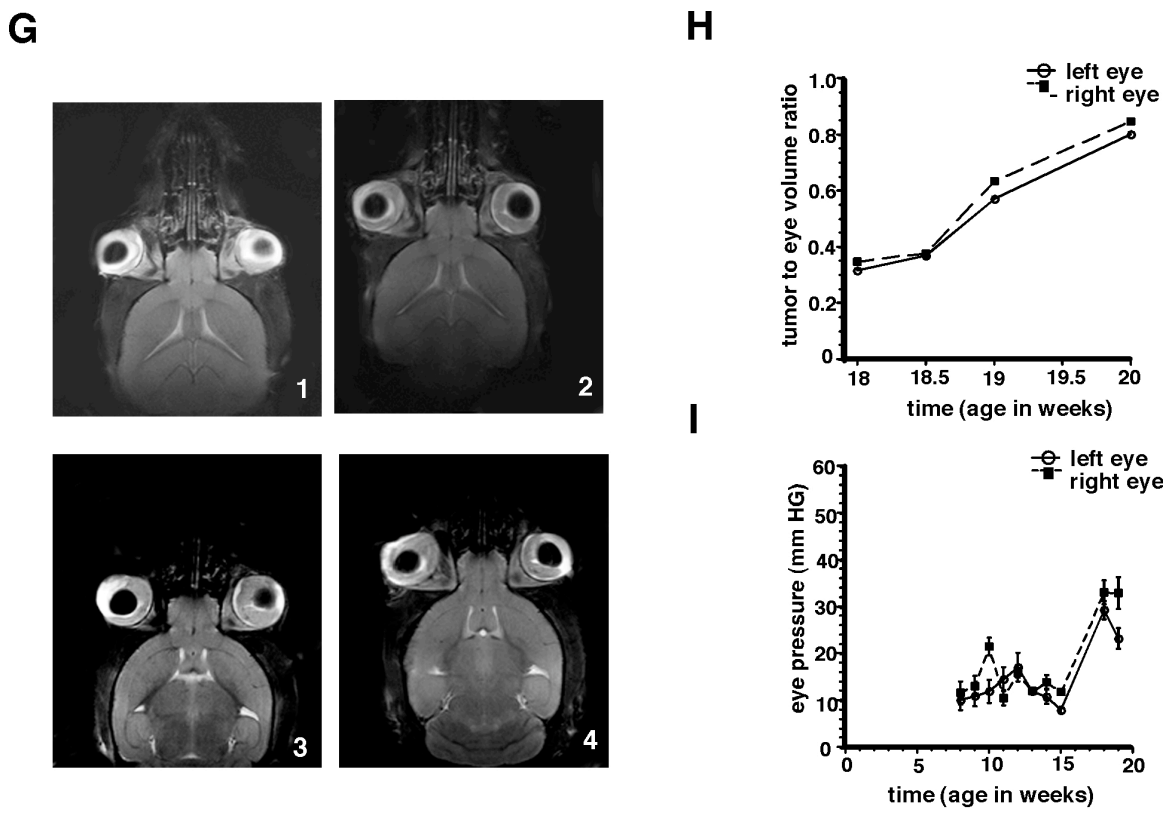

Figure 3-6 (Continued).

IOP was measured for each eye. As previously discussed, the tonometer is a straightforward device to monitor pressure changes in the anterior chamber. The goal was to see if there was a correlation between the extent of endophytic growth and increase in IOP. All eyes studied displayed an increase in IOP when significant tumor invasion into the anterior chamber occurred, prior to ocular rupture **(Fig. 3-6A-I)**.

3.3.2 A comparative volumetric study with ultrasound, MRI and serial sections

The historical approach to studying pathology and size of tumors has been by the invasive histological analyses. While this time consuming technique has been the traditional method for a number of years, we wanted to learn if the software capabilities of MRI and ultrasound would be more efficient and comparable. To answer this question, five eyes from different retinoblastoma models were used to compare these modern techniques to the standard approach. There were some differences in eye to tumor ratio obtained from the three methods **(Table 3-1)**. This data represents that there was good correlation for some of the samples. This is likely due to the difficulty in defining the posterior boundaries of the tumors. An increase in sample number may resolve the slight variability seen.

3.3.3 A longitudinal study using multiple preclinical modalities and mouse models

To understand the role of different genes in tumor progression and growth and their influence on ocular health, eye pressure and vision, six different mouse models were compared. These phenotype studies were carried out with multiple observations using the retina camera, tonometer and optomotry modalities. In general, animals were enrolled at an age of 50 ± 15 days. The majority of the genotypes had 7 to 16 mice. Previous established Kaplan Meier morbidity data was used to estimate age of tumor development. If tumors did not develop when 50% of the animals showed morbidity they were removed from the longitudinal study. Each eye was analyzed independently (7D had 8 samples, 3D had 15 samples, MDMDX had 8 samples, p107s had 16 samples, p53 TKO has 14 samples and Rb TKO had 10 samples). When tumor presence was established by retina camera, the mouse was followed until the eye's rupture was inevitable, then it was humanely sacrificed. Inevitable rupture status was defined as an

Table 3-1. Eye/Tumor Ratios from Three Different Modalities.

Sample	Gold standard eye/tumor ratio	MRI eye/tumor ratio	Ultrasound eye/tumor ratio
Eye 1	0.27	0.29	0.65
Eye 2	0.38	0.23	0.78
Eye 3	0.13	0.38	0.16
Eye 4	0.27	0.21	0.43
Eye 5	0.25	0.21	0.17

increase in IOP, inability to view the posterior chamber with retina camera, gross detection of tumor, an increase in eye size or poor animal health.

To begin the longitudinal study, a retinal camera was used for a visual inspection of the eye's posterior chamber to determine the date of tumor onset detection for each genotype. Mice were monitored approximately every 2 weeks and followed until tumor invaded the anterior chamber and the posterior chamber could no longer be viewed. The majority of genotypes developed tumors approximately at 63 ± 10 days **(Fig. 3-7)**.

More specifically, p107s mice developed tumors at 73 ± 3.6 days old, p53 TKO at 60.3 ± 3.8 days, MDMX at 66 ± 2.3 days old and Rb TKO at 53 ± 2.5 days old. The time of tumor development was similar among p53 TKO, MDMX ^{tg}, p107s and RB TKO groups which were collectively different to 3D($p < 0.001$ to $p < 0.05$). Interestingly the 7D group showed a slight difference of time of onset to all ($p < 0.5$). Interestingly, the 7D and 3D group did not show a significant difference between each other, 114 ± 11.2 and 123 ± 16.3 days old.

The next obvious question was to look at morbidity to see if there were similar differences among groups. As previously mentioned, the morbid status was marked by the time before, imminent eye rupture based on the loss of vision and/or an increase in IOP. Noticeably the first genotype to reach morbid status was Rb TKO at 80.4 ± 8.3 days old; whereas 3D and 7D were the last, at 256 ± 28 and 342 ± 9.2 days old, respectively. Interestingly, the three of the genotypes MDMX, p107s and p53 TKO, were similar in their moribund ages, 105 ± 12, 112 ± 3 and 112.4 ± 9 days old, respectively **(Fig. 3-8)**. There was no significant difference among theses groups; however there was a great difference to these and 7D and 3D genotypes. Even though the 7D and 3D genotypes reached morbid status last, there was a significant difference between them ($p \geq 0.01$).

From the above data sets, the tumor onset to morbid status or tumor progression period was calculated **(Fig. 3-9)**. Tumor progression time was ranked in the following order, from shortest time to the longest, RB TKO (16.8 ± 6 days), MDMX (39 ± 10), p107s (39.4 ± 4.3), p53 TKO (47 ± 7.8), 3D (133 ± 22) and 7D (228 ± 15.3). The groups with rapid tumor progression (MDMX, p53 TKO and p107s) were very similar to each other, except for RB TKO, but very different from 3D and 7D subjects ($p < 0.001$). Additionally the 3D and 7D mice were different from each other ($p < 0.001$). These calculations of the tumor progression period will be helpful in developing an optimal time of treatment for future preclinical studies.

In order to develop a comprehensive preclinical study, the six genotypes' loss of vision was followed using optometry. Interestingly the time of tumor onset did not immediately affect the animals' cone vision. In these cohorts some mice were blind upon enrollment, poor trackers or were uncooperative. Their visual acuity or loss could not be assessed and therefore the animals were not used for these optomotry studies. Upon enrollment age (50 ± 15 days) each eye was tested for a baseline approximately 2 ± 1 times during one week to obtain a baseline. Visual acuity was then assessed approximately every 3 (±1) weeks. Typically animals with advanced tumors were

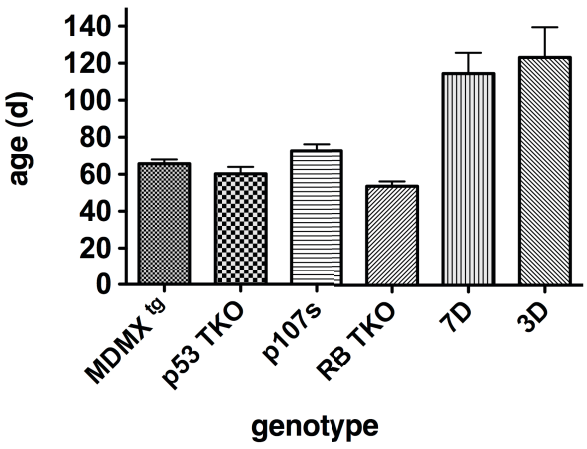

Figure 3-7. Comparison of Age of Tumor Onset.
Tumor detection with retina camera. The y-axis represents the age in days from birth and the y-axis represents each genotype. Data is expressed as mean ± S.E.M. See text for analyses. A one-way ANOVA and a Tukey's correction were used to compare groups. d= day; MDMX ^{tg} (Chx10-Cre- $Rb^{Lox/Lox}$; $p107^{-/-}$;$MDMX^{tg}$); p53 TKO (Chx10-Cre; $Rb^{Lox/Lox}$; $p107^{-/-}$; $p53^{Lox/Lox}$); p107s Rb (Chx10-Cre; $Rb^{Lox/Lox}$; $p107^{-/-}$); RB TKO (Chx10-Cre- $Rb^{Lox/Lox}$; $p107^{-/-}$; $p130^{Lox/Lox}$);7D (Chx10-Cre- $Rb^{Lox/Lox}$; $p107^{-/-}$); 3D (Chx10-Cre- $Rb^{Lox/Lox}$; $p130^{-/-}$).

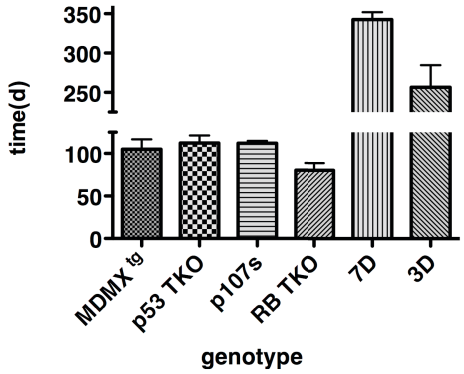

Figure 3-8. Comparison of Morbid Status among Retinoblastoma Mice.
Morbid status for the six different genotypes was defined as imminent ocular rupture. A one-way ANOVA and a Tukey's correction were used to compare groups. d = day; MDMX ^{tg} (Chx10-Cre- $Rb^{Lox/Lox}$; $p107^{-/-}$;$MDMX^{tg}$); p53 TKO (Chx10-Cre; $Rb^{Lox/Lox}$; $p107^{-/-}$; $p53^{Lox/Lox}$); p107s Rb (Chx10-Cre; $Rb^{Lox/Lox}$; $p107^{-/-}$); RB TKO (Chx10-Cre- $Rb^{Lox/Lox}$; $p107^{-/-}$; $p130^{Lox/Lox}$);7D (Chx10-Cre- $Rb^{Lox/Lox}$; $p107^{-/-}$); 3D (Chx10-Cre- $Rb^{Lox/Lox}$; $p130^{-/-}$).

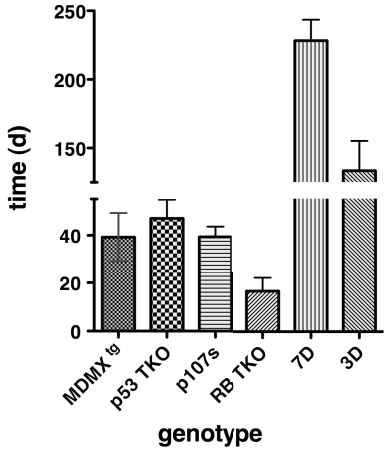

Figure 3-9. Comparison of Tumor Progression Period.
Age at tumor onset and morbid status were subtracted to determine tumor progression period. Data is expressed as mean ± S.E.M. See text for analyses. A one-way ANOVA and a Tukey's correction were used to compare groups. d = day; MDMX ^{tg} (Chx10-Cre-$Rb^{Lox/Lox}$; $p107^{-/-}$;$MDMX^{tg}$); p53 TKO (Chx10-Cre; $Rb^{Lox/Lox}$; $p107^{-/-}$; $p53^{Lox/Lox}$); p107s Rb (Chx10-Cre; $Rb^{Lox/Lox}$; $p107^{-/-}$); RB TKO (Chx10-Cre- $Rb^{Lox/Lox}$; $p107^{-/-}$; $p130^{Lox/Lox}$);7D (Chx10-Cre- $Rb^{Lox/Lox}$; $p107^{-/-}$); 3D (Chx10-Cre- $Rb^{Lox/Lox}$; $p130^{-/-}$).

screened near or on the day of euthanasia. Vision loss was defined as a 50% or greater decrease from the baseline measurement. Eyes were not considered to have a change if vision loss was less than 50%. For the mice that meet the above criteria, the loss of vision occurred in more than 40% of eyes for all genotypes, except the 3D group where about 30% lost vision. The age of enrollment where vision was lost was in the following order, earliest to latest, Rb TKO (16.5 ± 5.5 days), mdmx (20 ± 1), p53 TKO (34 ± 7), p107s (35 ± 11), 7D (51 ± 17) and 3D (168 ± 31.46) **(Fig. 3-10)**. Again the Rb TKO mice had the earliest onset of vision loss and earliest tumor onset (53 ± 2.5 days old); whereas 3D mice were the last group to have an effect on vision, in agreement with their late age of tumor development (123 ± 16.3 days old). The vision loss of 3D was significantly different to the other groups and some to no difference among the others.

Tumor mass can cause an increase in IOP by pressing on the lens and disrupting the anterior fluid (aqueous humor) flow. Ultimately damage of the optic nerves result in blindness. Upon enrollment of a mouse in the longitudinal study (50 ± 15 days) a baseline IOP measurement was taken. There after, IOP measurements (taken in sextuplet) occurred approximately bimonthly. An increase in IOP was defined as 18 mm HG or more. Unlike loss of visual acuity, an increase in IOP occurred in approximately 20-40% of eyes in all genotypes, except the 7D genotype, which never showed an increase in IOP **(Fig. 3-11)**. IOP increase was usually detected with a large increase in tumor mass and immediately prior to a rupture. The p53 TKO (23 ± 7 days) and Rb TKO30 ± 11 days) genotypes showed the earliest increase in IOP, followed by p107s (58 ± 9 days) and MDMX (60 ± 11 days) and finally 3D (176 ± 62 days) **(Fig. 3-12)**.

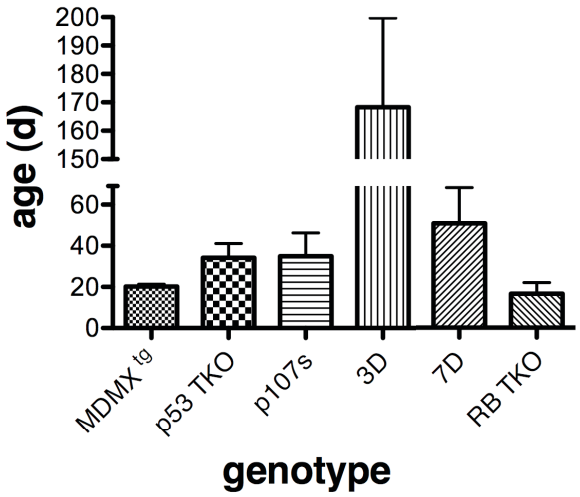

Figure 3-10. Comparison of Age of Vision Loss.
Time (days) for each genotype when vision decrease by at least 50%. Data is expressed as mean ± S.E.M. See text for analyses. A one-way ANOVA followed by a Tukey's multiple comparison test. d = day; MDMX ^{tg} (Chx10-Cre- $Rb^{Lox/Lox}$; $p107^{-/-}$; $MDMX^{tg}$); p53 TKO (Chx10-Cre; $Rb^{Lox/Lox}$; $p107^{-/-}$; $p53^{Lox/Lox}$); p107s Rb (Chx10-Cre; $Rb^{Lox/Lox}$; $p107^{-/-}$); RB TKO (Chx10-Cre- $Rb^{Lox/Lox}$; $p107^{-/-}$; $p130^{Lox/Lox}$);7D (Chx10-Cre- $Rb^{Lox/Lox}$; $p107^{-/-}$); 3D (Chx10-Cre- $Rb^{Lox/Lox}$; $p130^{-/-}$).

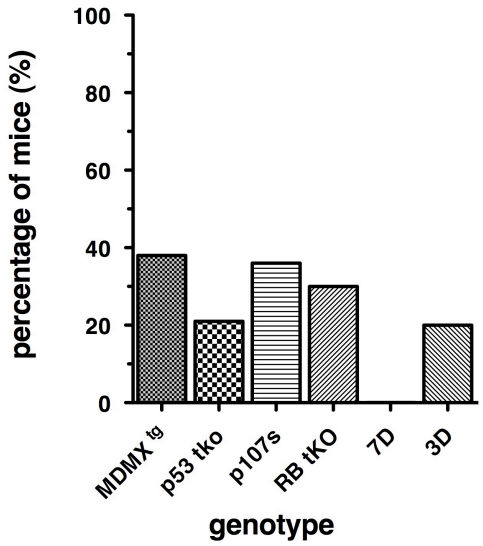

Figure 3-11. Comparison of Percentage of Mice with an Increase in IOP.
Data is expressed as percentage of total mice studied in each genotype. An increase in IOP was never seen in the 7D genotype.

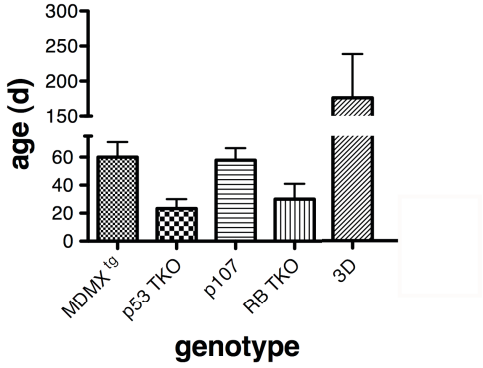

Figure 3-12. Comparison of Age of Increase in IOP Relative to Tumor Detection.
Data is expressed as mean ± S.E.M. See text for analyses. Data determined by one-way ANOVA followed by Tukey's multiple comparison test.

As seen with the loss of visual acuity, the eyes from the 3D genotype were the last to show an increase in IOP and was the greatest difference. From these results, the tonometer data has shown the growth characteristics vary for each genotype**.** In addition, these different mouse models of retinoblastoma allow genetic analysis of a specific gene's contributions to tumor susceptibility, progression and resistance.

In the clinic retinoblastoma patients often have ocular nerve damage and loss of vision due to tumor invasion of the anterior chamber. This invasion causes an increase in IOP. In the presence of a tumor the IOP can change and therefore tumor mice were followed to see if the tumor could be detected with this tool. However, prior to detecting tumors we characterized this modality with wild type animals and various retinoblastoma mice. The wild type mice showed no difference in day-to-day variability or animal-to animal variability. Since all of the retinoblastoma mice are crossed on the RB $^{Lox/Lox}$; p107$^{-/-}$ background we wanted to determine if this genotype's baseline was similar to the wild type findings. We found that they both had similar baselines. When we looked at the tonometer's ability to detect tumors in the p53 TKO group, we found an increase in IOP typically when the tumor could be seen upon gross inspection. In support of this conclusion, a pilot p53 TKO MRI study group (see below) also showed an increase in IOP when tumor invades anterior chamber. Based on these studies it also appears that the IOP increase occurs quickly and precludes an ocular rupture. We concluded that this modality was not effective at detecting early retinoblastomas. In future studies this modality should be used on a weekly bases for tumor animals. For early tumor progression, other modalities should be relied on more heavily

In the clinic, physicians see a decrease in visual acuity with an increase in IOP. Previous studies have shown that the optomotry machine is the standard for visual assessment in wild type mice [132]. We confirmed that visual acuity was consistent over many daily readings in different wild type mice. Reports have found that in the absence of the *Rb1* protein in a developing murine retina, rod photoreceptors fail to develop and could affect cone development [137]. When a small cohort of RB $^{Lox/Lox}$ mice was monitored we found their cone vision was normal. Young tumor prone double knockout 7D mice where followed for multiple days and found to have relatively normal vision. This group was important to monitor since all of retinoblastoma mouse models were breed on this genetic background**.** In addition, some vision loss could in tumor mice could be detected in all genotypes. We concluded that the visual acuity of the tumor-bearing mice could be followed over time, show accurate measurements and could detect tumors sooner than the tonometer.

The most common approached to visualize the posterior chamber of the eye and to detect an early tumor in the clinic is a retina camera**.** Previous reports have developed a reliable procedure to view the fundus posterior chamber in mice with the human Kowa camera fitted with a 78 diopter lens [134]. We confirmed our ability to detect an abnormal retina using a Nr2e3$^{-/-}$ mouse. As expected, the mutant had a marked phenotype of retinal spots all over the fundus, a phenotype originally described by Chang and colleagues [142]. Next, retinoblastoma mouse models were followed over several weeks to test the modality's ability to detect tumor formation. As expected tumors were seen and changes in tumor growth and/or seeding were noted over time. This finding assured us of the retinal camera's comparability to the clinic. The retina

camera is an excellent tool for the tumor onset diagnosis and for following moderately sized tumors.

3.4 CONCLUSION

3.4.1 Modality characterization

While retinoblastoma has been in the research spotlight for nearly 40 years, advancement in clinical treatment has not progressed rapidly. This is due to translational limitations, such as the late development of mouse models and the inability to follow tumors in real time with diagnostic tools. The ability to non-invasively follow tumor development in preclinical models amount other fields, including pediatric renal tube malignancies, neuroblastoma and prostate cancer, has become the standard method in testing new therapies [143-145]. Until recently, similar modalities, tonometer, optomotry, retina camera, ultrasound and MRI, were not readily available to monitor tumor progression in retinoblastoma mice. In this study, we characterized the multiple modalities using several mouse models of retinoblastoma in a noninvasive manner. In addition, these different mouse models of retinoblastoma allow genetic analysis of a specific gene's contributions to tumor susceptibility, progression and resistance.

In the clinic retinoblastoma patients often have ocular nerve damage and loss of vision due to tumor invasion of the anterior chamber. This invasion causes an increase in IOP. In the presence of a tumor in IOP can change and therefore tumor mice were followed to see if the tumor could be detected with this tool. However, prior to detecting tumors we characterized this modality with wild type animals and various retinoblastoma mice. The wild type mice showed no difference in day-to-day variability or animal-to animal variability. Since all of the retinoblastoma mice are crossed on the RB Lox/Lox;p107-/- background we wanted to determine if this genotype's baseline was similar to wild type findings. We found that they both had similar baselines. When we looked at the tonometer's ability to detect tumors in the p53 TKO group, we found an increase in IOP typically when the tumor could be seen upon gross inspection. In support of this conclusion, a p53 TKO MRI study group (see below) also showed an increase in IOP when tumor invades anterior chamber. Based on these studies it also appears that the IOP increase occurs quickly and precludes an ocular future. We concluded that this modality was not effective at detecting early retinoblastomas. In the future studies this modality should be used on a weekly bases for tumor animals. For early tumor progression, other modalities should be relied on more heavily.

In the clinic, physicians see a decrease in visual acuity with an increase in IOP. Previous studies have shown that the optomotry machine is the standard for visual assessment in wild type mice [132]. We confirmed that visual acuity was consistent over many daily readings in different wild type mice. Reports have found that in the absence of the Rb1 protein in a developing murine retina, rod photoreceptors fail to develop and could affect cone development [137]. When a small cohort of RB lox/lox mice was monitored we found their cone vision was normal. Young tumor prone double knockout 7D mice where followed for multiple days and found to have relatively normal vision. This group was important to monitor since all of retinoblastoma mouse models were

breed on this genetic background. In addition, some vision loss could in tumor mice could be detected in all genotype. We concluded that the visual acuity of the tumor-bearing mice could be followed over time, show accurate measurements and could detect tumors sooner than the tonometer.

The most common approached to visualize the posterior chamber of the eye and to detect an early tumor in the clinic is a retina camera. Previous reports have developed a reliable procedure to view the fundus posterior chamber in mice with the human Kowa camera fitted with a 78 diopter lens [134]. We confirmed our ability to detect an abnormal retina using a $Nr2e3^{-/-}$ mouse. As expected, the mutant had a marked phenotype of retinal spot all over the fundus, a phenotype originally described by Chang and colleagues. Next, retinoblastoma mouse models were followed over several weeks to test the modality's ability to detect tumor formation. As expected tumors were seen and changes in tumor growth and/or seeding were noted over time. This finding assured us of the retinal camera's comparability to the clinic. The retina camera is an excellent tool for the tumor onset diagnosis and for following moderately sized tumors.

Over the past few years a number of animal studies using ultrasound and MRI has greatly increased. For many preclinical models in other fields the ultrasound detection is limited by the tumor's location in the body cavity. One advantage of the retinoblastoma tumor is its accessibility by the ultrasound probe. In general, the average wild type inbreed mouse eye is 3.33 mm long and the ultrasound probe can emit waves approximately 4.5 mm [146]. Based on these measurements we expected this modality to be ideal for retinoblastoma detection.

When we scanned the eyes of tumor animals we found several examples of anterior chamber invasion. This promising data correlated well with the clinical detection of tumors using high-frequency ultrasound [147]. Therefore the small rodent ultrasound appears to be fairly compatible to the clinic. Unfortunately, like the clinic the major challenge was the precise detection of the tumor boundaries when near the optic nerve [148]. Based on the probes penetration depth and the average wild type eye's length, good penetration of the posterior chamber was expected; however, this was not the case for the majority of eyes tested. This could be due to the assumption that eye depth is same for all mouse strains, but a more likely reason may be due to the common characteristic of calcification and shadowing which is a leading cause of sound eave obstruction in retinoblastomas [141]. This is a leading cause to sound wave obstruction in retinoblastomas. Even with these drawbacks, the ultrasound's single field of view and the clear detection of the anterior chamber was beneficial.

One unique asset to this imaging modality is its ability to detect tumor blood flow with its Doppler mode. In the clinic, ultrasound can detect tumor vasculature and can be beneficial in the design of a chemotherapy plan. The small animal ultrasound could detect an increase in blood flow in retinoblastoma tumors; however, it was unclear if the variability seen was direct characteristic of the tumor or a technical limitation of this rodent modality. One way to resolve this uncertainty would be to use immunohistochemical markers specific for vessel detection in serial sections. An additional method would be to use contrasting agents as used in the clinic [143]. To our knowledge no study has been completed looking at these agents in the rodent eye. Perhaps as technology improves this will be an added benefit in ultrasound imaging.

A clear, noninvasive image of a single view of retinoblastomas was more challenging than originally expected. To compliment the pervious imaging modalities, the use of the 7T small animal MRI was explored. As mentioned previously, this modality can visualize the orbit, external orbit and the brain [131]. An image more detailed than the clinic was expected due to the doubling of tesla, which increases resolution. The anterior and posterior chambers, as well as the external orbital tissue, could be easily seen in our retinoblastoma mouse models; however, it was impossible to determine if the tumor expanded into the different layers of the eye tissues. This lack of detection could be due to the technologic limitations, such as the tesla strength. To determine if tumor progression could be seen over time a small cohort of retinoblastoma mice, p53 TKO, were scanned weekly for several weeks. When we looked at the individual mouse images, tumor growth progression could be seen qualitatively and quantitatively, by calculating volumes ratios using MRIcro program. From this pilot study we determine that a progression could be seen and quantified easily with MRI.

Tumor volume and size using diagnostic images are typically measured to assess the treatment's success in the clinic. High-resolution microimaging ultrasound has advanced and made it possible to also measure these characteristics in mouse prostate tumors with strong correlation to calculations made by serial sections [144]. Therefore we wanted to determine if tumor volume measured by ultrasound or MRI were comparable to the hand tracing method of volume measurements using histology images. We found that there was correlation between the ultrasound and hand trace, but even less with the ultrasound, which is likely due to the limited number of serial sections tumor's data collected by MRI. Future studies should include a smaller step size for MRI data collection, however due to the poor animals' health this may not be possible because it will increase the time of sedation.

This variation could be a result of many different factors. First, the eye and tumor tissue contain a different level of hydration *in vivo* and *ex vivo*. In addition the histological process often involves several dehydration steps that could alter the volume of the eye when compared to *in vivo* images. This had been commonly seen by researchers who compared ultrasound volume measurements of the kidney to histological sections [145]. Again, one would expect the ratio to correct these differences, but it is important to consider that the tissue shrinkage for the eye could be different for tumor tissue compared to normal tissue. Second, comparison between *ex vivo* imaging, MRI and ultrasound was limited by the definition of clear defined boundaries. This is particular true for the ultrasound where tumor shadowing is common. Third the MRI is known to be the highest soft tissue resolution when compared to ultrasound. After all of these perimeters are taken in consideration, it is not surprising that there is some variation between modalities.

Until recently the retinoblastoma field has had translational limitations, such as the inability to follow tumors in real time with diagnostic tools. In this study, we characterized the multiple modalities using several mouse model of retinoblastoma in a noninvasive manner. While the tonometer is a straightforward tool, it was found to only detect tumors toward prior to ocular rupture. In addition it did not detect tumors if they did not invaded the anterior chamber. Even though the optomotry is heavily dependant on mouse behavior, we found it to provided sound measurements and was useful in

showing the tumor's progression on vision loss. The retina camera's detection of early tumor mass was found to be highly superior to the previous modalities. The other imaging tools, MRI and US, strength was in imaging the tumor and eye in one field of view. The ultrasound allowed good imaging of the anterior chamber. In addition it could detect blood flow in some of the tumors. Tumors could be detected much sooner using MRI. We concluded that MRI shows tumor progression over time, measure volume, but also predicts tumor presence prior to tumor detection by tonometer. Finally, the comparison of MRI and US volume data sets to histological hand tracing data correlated better with the MRI than the US.

3.4.2 Longitudinal study

Tumor onset was identified with the retina camera, which provided the earliest detection. Observation of all six genotypes of retinoblastoma mouse models concluded that the age of tumor onset was similar for MDMX, p53 TKO, Rb TKO and p107; however, tumor onset was delayed in the two double knockout groups, 3D and 7D. Similar results were found for the age of morbidity. Triple knockout mice were younger at the time of morbidity status (80-100 days) than the 3D and 7D double knockout (morbid status > 200 days old). It is important to note that there was difference between these double knockout groups with 7D mice being the last to die. It is also important to note that there is some variability with these two genotypes. This could suggest heterogeneity for mice that have only two genes deleted perhaps due to genomic instability. Logically tumor progression period followed suit to this pattern and in particular we found that the Rb TKO had the shortest progression period. This suggests insult to all three Rb family members greatly increases tumor progression; thus reinforcing the common held belief that an increase in the genomic instability leads to an aggressive cancer.

In addition, vision loss was monitored throughout the animal's life span. As previously mentioned, vision loss was defined as a loss of at least 50% the individual baseline for each eye. Of the six genotypes, 40% of all enrolled eyes have a vision loss, except 3D group. This did not include eyes that were blind at the beginning. It is important to note that the blind eyes were not specific to one particular genotype. This blindness could be due to small genetic lesions that could not have been detected with retina camera until they were full-blown tumors. It is also important to note that animals that did not have a 50% reduction in visual acuity were not considered to have vision loss. This could be due to the fact that the mouse's eye does not have a fovea, a cluster of cone cells, therefore a degrees of vision may still be possible based on tumor placement. Perhaps more important to note is that the measurements were done every three weeks. While it would be ideal to measure visual acuity more often, the time constrains and manpower made this impossible for the number of enrolled animals.

Typically it is seen that the intraocular pressure increases when the tumor mass invades the anterior chamber and presses on the lens or a small tumor seed blocks then flow of fluid drainage. An increase in IOP was defined at 20 ± 2 mm HG. We found that 20-40% of eyes had an increase in IOP from all genotypes, except the 7D groups. This was expected from previous studies, which showed no anterior invasion with this model [110]. Again the triple knockout mice show an increase in IOP the earliest.

Triple knockout mice were younger at the time of morbidity status and the tumors were more aggressive than the 3D and 7D double knockouts. Of the double knockouts 7D was the least aggressive than the 3D and 7D double knockout. Of the double knockouts 7D was the least aggressive. We found the most aggressive genotype to be Rb TKO. Its short progression period suggested that insult to all three Rb family members greatly increases tumor progression. Of the six genotypes, 40% of all enrolled eyes had a vision loss (50% decrease form baseline), except for the 3D group. This could be due to the fact the mouse's eye does not have a fovea and some vision could still be possible based on tumor placement. However more frequent monitoring, other than every three weeks, may improve this percentage. Additionally a small portion of eyes had an increase in IOP in all genotypes, except the 7D group. To date in the clinic there is little evidence that relates the retinoblastoma tumors; phenotypes to related to specific gene mutation. As more human enucleated tumors are studies, insight will be gained and further therapeutic can be designed based on preclinical studies.

By using the above modalities in this collective we have shown that similar clinical tests could be used to characterized and monitor tumor progression in models of retinoblastoma in mice. We found all the five of the modalities to fully understand the picture of tumor progression and its growth pattern. This is the first time that any of these tools have been used in the characterization of retinoblastoma tumors. Along with gene array studies of the tumors in the retinoblastoma models these tools could give a comprehensive picture of specific gene involvement in tumor progression and phenotype.

CHAPTER 4. DISCUSSION AND FUTURE DIRECTIONS

4.1 PHARMACOKINETIC STUDIES

The administration of carboplatin and topotecan, as single agents, has been successfully tolerated in the retinoblastoma pediatric population [65, 67]; however, the long-term success rate for tumor treatment with the single agent, carboplatin, has not been promising. Therefore additional therapy or therapeutic agents are needed. To explore different drug combinations and the effects of a subconjunctival injection in our preclinical rodent model, we performed multiple pharmacokinetic and pharmacodynamic experiments in juvenile rats. From these studies we found that there was greater drug exposure to the vitreous with a subconjunctival injection. The subconjunctival data suggested there was an increase drug exposure to the vitreous in the presence of the tumor.

This finding is likely due to the physiological changes in the eye, such as vasculature, disruption of the blood-retinal-barrier, the pressure dynamics or the amount of vitreous present. Increase in vessels could affect the drug concentration either by an increase in concentration or a decrease in concentration. Our data shows an increase in drug concentration. Ultimately it is essential to determine if there are indeed more vessels. This could be done with immunohistochemical analyses on dissected eyes of tumor and non-tumor rats [149]. Alternatively the ultrasound Doppler function could identify an increase in vascular presence in a rat eye. Additionally, fluroescein angiography could be used to image vessels and compare tumor and non-tumor eyes. If these methods show an increase in vascular drug concentration, it could be affected three different ways. First, more vessels could result in an increase of drug delivered to the eye, however this is unlikely since tumor vascular systems are often inefficient. Second, the increase in vessels could move the drugs into the systemic circulatory system more rapidly. From our data this appears not to be the case since both carboplatin and topotecan pharmacokinetic experiments in tumor animals showed an increase drug in the vitreous. Lastly, the increase in vessels, which are likely to be leaky and disorganized, could prevent the drug from leaving the eye. An increase in new, and perhaps poorly formed, vessels would support the conclusion of the difference in drug concentrations.

Alternatively the increased vessels could have a greater vascular permeability or leakiness could result in an increase the concentration. Recently there have been reports suggesting permeability could increase the concentration of molecules [149]. An indirect way to answer this question is to do a pharmacokinetic study and compare, intravenous delivery of drugs to the subconjunctival studies in tumor bearing rats. If an increase in drug exposure to the vitreous is seen, as in subconjunctival injections, it is likely that the increased permeability is the result. However, if this pharmacokinetic study does not show an increase in drug exposure this could suggest that the vessels are not leaky.

Additionally the tumor could affect protective barriers of the eye, such as the blood-retina-barrier either by the tumor release of growth factors or actual growth into it. Tumors release a number of growth factors, such as VEGF, to be advantageous to their

survival. The blood-brain-barrier is often compared to the retina-brain-barrier. Previous reports have suggested that the VEGF disrupts the brain's barrier in the rat by increasing the permeability to drugs [150]. Since it is similar to blood-retina-barrier, this could also affect the drug exposure to the eye. To explore this further, antibody markers could be used to detect the growth factor in the eye's barrier. On the other hand, the actual growth of the tumor into the barrier could affect the tissue integrity and thus the protection. Assessment of tight junction proteins would give some insight to this idea. In addition, histological analyses and electron microscopy could give a gross idea of the potential changes. If there were disruptions in the barrier we would expect the layers to be non-homogenous.

Alternatively the internal or external pressure dynamics of the tumor or the injection could affect the drug exposure to the vitreous. Olsen and colleagues suggested an increase in IOP by decreasing the sclera-choroid-retina permeability [151]. Pressure gradients are greater in the presence of a tumor, which would result in a decrease the transscleral diffusion; however an increase in drug concentration was seen in our tumor modal. On the other hand, the external pressure from the subconjunctival injection could be the cause. If this were true the non-tumor bearing would have a higher drug concentration than tumor bearing rats. This is contrary to our data findings. Additionally the anterior pressure change could affect the clearance of the drug from the eye. This pathway is thought to be one of the potential routes of drug clearance. Finally, more simply, pressure dynamics could indirectly affect the cellular junctions of the barriers, leading to less selective barriers and increasing the drug concentration in the tumor rats.

The final idea could be due to the vitreous volume. There is less vitreous in the tumor eye and therefore the drug is less diluted, causing an increase in concentration. One simple way to determine if this explanation is correct, is to measure the vitreous fluid both the tumor and non-tumor bearing animals. If there is less vitreous in the tumor eyes this may be the cause of the data increase in drug concentration.

Additionally we looked at the drug exposure to the contralateral untreated eye with pharmacokinetic experiments. We found the untreated eyes were exposed to the drugs, but at a lower concentration than the treated eye. We suggested the contralateral exposure was due to the uptake of drug by the systemic circulation. This conclusion was supported by untreated eye's AUC ratio of vitreous/plasma was similar to previous systemic pharmacokinetic studies [60]. To confirm that the contralateral eye is exposed by the system an additional postmortem pharmacokinetic experiment could be carried out as Carcaboso and colleagues [152]. Rats could be sacrificed just prior to the subconjunctival injection and samples would we harvested a couple hours after administration [152]. If the contralateral eye exposed by the systemic circulation, we would expect the postmortem untreated eye to be drug free.

Additionally, our data suggests the treated eye has higher drug concentration than the untreated eye, suggesting a transscleral mechanism. Two observations support this idea. One, the vitreal AUC ratios are higher with the treated compared to untreated eyes. Two, the plasma AUC values of subconjunctival injections was less than the intravenous injections [60]. However, further exploration needs to be carried out to learn about the drug transport with subconjunctival injections of topotecan and carboplatin. More conclusive experiments would include an experiment where the

choroid vasculature is disrupted with freezing or heating the vessels. This would allow us to isolate the subconjunctival mechanisms. Additionally, a window administration of the drug in the subconjunctival space would allow the study of the choroid vascular influence.

Lastly, we found the vitreous was exposed to a greater concentration of carboplatin and topotecan in the presence of a tumor. Previous intravenous pharmacokinetic experiments with carboplatin and topotecan were only studied in non-tumor barrier animals [60]. To better recapitulate the pharmacokinetics in a retinoblastoma model with intravenous injection, it would be of interest to determine if vitreal concentration also increased in the presence of a tumor. Based on our current studies and clinical reports, we would expect a tumor to also increase the vitreal drug exposure with a intravenous injection [153].

4.2 ALTERNATIVE RAT MODELS FOR PHARMACODYNAMIC STUDIES

The understanding of a drug's pharmacokinetic properties leads to the comprehensive understanding of a drug when pharmacodynamic experiments are also carried out. The previous tumor response studies were carried out in our orthotropic rat xenograft model. We found tumor stability and reduction occurred in animals that were treated with an AUC guided dose. One limitation of this experiment was the length of the study. In these studies, rats developed detectable tumors quickly. This rapid increase in tumor mass is likely a result of the 33 hour doubling time of the Y79 cells [154]. After tumor detection rats could only be followed for 7-10 days before ocular rupture of untreated animals was inevitable or the limit of detection was reached with the Xenogen software. The use of an alterative retinoblastoma cell line, with a slower doubling time, could be engineered with the luciferane report gene. The well-characterized retinoblastoma Weri cell line is an ideal choice for two reasons. First, the original characterization found its doubling time to be approximately 4 days which would allow the study to be carried out for a longer period of time [154]. Second, the line was recently discovered to have the common genetic lesion, an over application of MDMX, in the p53 pathway [125]. Thus using WERI cells would give a better understanding of how retinoblastomas respond to chemotherapeutics and allow the potential of a long-term study so the schedule of drug delivery could also be investigated.

4.3 PRECLINICAL STUDIES AND CONSIDERATIONS

4.3.1 Preclinical studies

The major challenge in developing new protocols for pediatric cancers is the small patient population. The use of preclinical rodent models can accelerate the development of new therapies and combinations. Prior to conducting a study there are many model considerations that need to be addressed. The tumor needs to have the same genetic lesions as found in the human disease, the same tumor phenotype therapeutic response used in humans, time to evaluate the therapy, an endpoint of study

and a way to monitor the tumor response [155]. In meeting all of these conditions a proper noninvasive longitudinal preclinical study can have great predicative strength.

With these considerations, the present extensive pharmacological studies in the rat, proper calculations for the drug dose and characterization of multiple modalities were used to carry out a preclinical study in two of our mouse models. Enrolled mice received the drug combination of a subconjunctival injection of carboplatin and an i.p. injection of topotecan (daily x 5) on a clinical schedule (0.7 mg/kg and 0.1 mg/kg for five days). After the six rounds of therapy, similar to the clinic, it was found that thirteen of the eyes had either partial to full response or stable disease. Surprisingly the use of only two agents and no focal therapies showed promising results. Previous studies in the clinic have shown that focal therapy can help in tumor response. Even though focal therapy was not used in the current preclinical mouse study, it may provide an added benefit. Since our results predict good response in the rat and mouse model, the focal treatment may be a good alternative to the three-drug protocol with focal therapies currently used in the clinic. This would lessen systemic exposure, which would be significantly beneficial to children with germline mutations.

An additional preclinical study with the added focal therapy could confirm this proposal, which would likely expedite the translation time to the clinic. Other preclinical studies with retinoblastoma mouse models have used focal therapies, such as EBRT and cryotherapy, and found them to disrupt the blood-ocular barrier, increasing drug delivery [64, 118, 156]. Ideally, the use of cryotherapy is more attractive than EBRT due to the risks to patients with germline mutations. From these studies it is likely that the systemic delivery will be enhanced greater than the subconjunctival delivery [64, 157]. This would allow a better penetration of topotecan (daily x 5) and may increase the response seen in the preclinical mouse study. To date there have been no reports of two chemotherapy drugs and focal therapy delivery in preclinical retinoblastoma studies and therefore it is of interest to explore this combination.

4.3.2 Preclinical considerations

Organ and animal development is important to fully understand because it affects the pharmacokinetics of a drug. Surprisingly this is often overlooked in preclinical and clinical trials. Typically the clinic has treated children as small adults with dose levels adjusted only based on body weight or surface area [158]. This approach fails to recognize the different developmental stages and can be lead to toxicity. Many species, including humans, have significant postnatal development, organogenesis, increase in plasma protein concentration and drug transporter protein development [155]. These changes are important to consider for each pharmacokinetic stage: absorption, distribution, metabolism and elimination (ADME).

The toxic effects of drugs can occur at any one of the four above pharmacokinetic phases. As previously mentioned in our study group, rats which received carboplatin i.p. and topotecan subconjunctival experienced toxicity after a few days. Since death was not immediate the toxicity is likely due to the drug's elimination. Carboplatin's primary clearance organ is the kidney. As in human newborns, there is significant nephrogenesis postnatally in the rat [159]. To determine if the kidney was the

culprit for carboplatin's toxicity different perimeters, such as the glomerular filtration rate, gross inspection with H and E staining and expression drug transporters could be measured. The filtration rate is the traditional method to measure renal and evaluate maturation. Interestingly a comprehensive study of kidney development in rats found its maturation was completed at eight weeks of age [160]. Today exogenous markers, such as creatinine, in the blood or urine are measured over a period of time [159]. Given this previous study and our chemistry results in our rats, young than 8 weeks of age, it is likely that they did not have necessary filtration rate, which could have affected the animals' clearance and overall exposure to the drug.

However, it is more important to look at the to the developmental changes affecting the glomerular filtration rate closer, such as the ontogeny of drug transporters. They play a critical role in kidney function or transport. In general, the number of transporters increases absorption or elimination of a xenobiotic. In brief, the renal transport takes place in the tubules where different transporters are located on the basolateral membrane and the apical sides. Xenobiotics are absorbed from the blood on the basolateral side and either removed by the urine or effluxed back into the body [161]. Each drug is a substrate for specific transporters. The transporters for carboplatin are multidrug resistance protein 2, copper transporter receptor 1 and organic cation transporter 1: whereas, the topotecan is a substrate for p-glycoproteins, multidrug resistance-protein 1 and breast cancer resistance protein [162, 163]. Typically when the blood with carboplatin passes the basolateral side of renal tubules, it is primarily absorbed by the organic cation transport 1 [159]. Interestingly the developing rat kidney does not have a high expression of organic cation transporter mRNA doesn't fully mature until six weeks of age [164]. Decreased expression of organic cation transporter 1 could result in a slow elimination of the drug and thus increase exposure of carboplatin. The other transporters, multidrug resistance protein 2 and copper transporter, are also expressed at levels that are greater than adult and may, theoretically, compensate for the lack of organic transporter 1 elimination [158]. In addition, it is necessary to consider the transporters for topotecan, since both drugs are given at the same time. Previous publications have found that mRNA expression of two of three transporters (multidrug resistance protein 1 and breast cancer resistance protein) in the kidney are greater as an adult than at birth; however, previous reports have suggested that p-glycoprotein reach full mature levels at approximately two weeks of age [158]. While these finding help guide us to the cause of toxicity, all of these studies only measured the mRNA levels and not protein expression. Therefore it would be necessary to measure protein expression of the various transporters in our model's kidney to fully understand the pharmacokinetic properties of our model.

An additional developmental factor that could affect pharmacokinetics is the plasma protein and albumin concentrations, which both affect the bioavailability. Typically a circulating drug has two different states, bound and unbound. Unbound drug is the amount of drug that is active and available to carry out its function; whereas, the bound drug is unavailable to be active because it is bound to circulating proteins. Each drug has a different affinity for the plasma proteins, which can affect their available concentration. Zwart and colleagues looked at these levels in rats younger than six weeks and found that they are nearly half that of an adult level [158]. While this is an interesting developmental parameter to consider it is unlikely that this is the cause of the

toxicity we observed. Both carboplatin and topotecan have a low affinity for plasma proteins and therefore this development would not be an influencing factor.

4.4 DIAGNOSTIC APPROACHES

Characterization of the five modalities, tonometer, optomotry, retina camera, ultrasound and MRI, strengthened our tumor progression studies; however, we were surprised by their limitations. In the clinic, IOP changes are used to monitor tumor progression; however, with the rodent tonometer, early tumor detection was not seen, as seen in a comparison of tumor development using MRI and tonometer. Additional longitudinal studies of tumor progression in various genotypes also did not show a gradual increase in IOP. This difference seen between the human and rodent indentation tonometer system could be a result of species difference in eye pressure and anterior fluid regulation. Thus our data suggests it is not a good tool to measure the progression of retinoblastomas. Traditionally the alternative method to measure IOP is with cannulation; however, this is not ideal for mice with retinoblastoma because of a microneedle. This could lead to tumor dissemination [165]. Therefore, we conclude that the tonometer may a good supportive tool for late stage tumor anterior invasion.

Even though optomotry did showed a more gradual decrease in vision with tumor progression, this modality strongly depends on the behavior of mice and limited to a four hour testing time. These restrictions led to a three-week schedule of visual assessment. This modality may have shown more heterogeneity between retinoblastoma genotypes if the animals could have been measured more frequently. We defined vision loss as a 50% decrease from the baseline vision. Interestingly not all of the mice showed reduction in vision. This may have been due to the frequency of monitoring, but more likely to the tumor's location in the eye or the lack of anterior invasion not causing severe nerve damage. It would be ideal to conduct a longitudinal study with visual assessment with imaging, such as ultrasound and MRI.

Of the modalities, the retina camera detected tumors the earliest and was used to define tumor onset for each genotype (see below). The noninvasive technique also had limitations. From our data, tumors were detected in 3D and 7D genotypes at the same time, approximately at sixteen weeks of age; however previous histological analysis studies have shown genetic lesions beginning as early as two weeks in the 7D genotype [110]. Similarly, we found the p53 TKO genotype's tumor onset to be around nine weeks of age, whereas earlier histological studies found the tumors to be present as early as six weeks of age [4]. Further comparison of the two methods with the additional genotypes would give a clear understanding of this modality's limits. Nonetheless, retina camera's tumor detection is noninvasive and therefore ideal for preclinical longitudinal studies.

Additionally volume comparison studies between ultrasound, MRI and hand-trace BioQuant were conducted to determine if the noninvasive methods were comparable to the traditional hand tracing of serial sectioning. We found some correlation between the eye tumor ratios of the three ways. The difference could be due to a couple of factors. First, the MRI scans consisted of a lower density of slices. The majority of the scans, that had clear tumor and eye margins, were only about 3-5 image slices for each animal.

Second, the MRI images are based off of the proton environment, not absolute tissue density like the ultrasound modality. Perhaps, a longer scan session for MRI data acquisition is likely to increase the number of slices thus improving the tumor volume measurements. In addition, further exploration with enhancing dyes for both ultrasound and MRI would provide clear tumor/ eye boundaries and thus lead to confident distinctions would be beneficial in that they could improve tumor detection parameters.

4.5 LONGITUDINAL STUDY OF TUMOR PROGRESSION

The different tumor phenotypes seen in the six genotypes were likely to be a result of the combination of the different deleted genes. The retinoblastoma gene family is unique in that it has different temporal expression levels and roles, either redundant or compensatory. Previous developmental data has shown that p107 can compensate for the loss of RB [166]. Interestingly this compensation is only possible if both copies of the p107 gene are intact. In addition, the p130 protein provides additional protection from tumors in the postnatal developing mouse eye. In the same study, Donovan and colleagues found that p130 function is redundant to that of RB. To get a better understanding of how the loss of different genes could affect the tumor phenotypes, a longitudinal study with six different retinoblastoma genotypes was conducted.

In our current study, we looked at tumor onset, progression and morbidity to get an understanding of potential roles of the various deleted genes in the phenotypes of retinoblastoma. These differences are likely due to the different combination of deleted genes, creating genetic instability, uncontrolled cell growth leading to potential tumors. It is well known that a cell needs at least two genetic hits to reach this state, however with more mutations the cells, generally, becomes more instable. Given this, it is not surprising that the double knockout mice, 7D and 3D, had the latest age of tumor onset. And as expected the mice with the greater number of gene deletions took less time to develop tumors (RB TKO, p53 TKO, p107s and $MDMX^{tg}$). Interestingly, the 7D and 3D groups developed tumors the around the same time, but time it took for tumors to progress and mice reach morbid status was different. Tumors in the 3D mice progressed faster, thus leading to a younger morbid age than the other double knockout group. In the 3D group p107 compensated for RB1 loss, whereas the late detection of the 7D tumors is likely due to the redundant nature of p130 for RB1. As for the other genotypes, p53 TKO, p107s and $MDMX^{tg}$, there was little to no difference in the progression and time to reach morbid status. This is not surprising for the p53 and $MDMX^{tg}$, since the over amplification MDMX prevents p53 from activating downstream targets, similar to the deletion of p53. In addition, early reports of histological analyses found there to little difference in the tumor morphology [125]. Interestingly, with only one intact copy of p107, the p107s group tumors' phenotype was similar. Even though p107 is haploinsufficient it did impact tumor development [166]. This may suggest that the one copy still has some cell cycle control that affect the tumor progression and morbidity. The RB TKO group had similar tumor onset age to the other triple knockouts, but the time for the tumor to progress and morbid age was the earliest. Therefore, the loss of all RB family members, thus complete loss of cell cycle control, lead to fast and aggressive tumors. While this analyses are informative, they are not conclusive can be strengthened with genetic studies on the tumors and compared to human tumors. These would include microarray analyses, comparative genomic hybridization and SKY assay.

My graduate thesis work has addressed two specific issues relevant to the assessment and development of preclinical approaches for the treatment of retinoblastoma. First, I conducted a preclinical study looking at the combination of a local and systemic administration of carboplatin and topotecan. I found a local injection could increase the drug exposure in the vitreous and decrease systemic exposure. This is an important finding for children with the germline mutation. In addition, an ideal combination of two well-studied board spectrum chemotherapy agents, carboplatin in the subconjunctival space and topotecan i.p., has shown good tumor response with minimal systemic and local toxicity. I have also optimized the use of clinical modalities for mice and determined tumor progression in various models. Not only does this non-invasive longitudinal study make the preclinical research truly translational, but also gives a sense of retinoblastoma growth and progression in various mouse models of retinoblastoma. These finding will lay the foundation for future preclinical studies and help define the role of different genes in retinoblastoma tumor formation.

LIST OF REFERENCES

1. Nemeth, K.M.et.al., *Improved retinoblastoma treatment using subconjunctival carboplatin and systemic topotecan in preclinical models.* Cancer, 2010 (in press).
2. Vander, A., J. Sherman and D. Luciano, *Human Physiology*. 8 ed. 2001, New York: McGraw-Hill Higher Education. 800.
3. Snell, R.S. and M.A. Lemp, *Clinical Anatomy of the Eye*. 2 ed. 2007, Malden: Blackwell Publishing. 423.
4. Dyer, M.A. and R. Bremner, *The search for the retinoblastoma cell of origin.* Nat Rev Cancer, 2005. **5**(2): p. 91-101.
5. Bill, A., *Blood circulation and fluid dynamics in the eye.* Physiol Rev, 1975. **55**(3): p. 383-417.
6. Turner, D.L. and C.L. Cepko, *A common progenitor for neurons and glia persists in rat retina late in development.* Nature, 1987. **328**(6126): p. 131-6.
7. Turner, D.L., E.Y. Snyder and C.L. Cepko, *Lineage-independent determination of cell type in the embryonic mouse retina.* Neuron, 1990. **4**(6): p. 833-45.
8. Schoenwald, R.D., et al., *Ophthalmic bioequivalence of steroid/antibiotic combination formulations.* Biopharm Drug Dispos, 1987. **8**(6): p. 527-48.
9. Cepko, C.L., et al., *Cell fate determination in the vertebrate retina.* Proc Natl Acad Sci U S A, 1996. **93**(2): p. 589-95.
10. Burkhart, D.L. and J. Sage, *Cellular mechanisms of tumour suppression by the retinoblastoma gene.* Nat Rev Cancer, 2008. **8**(9): p. 671-82.
11. Nevins, J.R., *The Rb/E2F pathway and cancer.* Hum Mol Genet, 2001. **10**(7): p. 699-703.
12. Classon, M. and N. Dyson, *p107 and p130: versatile proteins with interesting pockets.* Exp Cell Res, 2001. **264**(1): p. 135-47.
13. Stengel, K.R., et al., *Retinoblastoma/p107/p130 pocket proteins: protein dynamics and interactions with target gene promoters.* J Biol Chem, 2009. **284**(29): p. 19265-71.
14. Donovan, S.L. and M.A. Dyer, *Regulation of proliferation during central nervous system development.* Semin Cell Dev Biol, 2005. **16**(3): p. 407-21.
15. Sparkes, R.S., et al., *Regional assignment of genes for human esterase D and retinoblastoma to chromosome band 13q14.* Science, 1980. **208**(4447): p. 1042-4.
16. Mannermaa, E., K.S. Vellonen and A. Urtti, *Drug transport in corneal epithelium and blood-retina barrier: emerging role of transporters in ocular pharmacokinetics.* Adv Drug Deliv Rev, 2006. **58**(11): p. 1136-63.
17. Godbout, R., et al., *Somatic inactivation of genes on chromosome 13 is a common event in retinoblastoma.* Nature, 1983. **304**(5925): p. 451-3.
18. Friend, G., *Correction of iatrogenic floating toe following resection of the base of the proximal phalanx.* Clin Podiatr Med Surg, 1986. **3**(1): p. 57-64.
19. Carlson, R.W., et al., *Late consolidative radiation therapy in the treatment of limited-stage small cell lung cancer.* Cancer, 1991. **68**(5): p. 948-58.
20. Weinberg, R.A., *The retinoblastoma protein and cell cycle control.* Cell, 1995. **81**(3): p. 323-30.
21. Knudsen, E.S. and K.E. Knudsen, *Retinoblastoma tumor suppressor: where cancer meets the cell cycle.* Exp Biol Med (Maywood), 2006. **231**(7): p. 1271-81.

22. Knudson, A.G., Jr., *Mutation and cancer: statistical study of retinoblastoma.* Proc Natl Acad Sci U S A, 1971. **68**(4): p. 820-3.
23. Friend, S.H., et al., *A human DNA segment with properties of the gene that predisposes to retinoblastoma and osteosarcoma.* Nature, 1986. **323**(6089): p. 643-6.
24. Harbour, J.W., et al., *Abnormalities in structure and expression of the human retinoblastoma gene in SCLC.* Science, 1988. **241**(4863): p. 353-7.
25. Ellsworth, R.M., *The practical management of retinoblastoma.* Trans Am Ophthalmol Soc, 1969. **67**: p. 462-534.
26. Chintagumpala, M., et al., *Retinoblastoma: review of current management.* Oncologist, 2007. **12**(10): p. 1237-46.
27. Shields, C.L., et al., *Practical approach to management of retinoblastoma.* Arch Ophthalmol, 2004. **122**(5): p. 729-35.
28. Kaste, S.C., et al., *Retinoblastoma: sonographic findings with pathologic correlation in pediatric patients.* Am J Roentgenol, 2000. **175**(2): p. 495-501.
29. de Graaf, P., et al., *Retinoblastoma: MR imaging parameters in detection of tumor extent.* Radiology, 2005. **235**(1): p. 197-207.
30. Reese, A.B. and R.M. Ellsworth, *Management of retinoblastoma.* Ann N Y Acad Sci, 1964. **114**: p. 958-62.
31. Chantada, G., et al., *A proposal for an international retinoblastoma staging system.* Pediatr Blood Cancer, 2006. **47**(6): p. 801-5.
32. Albert, D.M., *Historic review of retinoblastoma.* Ophthalmology, 1987. **94**(6): p. 654-62.
33. Stallard, H.B., *Irradiation of retinoblastoma (glioma retinae).* Lancet, 1952. **1**(6717): p. 1046-9.
34. Schueler, A.O., et al., *High resolution magnetic resonance imaging of retinoblastoma.* Br J Ophthalmol, 2003. **87**(3): p. 330-5.
35. Roarty, J.D., I.W. McLean and L.E. Zimmerman, *Incidence of second neoplasms in patients with bilateral retinoblastoma.* Ophthalmology, 1988. **95**(11): p. 1583-7.
36. Eng, C., et al., *Mortality from second tumors among long-term survivors of retinoblastoma.* J Natl Cancer Inst, 1993. **85**(14): p. 1121-8.
37. Kupfer, C., *Retinoblastoma treated with intravenous nitrogen mustard.* Am J Ophthalmol, 1953. **36**(12): p. 1721-3.
38. White, L., *Chemotherapy in retinoblastoma: current status and future directions.* Am J Pediatr Hematol Oncol, 1991. **13**(2): p. 189-201.
39. White, L., *Chemotherapy for retinoblastoma: where do we go from here? A review of published literature and meeting abstracts, including discussions during the Vth International Symposium on Retinoblastoma, October 1990.* Ophthalmic Paediatr Genet, 1991. **12**(3): p. 115-30.
40. Gery, S., et al., *Ovarian carcinomas: CCN genes are aberrantly expressed and CCN1 promotes proliferation of these cells.* Clin Cancer Res, 2005. **11**(20): p. 7243-54.
41. Kingston, J.E., et al., *Results of combined chemotherapy and radiotherapy for advanced intraocular retinoblastoma.* Arch Ophthalmol, 1996. **114**(11): p. 1339-43.
42. Abramson, D.H. and C.M. Frank, *Second nonocular tumors in survivors of bilateral retinoblastoma: a possible age effect on radiation-related risk.* Ophthalmology, 1998. **105**(4): p. 573-9; discussion 579-80.

43. Servodidio, C.A. and D.H. Abramson, *Acute and long-term effects of radiation therapy to the eye in children.* Cancer Nurs, 1993. **16**(5): p. 371-81.
44. Shields, C.L., et al., *Plaque radiotherapy in the management of retinoblastoma. Use as a primary and secondary treatment.* Ophthalmology, 1993. **100**(2): p. 216-24.
45. Shields, J.A., et al., *Plaque radiotherapy for residual or recurrent retinoblastoma in 91 cases.* J Pediatr Ophthalmol Strabismus, 1994. **31**(4): p. 242-5.
46. Abramson, D.H. and R.M. Ellsworth, *The surgical management of retinoblastoma.* Ophthalmic Surg, 1980. **11**(9): p. 596-8.
47. Shields, C.L., et al., *Combined chemoreduction and adjuvant treatment for intraocular retinoblastoma.* Ophthalmology, 1997. **104**(12): p. 2101-11.
48. Gallie, B.L., et al., *Chemotherapy with focal therapy can cure intraocular retinoblastoma without radiotherapy.* Arch Ophthalmol, 1996. **114**(11): p. 1321-8.
49. Greenwald, M.J. and L.C. Strauss, *Treatment of intraocular retinoblastoma with carboplatin and etoposide chemotherapy.* Ophthalmology, 1996. **103**(12): p. 1989-97.
50. Bayar, E., M.G. Robinson and T.W. Kurczynski, *Unilateral retinoblastoma with acquired monosomy 7 and secondary acute myelomonocytic leukemia.* Cancer Genet Cytogenet, 1998. **105**(1): p. 79-82.
51. Hande, K.R., *Clinical applications of anticancer drugs targeted to topoisomerase II.* Biochim Biophys Acta, 1998. **1400**(1-3): p. 173-84.
52. Nishimura, S., et al., *Acute myeloblastic leukemia as a second malignancy in a patient with hereditary retinoblastoma.* J Clin Oncol, 2001. **19**(21): p. 4182-3.
53. Burden, D.A. and N. Osheroff, *Mechanism of action of eukaryotic topoisomerase II and drugs targeted to the enzyme.* Biochim Biophys Acta, 1998. **1400**(1-3): p. 139-54.
54. Hande, K.R., *Etoposide: four decades of development of a topoisomerase II inhibitor.* Eur J Cancer, 1998. **34**(10): p. 1514-21.
55. Rodriguez-Galindo, C., et al., *Treatment of intraocular retinoblastoma with vincristine and carboplatin.* J Clin Oncol, 2003. **21**(10): p. 2019-25.
56. Pratt, C.B., et al., *Phase I study of topotecan for pediatric patients with malignant solid tumors.* J Clin Oncol, 1994. **12**(3): p. 539-43.
57. Tubergen, D.G., et al., *Phase I trial and pharmacokinetic (PK) and pharmacodynamics (PD) study of topotecan using a five-day course in children with refractory solid tumors: a pediatric oncology group study.* J Pediatr Hematol Oncol, 1996. **18**(4): p. 352-61.
58. Thompson, J., et al., *Synergy of topotecan in combination with vincristine for treatment of pediatric solid tumor xenografts.* Clin Cancer Res, 1999. **5**(11): p. 3617-31.
59. Houghton, J.A., et al., *Determinants of intrinsic sensitivity to Vinca alkaloids in xenografts of pediatric rhabdomyosarcomas.* Cancer Res, 1984. **44**(2): p. 582-90.
60. Laurie, N.A., et al., *Topotecan combination chemotherapy in two new rodent models of retinoblastoma.* Clin Cancer Res, 2005. **11**(20): p. 7569-78.
61. Mendelsohn, M.E., et al., *Intraocular concentrations of chemotherapeutic agents after systemic or local administration.* Arch Ophthalmol, 1998. **116**(9): p. 1209-12.
62. Rootman, J. and G. Gudauskas, *Treatment of ocular leukemia with local chemotherapy.* Cancer Treat Rep, 1985. **69**(1): p. 119-22.

63. Rootman, J., N. Bussanich and G. Gudauskas, *Combined local chemotherapy for a spontaneously occurring intraocular tumour in a cat.* Can J Ophthalmol, 1983. **18**(4): p. 185-7.
64. Murray, T.G., et al., *Subconjunctival carboplatin therapy and cryotherapy in the treatment of transgenic murine retinoblastoma.* Arch Ophthalmol, 1997. **115**(10): p. 1286-90.
65. Abramson, D.H., C.M. Frank and I.J. Dunkel, *A phase I/II study of subconjunctival carboplatin for intraocular retinoblastoma.* Ophthalmology, 1999. **106**(10): p. 1947-50.
66. Abramson, D.H., et al., *Systemic carboplatin for retinoblastoma: change in tumour size over time.* Br J Ophthalmol, 2005. **89**(12): p. 1616-9.
67. Chantada, G.L., et al., *A phase I study of periocular topotecan in children with intraocular retinoblastoma.* Invest Ophthalmol Vis Sci, 2009. **50**(4): p. 1492-6.
68. Burton, M.E., et al., *Applied Pharmacokinetics and Pharmacodynamics; Priniciples of Therapeutic Drug Monitoring*. 4 ed. 2006, Baltimore: Lippincott Williams and Wilkins. 867.
69. O'Dwyer, P.J., et al., *Etoposide (VP-16-213). Current status of an active anticancer drug.* N Engl J Med, 1985. **312**(11): p. 692-700.
70. Belani, C.P., L.A. Doyle and J. Aisner, *Etoposide: current status and future perspectives in the management of malignant neoplasms.* Cancer Chemother Pharmacol, 1994. **34** Suppl: p. S118-26.
71. Stewart, C.F., et al., *Prospective evaluation of a model for predicting etoposide plasma protein binding in cancer patients.* Cancer Res, 1990. **50**(21): p. 6854-6.
72. Stine, K.C., et al., *Secondary acute myelogenous leukemia following safe exposure to etoposide.* J Clin Oncol, 1997. **15**(4): p. 1583-6.
73. Nichols, C.R., et al., *Secondary leukemia associated with a conventional dose of etoposide: review of serial germ cell tumor protocols.* J Natl Cancer Inst, 1993. **85**(1): p. 36-40.
74. Takimoto, C.H. and S.G. Arbuck, *Clinical status and optimal use of topotecan.* Oncology (Williston Park), 1997. **11**(11): p. 1635-46; discussion 1649-51, 1655-7.
75. Pommier, Y., *Topoisomerase I inhibitors: camptothecins and beyond.* Nat Rev Cancer, 2006. **6**(10): p. 789-802.
76. Vassal, G., et al., *Preclinical development of camptothecin derivatives and clinical trials in pediatric oncology.* Biochimie, 1998. **80**(3): p. 271-80.
77. Teicher, B.A., *Next generation topoisomerase I inhibitors: rationale and biomarker strategies.* Biochem Pharmacol, 2008. **75**(6): p. 1262-71.
78. Sieber, S.M., J.A. Mead and R.H. Adamson, *Pharmacology of antitumor agents from higher plants.* Cancer Treat Rep, 1976. **60**(8): p. 1127-39.
79. Zhou, X.J. and R. Rahmani, *Preclinical and clinical pharmacology of vinca alkaloids.* Drugs, 1992. **44** Suppl 4: p. 1-16; discussion 66-9.
80. Rahmani, R. and X.J. Zhou, *Pharmacokinetics and metabolism of vinca alkaloids.* Cancer Surv, 1993. **17**: p. 269-81.
81. Von Hoff, D.D., *Whither carboplatin?--A replacement for or an alternative to cisplatin?* J Clin Oncol, 1987. **5**(2): p. 169-71.
82. Muggia, F.M., *Overview of carboplatin: replacing, complementing and extending the therapeutic horizons of cisplatin.* Semin Oncol, 1989. **16** Suppl 5: p. 7-13.
83. Ozols, R.F., *Optimal dosing with carboplatin.* Semin Oncol, 1989. **16** Suppl 5: p. 14-8.

84. Judson, I. and L.R. Kelland, *New developments and approaches in the platinum arena.* Drugs, 2000. **59** Suppl 4: p. 29-36; discussion 37-8.
85. Ranta, V.P. and A. Urtti, *Transscleral drug delivery to the posterior eye: prospects of pharmacokinetic modeling.* Adv Drug Deliv Rev, 2006. **58**(11): p. 1164-81.
86. Edelhauser, H.F., J.H. Boatright and J.M. Nickerson, *Drug delivery to posterior intraocular tissues: third Annual ARVO/Pfizer Ophthalmics Research Institute Conference.* Invest Ophthalmol Vis Sci, 2008. **49**(11): p. 4712-20.
87. Hosoya, K., V.H. Lee and K.J. Kim, *Roles of the conjunctiva in ocular drug delivery: a review of conjunctival transport mechanisms and their regulation.* Eur J Pharm Biopharm, 2005. **60**(2): p. 227-40.
88. Davies, N.M., *Biopharmaceutical considerations in topical ocular drug delivery.* Clin Exp Pharmacol Physiol, 2000. **27**(7): p. 558-62.
89. Geroski, D.H. and H.F. Edelhauser, *Transscleral drug delivery for posterior segment disease.* Adv Drug Deliv Rev, 2001. **52**(1): p. 37-48.
90. Cruysberg, L.P., et al., *The influence of intraocular pressure on the transscleral diffusion of high-molecular-weight compounds.* Invest Ophthalmol Vis Sci, 2005. **46**(10): p. 3790-4.
91. Cheruvu, N.P., A.C. Amrite and U.B. Kompella, *Effect of eye pigmentation on transscleral drug delivery.* Invest Ophthalmol Vis Sci, 2008. **49**(1): p. 333-41.
92. Steuer, H., et al., *Functional characterization and comparison of the outer blood-retina barrier and the blood-brain barrier.* Invest Ophthalmol Vis Sci, 2005. **46**(3): p. 1047-53.
93. Hosoya, K. and M. Tomi, *Advances in the cell biology of transport via the inner blood-retinal barrier: establishment of cell lines and transport functions.* Biol Pharm Bull, 2005. **28**(1): p. 1-8.
94. Lee, V.H., *Membrane transporters.* Eur J Pharm Sci, 2000. **11** Suppl 2: p. S41-50.
95. Gallie, B.L., et al., *Heterotransplantation of retinoblastoma into the athymic "nude" mouse.* Invest Ophthalmol Vis Sci, 1977. **16**(3): p. 256-9.
96. Kobayashi, S. and N. Mukai, *Retinoblastoma-like tumors induced in rats by human adenovirus.* Invest Ophthalmol, 1973. **12**(11): p. 853-6.
97. Howes, K.A., et al., *Photoreceptor cell tumors in transgenic mice.* Invest Ophthalmol Vis Sci, 1994. **35**(2): p. 342-51.
98. Marcus, D.M., et al., *Trilateral tumors in four different lines of transgenic mice expressing SV40 T-antigen.* Invest Ophthalmol Vis Sci, 1996. **37**(2): p. 392-6.
99. Windle, J.J., et al., *Retinoblastoma in transgenic mice.* Nature, 1990. **343**(6259): p. 665-9.
100. Mills, M.D., J.J. Windle and D.M. Albert, *Retinoblastoma in transgenic mice: models of hereditary retinoblastoma.* Surv Ophthalmol, 1999. **43**(6): p. 508-18.
101. Dyson, N., et al., *The human papilloma virus-16 E7 oncoprotein is able to bind to the retinoblastoma gene product.* Science, 1989. **243**(4893): p. 934-7.
102. Mukai, N., et al., *Retinal tumor induced in the baboon by human adenovirus 12.* Science, 1980. **210**(4473): p. 1023-5.
103. Jacks, T., et al., *Effects of an Rb mutation in the mouse.* Nature, 1992. **359**(6393): p. 295-300.
104. Lee, E.Y., et al., *Mice deficient for Rb are nonviable and show defects in neurogenesis and haematopoiesis.* Nature, 1992. **359**(6393): p. 288-94.

105. Clarke, A.R., et al., *Requirement for a functional Rb-1 gene in murine development.* Nature, 1992. **359**(6393): p. 328-30.
106. Maandag, E.C., et al., *Developmental rescue of an embryonic-lethal mutation in the retinoblastoma gene in chimeric mice.* EMBO J, 1994. **13**(18): p. 4260-8.
107. Williams, B.O., et al., *Extensive contribution of Rb-deficient cells to adult chimeric mice with limited histopathological consequences.* EMBO J, 1994. **13**(18): p. 4251-9.
108. Sauer, B. and N. Henderson, *Site-specific DNA recombination in mammalian cells by the Cre recombinase of bacteriophage P1.* Proc Natl Acad Sci U S A, 1988. **85**(14): p. 5166-70.
109. Robanus-Maandag, E., et al., *p107 is a suppressor of retinoblastoma development in pRb-deficient mice.* Genes Dev, 1998. **12**(11): p. 1599-609.
110. Zhang, J., B. Schweers and M.A. Dyer, *The first knockout mouse model of retinoblastoma.* Cell Cycle, 2004. **3**(7): p. 952-9.
111. Dannenberg, J.H., et al., *Tissue-specific tumor suppressor activity of retinoblastoma gene homologs p107 and p130.* Genes Dev, 2004. **18**(23): p. 2952-62.
112. Shih, C.S., et al., *AAV-mediated local delivery of interferon-beta for the treatment of retinoblastoma in preclinical models.* Neuromolecular Med, 2009. **11**(1): p. 43-52.
113. Dyer, M.A., *Mouse models of childhood cancer of the nervous system.* J Clin Pathol, 2004. **57**(6): p. 561-76.
114. Brandt, C.R., et al., *Treatment of spontaneously arising retinoblastoma tumors in transgenic mice with an attenuated herpes simplex virus mutant.* Virology, 1997. **229**(1): p. 283-91.
115. Albert, D.M., et al., *The antineoplastic effect of vitamin D in transgenic mice with retinoblastoma.* Invest Ophthalmol Vis Sci, 1992. **33**(8): p. 2354-64.
116. Harbour, J.W., et al., *Local carboplatin therapy in transgenic murine retinoblastoma.* Invest Ophthalmol Vis Sci, 1996. **37**(9): p. 1892-8.
117. Shternfeld, I.S., et al., *Antineoplastic effect of 1,25-dihydroxy-16-ene-23-yne-vitamin D3 analogue in transgenic mice with retinoblastoma.* Arch Ophthalmol, 1996. **114**(11): p. 1396-401.
118. Murray, T.G., et al., *Radiation therapy and ferromagnetic hyperthermia in the treatment of murine transgenic retinoblastoma.* Arch Ophthalmol, 1996. **114**(11): p. 1376-81.
119. Kang, S.J., et al., *Subconjunctival nanoparticle carboplatin in the treatment of murine retinoblastoma.* Arch Ophthalmol, 2009. **127**(8): p. 1043-7.
120. Hayden, B.H., et al., *Subconjunctival carboplatin in retinoblastoma: impact of tumor burden and dose schedule.* Arch Ophthalmol, 2000. **118**(11): p. 1549-54.
121. Singh, M. and L. Johnson, *Using genetically engineered mouse models of cancer to aid drug development: an industry perspective.* Clin Cancer Res, 2006. **12**(18): p. 5312-28.
122. Reagan-Shaw, S., M. Nihal and N. Ahmad, *Dose translation from animal to human studies revisited.* FASEB J, 2008. **22**(3): p. 659-61.
123. van Hennik, M.B., et al., *Comparative pharmacokinetics of cisplatin and three analogues in mice and humans.* Cancer Res, 1987. **47**(23): p. 6297-301.
124. Dyer, M.A., C. Rodriguez-Galindo and M.W. Wilson, *Use of preclinical models to improve treatment of retinoblastoma.* PLoS Med, 2005. **2**(10): p. e332.

125. Laurie, N.A., et al., *Inactivation of the p53 pathway in retinoblastoma.* Nature, 2006. **444**(7115): p. 61-6.
126. Prusky, G.T. and R.M. Douglas, *Characterization of mouse cortical spatial vision.* Vision Res, 2004. **44**(28): p. 3411-8.
127. Rygaard, J. and C.O. Povlsen, *Heterotransplantation of a human malignant tumour to "Nude" mice.* Acta Pathol Microbiol Scand, 1969. **77**(4): p. 758-60.
128. Kelland, L.R., *Of mice and men: values and liabilities of the athymic nude mouse model in anticancer drug development.* Eur J Cancer, 2004. **40**(6): p. 827-36.
129. Teicher, B.A., *Tumor models for efficacy determination.* Mol Cancer Ther, 2006. **5**(10): p. 2435-43.
130. Hollingshead, M.G., *Antitumor efficacy testing in rodents.* J Natl Cancer Inst, 2008. **100**(21): p. 1500-10.
131. Ajioka, I., et al., *Differentiated horizontal interneurons clonally expand to form metastatic retinoblastoma in mice.* Cell, 2007. **131**(2): p. 378-90.
132. Prusky, G.T., et al., *Rapid quantification of adult and developing mouse spatial vision using a virtual optomotor system.* Invest Ophthalmol Vis Sci, 2004. **45**(12): p. 4611-6.
133. Dyer, M.A., et al., *Retinal degeneration in Aipl1-deficient mice: a new genetic model of Leber congenital amaurosis.* Brain Res Mol Brain Res, 2004. **132**(2): p. 208-20.
134. Hawes, N.L., et al., *Mouse fundus photography and angiography: a catalogue of normal and mutant phenotypes.* Mol Vis, 1999. **5**: p. 22.
135. Savinova, O.V., et al., *Intraocular pressure in genetically distinct mice: an update and strain survey.* BMC Genet, 2001. **2**: p. 12.
136. Akey, D.T., et al., *The inherited blindness associated protein AIPL1 interacts with the cell cycle regulator protein NUB1.* Hum Mol Genet, 2002. **11**(22): p. 2723-33.
137. Donovan, S.L. and M.A. Dyer, *Developmental defects in Rb-deficient retinae.* Vision Res, 2004. **44**(28): p. 3323-33.
138. Alexander, J.J., et al., *Restoration of cone vision in a mouse model of achromatopsia.* Nat Med, 2007. **13**(6): p. 685-7.
139. DiLoreto, D., Jr., et al., *A new procedure for fundus photography and fluorescein angiography in small laboratory animal eyes.* Curr Eye Res, 1994. **13**(2): p. 157-61.
140. Chang, B., et al., *Mouse models of ocular diseases.* Vis Neurosci, 2005. **22**(5): p. 587-93.
141. Abramson, D.H., *The diagnosis of retinoblastoma.* Bull N Y Acad Med, 1988. **64**(4): p. 283-317.
142. Chang, B., et al., *Retinal degeneration mutants in the mouse.* Vision Res, 2002. **42**(4): p. 517-25.
143. McCarville, M.B., et al., *Angiogenesis inhibitors in a murine neuroblastoma model: quantitative assessment of intratumoral blood flow with contrast-enhanced gray-scale US.* Radiology, 2006. **240**(1): p. 73-81.
144. Wirtzfeld, L.A., et al., *A new three-dimensional ultrasound microimaging technology for preclinical studies using a transgenic prostate cancer mouse model.* Cancer Res, 2005. **65**(14): p. 6337-45.
145. Jouannot, E., et al., *High-frequency ultrasound detection and follow-up of Wilms' tumor in the mouse.* Ultrasound Med Biol, 2006. **32**(2): p. 183-90.
146. Remtulla, S. and P.E. Hallett, *A schematic eye for the mouse, and comparisons with the rat.* Vision Res, 1985. **25**(1): p. 21-31.

147. Finger, P.T., et al., *High-frequency ultrasound of anterior segment retinoblastoma.* Am J Ophthalmol, 2004. **137**(5): p. 944-6.
148. Brockmann, M.A., A. Kemmling and C. Groden, *Current issues and perspectives in small rodent magnetic resonance imaging using clinical MRI scanners.* Methods, 2007. **43**(1): p. 79-87.
149. Yang, A.D., et al., *Improving delivery of antineoplastic agents with anti-vascular endothelial growth factor therapy.* Cancer, 2005. **103**(8): p. 1561-70.
150. Zhang, Z.G., et al., *VEGF enhances angiogenesis and promotes blood-brain barrier leakage in the ischemic brain.* J Clin Invest, 2000. **106**(7): p. 829-38.
151. Olsen, T.W., et al., *Human scleral permeability. Effects of age, cryotherapy, transscleral diode laser and surgical thinning.* Invest Ophthalmol Vis Sci, 1995. **36**(9): p. 1893-903.
152. Carcaboso, A.M., et al., *Topotecan vitreous levels after periocular or intravenous delivery in rabbits: an alternative for retinoblastoma chemotherapy.* Invest Ophthalmol Vis Sci, 2007. **48**(8): p. 3761-7.
153. Abramson, D.H., et al., *Intraocular carboplatin concentrations following intravenous administration for human intraocular retinoblastoma.* Ophthalmic Genet, 1999. **20**(1): p. 31-6.
154. McFall, R.C., T.W. Sery and M. Makadon, *Characterization of a new continuous cell line derived from a human retinoblastoma.* Cancer Res, 1977. **37**(4): p. 1003-10.
155. Weiss, B. and K. Shannon, *Mouse cancer models as a platform for performing preclinical therapeutic trials.* Curr Opin Genet Dev, 2003. **13**(1): p. 84-9.
156. Sobrin, L., et al., *External beam radiation "salvage" therapy in transgenic murine retinoblastoma.* Arch Ophthalmol, 2004. **122**(2): p. 251-7.
157. Wilson, T.W., et al., *Penetration of chemotherapy into vitreous is increased by cryotherapy and cyclosporine in rabbits.* Arch Ophthalmol, 1996. **114**(11): p. 1390-5.
158. de Zwart, L., et al., *The ontogeny of drug metabolizing enzymes and transporters in the rat.* Reprod Toxicol, 2008. **26**(3-4): p. 220-30.
159. Chinnaswamy, G., et al., *Estimation of renal function and its potential impact on carboplatin dosing in children with cancer.* Br J Cancer, 2008. **99**(6): p. 894-9.
160. Wacker, G.R., H.S. Zarkowsky and H.B. Burch, *Changes in kidney enzymes of rats after birth.* Am J Physiol, 1961. **200**: p. 367-9.
161. Sweet, D.H., et al., *Organic anion and cation transporter expression and function during embryonic kidney development and in organ culture models.* Kidney Int, 2006. **69**(5): p. 837-45.
162. Horster, M. and J.E. Lewy, *Filtration fraction and extraction of PAH during neonatal period in the rat.* Am J Physiol, 1970. **219**(4): p. 1061-5.
163. Cheng, X. and C.D. Klaassen, *Tissue distribution, ontogeny and hormonal regulation of xenobiotic transporters in mouse kidneys.* Drug Metab Dispos, 2009. **37**(11): p. 2178-85.
164. Calcagno, P.L. and M.I. Rubin, *Renal Extraction of Para-Aminohippurate in Infants and Children.* J Clin Invest, 1963. **42**: p. 1632-9.
165. John, S.W., et al., *Intraocular pressure in inbred mouse strains.* Invest Ophthalmol Vis Sci, 1997. **38**(1): p. 249-53.
166. Donovan, S.L., et al., *Compensation by tumor suppressor genes during retinal development in mice and humans.* BMC Biol, 2006. **4**: p. 14.

167. Zamboni, W.C., et al., *Pharmacodynamic model of topotecan-induced time course of neutropenia.* Clin Cancer Res, 2001. **7**(8): p. 2301-8.
168. Freeman, B.B., 3rd, et al., *Using plasma topotecan pharmacokinetics to estimate topotecan exposure in cerebrospinal fluid of children with medulloblastoma.* Neuro Oncol, 2006. **8**(2): p. 89-95.
169. Stewart, C.F., et al., *Results of a phase II upfront window of pharmacokinetically guided topotecan in high-risk medulloblastoma and supratentorial primitive neuroectodermal tumor.* J Clin Oncol, 2004. **22**(16): p. 3357-65.
170. Freireich, E.J., et al., *Quantitative comparison of toxicity of anticancer agents in mouse, rat, hamster, dog, monkey and man.* Cancer Chemother Rep, 1966. **50**(4): p. 219-44.
171. Jeon, C.J., E. Strettoi and R.H. Masland, *The major cell populations of the mouse retina.* J Neurosci, 1998. **18**(21): p. 8936-46.
172. Newell, D.R., et al., *Carboplatin pharmacokinetics in children: the development of a pediatric dosing formula. The United Kingdom Children's Cancer Study Group.* J Clin Oncol, 1993. **11**(12): p. 2314-23.
173. Riccardi, R., et al., *Clinical pharmacokinetics of carboplatin in children.* Cancer Chemother Pharmacol, 1994. **33**(6): p. 477-83.
174. Clark, D.L., et al., *Predictive value of preclinical toxicology studies for platinum anticancer drugs.* Clin Cancer Res, 1999. **5**(5): p. 1161-7.
175. Aukunuru, J.V., et al., *Expression of multidrug resistance-associated protein (MRP) in human retinal pigment epithelial cells and its interaction with BAPSG, a novel aldose reductase inhibitor.* Pharm Res, 2001. **18**(5): p. 565-72.
176. Kennedy, B.G. and N.J. Mangini, *P-glycoprotein expression in human retinal pigment epithelium.* Mol Vis, 2002. **8**: p. 422-30.
177. Rajan, P.D., et al., *Expression of the extraneuronal monoamine transporter in RPE and neural retina.* Curr Eye Res, 2000. **20**(3): p. 195-204.
178. Ito, A., et al., *Distribution of rat organic anion transporting polypeptide-E (oatp-E) in the rat eye.* Invest Ophthalmol Vis Sci, 2003. **44**(11): p. 4877-84.
179. Merriman-Smith, B.R., et al., *Molecular identification of P-glycoprotein: a role in lens circulation?* Invest Ophthalmol Vis Sci, 2002. **43**(9): p. 3008-15.
180. Wu, J., et al., *P-glycoprotein regulates a volume-activated chloride current in bovine non-pigmented ciliary epithelial cells.* J Physiol, 1996. **491**(Pt 3): p. 743-55.
181. Kawazu, K., et al., *Characterization of cyclosporin A transport in cultured rabbit corneal epithelial cells: P-glycoprotein transport activity and binding to cyclophilin.* Invest Ophthalmol Vis Sci, 1999. **40**(8): p. 1738-44.
182. Yang, J.J., K.J. Kim and V.H. Lee, *Role of P-glycoprotein in restricting propranolol transport in cultured rabbit conjunctival epithelial cell layers.* Pharm Res, 2000. **17**(5): p. 533-8.
183. Attar, M., et al., *Ophthalmic drug delivery considerations at the cellular level: drug-metabolising enzymes and transporters.* Expert Opin Drug Deliv, 2005. **2**(5): p. 891-908.
184. Ueda, H., et al., *Functional characterization of organic cation drug transport in the pigmented rabbit conjunctiva.* Invest Ophthalmol Vis Sci, 2000. **41**(3): p. 870-6.

APPENDIX A. DRUG TRANSPORTERS IN THE EYE

Table A-1. An Abbreviated Summary of Drug Transporters in the Eye.

Tissue	Transporter	Species	Reference
Blood-retina-barrier	P-gp (MDR)	Porcine	[92]
	MRP1	Porcine	[92] [175]
RPE	P-gp	Human, rabbit	[16, 176]
	OCT3	Mouse, rabbit, human	[177]
	OATP-E	Rat	[178]
Lens	P-gp	Rat	[179]
Ciliary epithelium	P-gp	Bovine	[180]
Cornea	P-gp	Rabbit, human	[181]
	OATP-E	Rat	[178]
Conjunctiva	P-gp (apical /tear side)	Rabbit, human	[182, 183]
	OCTs	Rabbit, mouse, human	[183, 184]

APPENDIX B. PHARMACOKINETICS AND AUC GUIDED DOSING FOR CARBOPLATIN AND TOPOTECAN IN HUMANS AND RODENTS

B.1 SYSTEMIC TOPOTECAN

Preclinical studies have suggested that attaining a specific plasma topotecan lactone systemic exposure (i.e. AUC) was associated with an improved antitumor effect in pediatric solid tumor xenografts [167]. Thus, numerous clinical trials in children with cancer have used the approach of pharmacokinetically guided topotecan dosing to individualize topotecan therapy for a patient based upon that child's topotecan systemic clearance. This approach takes advantage of the linear relationship between topotecan dosage and plasma area under the concentration-time curve (AUC) to account for the wide interpatient variability noted in topotecan clearance [168] to achieve the target topotecan systemic exposure (AUC), which is defined differently for each clinical trial depending upon the therapeutic goal. For example, in a study of children with high-risk medulloblastoma administered topotecan intravenously daily for 5 days, the target was defined as a plasma topotecan lacton AUC of 120 to 160 ng/ml•hr (~0.26-0.35 μM•h topotecan lacton or ~0.79-1.1 uM•h topotecan total [lactone and carboxylate]) [169]. In this study, the median topotecan dosage associated with the studies that were within the target range was 3.2 mg/m^2/dose. In current institutional study for children with retinoblastoma, the same topotecan lactone target systemic exposure (i.e. 120 to140 ng/ml•hr) and dosing approach is used. Our orthotopic xenograft studies are carried our in juvenile rats (P14) [60]. To directly convert the human dosage in mg/m^2 to a juvenile rat dosage in mg/kg, we considered that although the size of our juvenile rats (~28-30 g) is similar to the size of an adult mouse, drug metabolism and clearance mechanisms (in particular, those depend on the liver and kidneys) may be significantly different in juvenile rats due to their incomplete development. Therefore, in order to calculate human-equivalent dosages in juvenile rats, we did not use species-specific conversion factors (based purely on body surface area and weight), which have been developed for adult rat (factor 6) and adult mice (factor 3), but not for juvenile rats [170]. Instead, we preferred a dosing approach that was "AUC guided," based first on determining a desired or appropriate systemic exposure or AUC in patients, and then with our knowledge of the pharmacokinetics of the drug in the animal model calculate what dosage would be required to attain that systemic exposure or value in animal model.

Using this approach we would first chose the topotecan lactone systemic exposure or AUC value form the retinoblastoma clinical trial as our "target" for the animal model (i.e., 120 to 60 ng/ml•h). Results of previous pharmacokinetic studies in this animal model juvenile (P14) rats reformed in our lab showed that after a 2 mg/kg i.p. injection of topotecan, the total topotecan AUC was 1230 ng/ml•hr (2.7 μM•h) [60]. This is approximately 2.7 to 3.4-fold higher than the above described topotecan AUC target for the clinical retinoblastoma protocol. Since the relationship between topotecan dosage and AUC is linear, a dosage of 0.7 mg/kg in P14 rats is estimated to yield the equivalent of a plasma topotecan lactone AUC of 140 ng/ml•h. Therefore, topotecan given at a dosage of 0.7 mg/kg i.p. daily x 5 is our candidate equivalent dosage based on pediatric plasma AUC measurements. A similar study in adult mice found that the dose of 0.6 mg/kg on a daily x 5 (x2) schedule was well tolerated and gave a topotecan

lactone AUC of 88 ng/ml•hr [170]. It may be necessary to increase 1.6-fold the dosage in adult mice to achieve the equivalent of the desired topotecan lactone AUC of 140 ng/ml•hr. Based on this approach, the human equivalent i.p. topotecan dosage for P14 rats is 0.7 mg/kg and 1 mg/kg for adult mice.

B.2 SUBCONJUNCTIVAL TOPOTECAN

In 2009, Chantada administered subconjunctival topotecan to children with retinoblastoma, and found that the maximum tolerated dose was 2 ml or 2 mg per eye [67]. A 30 lb child that is 25 inches tall and 30 months old (59^{th} percentile from growth charts) has a body surface area (BSA) of 0.49 m^2. Therefore, a dose a 2mg is equivalent to 4 mg/m^2. Based on previous topotecan AUC data for systemic administration, the plasma AUC should be 240-320 ng/ml•h if the drug is absorbed systemically in a manner similar to a 30 minute i.v. infusion. This assumption is not necessarily true. The total plasma AUC achieved from a 2 mg subconjunctival injection of topotecan was much lower at 104 ng/ml •h (G. Chantada, personal communication). The volume of the subconjunctival space and the drug concentration provided by the manufacturer limits the total dose.

The volume of an average child's eye with retinoblastoma is ~3600 mm^3. Therefore, if 2 mg is administered per eye, the maximum ocular concentration would be 0.55 mg/ml of eye volume. As an approach to calculate equivalent local topotecan dosages in P14 rats, we considered literature data on the volume of an adult mouse eye (19.1 mm^3) [171]. For a mouse eye of 19.1 mm^3 the dose would be ~0.01 mg per eye to achieve the same maximum exposure of 0.55 mg/ml of eye volume. In our pharmacokinetic studies, we administered 0.01 ml of a 1 mg/ml stock. This is equivalent to the human dose according to our rationale. We performed a pharmacokinetic study of subconjunctival topotecan (0.01 mg/eye) in both eyes of P14 rats to directly compare to the data from Chantada [67]. We analyzed total topotecan concentration in plasma and found that the topotecan AUC total from this experiment was 524 ng/ml•h. Thus, the plasma AUC from a single injection of topotecan to one eye was 104 ng/ml•h for humans as compared to 262 ng/ml•h per mouse eye. We have not performed a pharmacokinetic study in adult mice using subconjunctival injection of topotecan to determine if the systemic or vitreal exposure is different between adult mice and juvenile rats. It is also important to consider the possibility that there may be an increase in the side effects of subconjunctival topotecan in juvenile rats as compared to humans because of this increase in systemic exposure. Since no data are available from vitreal topotecan AUC values in humans, we could not compare our murine data and derive dosing recommendations as with systemic topotecan therapy. However, we believe that our selection of a topotecan dose of 0.01 mg/eye for our rodent studies is rational based upon the proposed eye volume approach.

B.3 TOPOTECAN SUMMARY

Based on these data, the human equivalent i.p. topotecan dosage for P14 rats is 0.7 mg/kg and 1 mg/kg for adult mice. The human equivalent dose for subconjunctival injection of topotecan in rodents is 0.01 mg/eye.

B.4 SYSTEMIC CARBOPLATIN

The dosage of intravenous carboplatin used in children with cancer including those with retinoblastoma is 550-560 mg/m^2 [123, 172]. The plasma AUC for the dose can range from 260-430 μM•hr [123, 172]. A linear relationship has been noted between AUC and carboplatin dosages. However, as with many anticancer drugs in children, wide interpatient variability in carboplatin systemic clearance has been reported [173].

The equivalent carboplatin dosage, using the conversion factors based on body surface area and weight, for the adult rat is ~90 mg/kg and ~180 mg/kg in adult mice [170]. As with topotecan, it is likely that the disposition of the carboplatin varies among species. The LD_{10} for adult mice was 165 mg/kg [174]. Therefore, it is impossible to administer the converted dose (180mg/kg) based on body weight in adult mice.

Previous studies using juvenile (P14) rats and a 70 mg/kg i.p. dose (equivalent to 210-420 mg/m^2 in children) gave a plasma AUC of 560 μM•h [60]. This is approximately 2-fold higher than the target AUC for children. Considering that the dose-to-AUC relationship is linear, a dose of 35 mg/kg should give a plasma AUC in P14 rats of ~280 μM•h. A similar study performed in adult mice found that the dose of 165 mg/kg resulted in a plasma AUC of 487 μM•h. Therefore, in adult mice found that the dose of 165 mg/kg resulted in a plasma AUC of 487 μM•h. Therefore, in adult mice, it may be necessary to increase the i.p. to ~80 mg/kg to achieve exposure similar to those seen in humans [172].

B.5 SUBCONJUNCTIVAL CARBOPLATIN

Abramson performed a human Phase I/II clinical trial of subconjunctival carboplatin with a maximum dose of 20 mg/eye [65]. Using the conversion described above based on the volume of the rodent eye compared to the human eye, a dose of 0.1 mg/eye is equivalent to the human dose. Our AUC analysis of P14 rats using bilateral injection of 0.1 mg/eye resulted in a plasma AUC of 63 μM•h. No plasma AUC data are available for the 20 mg subconjunctival injection in humans.

B.6 CARBOPLATIN SUMMARY

Based on these data, the human equivalent i.p. carboplatin dose for P14 rats is 34 mg/kg and 80 mg/kg for adult mice. The human equivalent dose for subconjunctival injection of topotecan in rodents is 0.2 mg/eye.

VITA

Katie Marie Nemeth was born in Hartford, Wisconsin in 1976. She graduated from West Bend West High School in June of 1994. In 1999, she completed her double major in French and Biology from Marquette University. She enrolled in the Interdisciplinary Program of Biomedical Sciences at the University of Tennessee in 2004. Her dissertation research was conducted at St. Jude's Children's Research Hospital. She completed her doctorate work May 2010.